The Design of Low-Leakage Modular Regenerators for Gas-Turbine Engines

by

James Anthony Kluka

B.S., Aeronautical and Astronautical Engineering
University of Illinois at Urbana-Champaign, 1990

Submitted to the Department of Aeronautics and Astronautics in Partial Fulfillment of the Requirements for the Degree of

Master of Science in Aeronautics and Astronautics

at the

Massachusetts Institute of Technology

June 1995

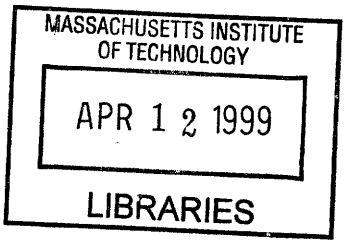

Author .....
Department of Aeronautics and Astronautics
May 22, 1995

Certified by .....
Professor David Gordon Wilson
Department of Mechanical Engineering
Thesis Supervisor

Accepted by .....
Professor Harold Y. Wachman
Chairman, Department Graduate Committee

The Design of Low-Leakage Modular Regenerators for Gas-Turbine Engines

by
James Anthony Kluka

Submitted to the Department of Aeronautics and Astronautics on May 22, 1995 in Partial Fulfillment of the Requirements for the Degree of Master of Science in Aeronautics and Astronautics.

Abstract

The design of a modular regenerator concept (patented by Wilson and MIT) for gas-turbine engines is investigated. Mechanical design analysis and theoretical performance calculations were made to show the concept's functionality and performance benefits over current regenerator designs.

The modular regenerator concept consists of a ceramic-honeycomb matrix discretized into rectangular blocks, called modules. The modules are exposed to hot (turbine exhaust) and cold (compressor outlet) streams, then are periodically transported through linear passages from one stream to the other. Separating the matrix into modules reduces the transverse sealing lengths substantially. Furthermore, the range of gas-turbine applications increases with the modular concept since larger matrix face areas are possible.

Module design is investigated which includes using current research results pertaining to manufacturing technology for rotary regenerators.

Mechanical design analysis was made to investigate the possible module-movement schemes. Several regenerator configurations and orientations are introduced. One particular concept balances the pressure forces such that the power requirement for module movement is reduced substantially. Design drawings of a possible modular prototype showing the general configuration and mechanical layout accompany the analysis.

A method for determining the regenerator size and measuring its fluid-mechanical and heat-transfer performance is given. An optimization study is made by analyzing the effects when several chosen design parameters are varied. Numerical results of a modular concept for a small gas-turbine engine (120 kW) are given.

Seal leakage calculations were made for two modular concepts and compared to the leakage rates for two rotary concepts. The total seal-leakage rates for both modular cases were considerably less than the rotary concepts and can be reduced to well under one percent. In addition, techniques for further leakage reduction are given.

Other design issues (to further prove the modular concept's feasibility) not covered in this study have been identified. Guidelines for investigating these issues are given.

Thesis Supervisor: David Gordon Wilson
Title: Professor Emeritus of Mechanical Engineering

Acknowledgments

I express my thanks to David Gordon Wilson, Professor Emeritus of Mechanical Engineering, on giving me the opportunity to work on a very exciting and interesting project. I also want to thank him on his efforts of raising funds to help with my financial situation.

In addition, I gratefully acknowledge the following people:

- Dean Arthur C. Smith of Undergraduate Education and Student Affairs and Dean John B. Vander Sande of the School of Engineering for their generous financial contributions.
- Andy Pfahnl, graduate student, for all of his technical assistance.
- My wife, Sandra, for her support and for making my life easier during the hectic times.
- My sister, Carol, and my mother, Naoko, for their moral support. If only this research could make Carol's Doberman, Tasha, well again.

Finally, I dedicate this work to my dad, Henry A. Kluka. Although he may not be here physically, he always lives within me and gives me the strength and endurance to overcome any obstacle.

Table of Contents

List of Figures

List of Tables

Nomenclature

Roman-Letter Symbols

a	≡	acceleration, m/sec^2
A_f	≡	face area, m^2
A_{ff}	≡	free face area, m^2
A_h	≡	heat-transfer area, m^2
AR	≡	aspect ratio
As	≡	matrix material area available for heat conduction, m^2
As'	≡	heat-conduction available-area ratio
C	≡	fluid velocity, m/s
$\overline{C}$	≡	mean fluid velocity, m/s
C_f	≡	coefficient of friction
c_P	≡	specific heat at constant pressure, J/kg-K
$\overline{c}_P$	≡	mean specific heat at constant pressure, J/kg-K
C_{rat}	≡	$(\dot{m}\,\overline{c}_p)_{min}/(\dot{m}\,\overline{c}_p)_{max}$ (heat-capacity-rate ratio)
C_{rot}	≡	$(\dot{m}\,\overline{c}_p)_{mat}/(\dot{m}\,\overline{c}_p)_{min}$
d	≡	diameter, m
d_h	≡	hydraulic diameter, m
$dist$	≡	distance or length, m
$dmod$	≡	distance traveled during actual module movement, m
F	≡	Force, N
FAR	≡	matrix face-area ratio
g	≡	gravitational acceleration, m/s^2
h	≡	seal-clearance height, m

h_t	≡	heat-transfer coefficient, W/m^2-K
$\left(h_t A_h\right)'$	≡	conductance ratio
k	≡	thermal conductivity, W/m-K
l	≡	length, m
m	≡	mass, kg
$\dot{m}$	≡	mass-flow rate, kg/s
n	≡	number of throttlings in labyrinth seal
$Nmod$	≡	number of modules
NTU	≡	number of transfer units
Nu	≡	Nusselt number
P	≡	pressure, Pa
$\bar{P}$	≡	mean pressure, Pa
P_{feed}	≡	feed pressure of pneumatic cylinder, Pa
Pr	≡	Prandtl number
q	≡	incompressible dynamic pressure, Pa
$\dot{Q}$	≡	heat-transfer rate, W
r	≡	compressor pressure ratio
R	≡	universal gas constant, J/kg-K
Re	≡	$(\rho C d_h)/\mu$ (Reynolds number)
s	≡	displacement, m
SC	≡	seal coverage
St	≡	Stanton number
t	≡	time, s
t_{net}	≡	total time, s
T	≡	temperature, K
$\bar{T}$	≡	mean temperature, K

th	≡	thickness, m
$tmod$	≡	time for actual module movement, s
U	≡	overall heat-transfer coefficient, W/m^2-K
v	≡	velocity, m/s
$\vec{v}$	≡	mean velocity, m/s
V	≡	volume, m^3
w	≡	width, m
$\dot{W}$	≡	power, W
$\overline{\dot{W}}$	≡	average power, W
$\dot{W}'$	≡	specific power
$\hat{\dot{W}}$	≡	normalized power requirement
x	≡	distance in the x-direction, m
Z	≡	number of passages

Greek Letter Symbols

α	≡	flow coefficient
ΔP	≡	pressure drop, Pa
ε	≡	regenerator effectiveness
$\hat{\varepsilon}$	≡	effectiveness estimate (calculated)
$\left(\frac{\Delta\varepsilon}{\varepsilon}\right)_{acsw}$	≡	axial-conduction-and-seal-width effect
ζ_{mat}	≡	proportion of channel area occupied by ceramic matrix
γ	≡	Egli's carry-over factor
η_{poly}	≡	total-to-total polytropic efficiency
$\eta_{thermal}$	≡	thermal efficiency
λ	≡	axial-conduction parameter
μ	≡	viscosity, kg/m-s

$\overline{\mu}$	≡	mean viscosity, kg/m-s
μ_s	≡	coefficient of static friction
ξ	≡	time proportion
ρ	≡	density, kg/m^3
$\overline{\rho}$	≡	mean density, kg/m^3
τ	≡	shear stress, Pa
Ψ	≡	porosity

Roman-Letter Subscripts

1	≡	station 1 in gas turbine engine
1-2	≡	associated with the compressor
2	≡	station 2 in gas turbine engine
3	≡	station 3 in gas turbine engine
3-4	≡	associated with the combustor
4	≡	station 4 in gas turbine engine
4-5	≡	associated with the turbine
5	≡	station 5 in gas turbine engine
6	≡	station 6 in gas turbine engine
acsw	≡	calculated assuming axial conduction and finite seal width
air	≡	associated with the air flow through the gas turbine
back	≡	associated with the back face of a module
bottom	≡	associated with the bottom face a module
carry-over	≡	associated with carry-over leakage
cer	≡	associated with the ceramic material of the regenerator
channel	≡	associated with the regenerator channel (header/regenerator interface)
chamber	≡	associated with the seal chamber for the gate-seal concept
cold	≡	associated with the cold side of the regenerator

config1	≡	associated with cylinder configuration #1
config2	≡	associated with cylinder configuration #2
cycle	≡	associated with the overall gas-turbine cycle
decel	≡	associated with the module-movement deceleration device
exposed	≡	associated with exposed to the flow
extension	≡	associated with the cylinder-rod extension stroke
f	≡	associate with an final condition
fillets	≡	associated with fillets along the module edges
friction	≡	associated with friction
front	≡	associated with the front face of a module
fuel	≡	associated with the gas-turbine engine fuel
gap	≡	associated with leakage through the seal-clearance gap
general	≡	associated with a general or generic term
GT	≡	associated with the gas-turbine engine
high	≡	associated with the high-pressure cold side of the regenerator
hot	≡	associated with the hot side of the regenerator
i	≡	associate with an initial condition
leak	≡	associated with the regenerator seal leakage
low	≡	associated with the low-pressure hot side of the regenerator
mat	≡	associated with the ceramic-honeycomb regenerator matrix
max	≡	maximum
min	≡	minimum
mod	≡	associated with a module
movement	≡	associated with module movement
nc	≡	calculated assuming no axial conduction
neg	≡	associated with negative module movement
net	≡	associated with a net or total result

orient1	≡	associated with regenerator orientation #1
orient2	≡	associated with regenerator orientation #2
pass	≡	associated with the ceramic matrix passages
pos	≡	associated with positive module movement
pressure	≡	associated with fluid pressure
regenerator	≡	associate with the modular regenerator
retraction	≡	associated with the cylinder-rod retraction stroke
rim	≡	associated with the module rim
rod	≡	associated with the cylinder piston rod
seal	≡	associated with the labyrinth seal along a module face
seal-channel	≡	associated with the seal-channel concept for leakage reduction
side	≡	associated with the side face of a module
slots	≡	associated with slots in the module rim
step	≡	associated with a module movement step
step1	≡	associated with step1 of module movement
step2	≡	associated with step2 of module movement
top	≡	associated with the top face of a module
unexposed	≡	associated with being not exposed to the flow
wall	≡	associated with the ceramic matrix walls

1. Introduction

Regenerators are heat exchangers which can be used to improve the thermal efficiency of gas-turbine engines. Most regenerator concepts have intrinsic compressed-air-leakage problems which lower an engine's thermal efficiency. Wilson and MIT have patented a new regenerator concept [1] that promises to offer substantially less leakage than current designs. The work presented is a design study for this concept called the modular regenerator. This chapter provides some fundamental aspects of regenerative gas-turbine cycles and regenerator performance. In addition, the different types of regenerators are introduced. In the next chapter, variations of the modular-regenerator concept are described. Thereafter, a detailed mechanical description is given. Finally, methods to design a modular regenerator and determine its heat-transfer and fluid-mechanical performance are presented.

1.1 Gas-Turbine Regenerative Cycle

The simple gas-turbine cycle consists of a compressor, combustor (also called a burner), and turbine. Air first enters the compressor where it is compressed, then fuel is added and burned with the air in the combustor, thus increasing the energy of the mixture. The combustion products enter the turbine where the energy is extracted to drive the

compressor and any external equipment. Upon exiting the turbine, the gas is released to the atmosphere. The exhaust temperature is relatively high; therefore, the thermal energy associated with the exhaust is wasted. Regenerators are used to recover some of this energy by reintroducing it back into the cycle just prior to combustion (hence the term "regeneration"). The compressed air now enters the combustor at a higher temperature, so less fuel is needed for the same amount of energy output. The result is an increase in thermal efficiency, which is defined as the work output divided by the heat input. The regenerative process can be represented on a temperature-entropy diagram as shown below with corresponding stations placed on the regenerative gas-turbine block diagram in Figure 1.2.

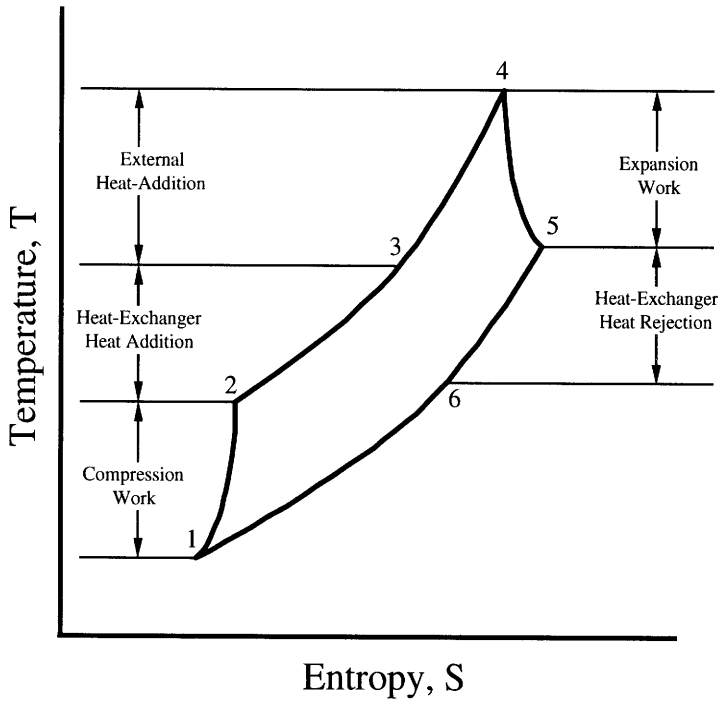

Figure 1.1 T-S diagram of regenerative gas-turbine cycle.

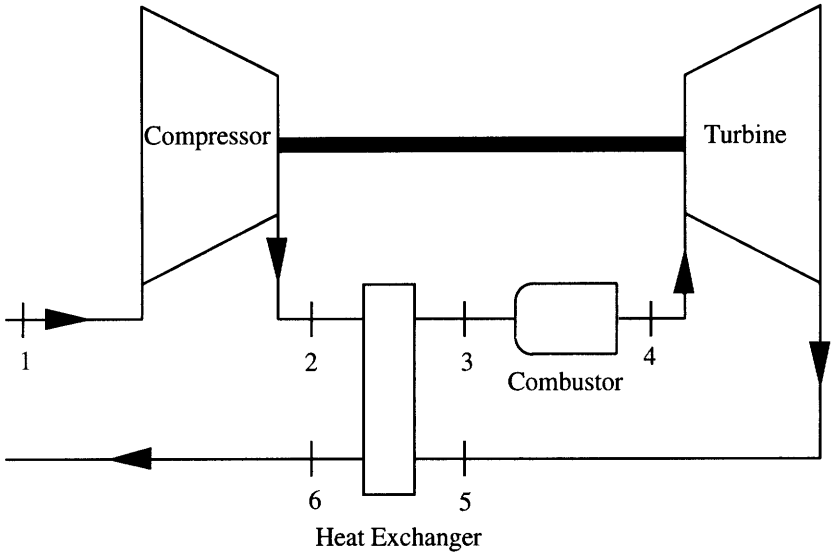

Figure 1.2 Block diagram of regenerative gas-turbine engine.

1.2 Regenerators

1.2.1 Regenerator Performance

This section discusses the fundamental performance aspects associated with regenerators. The performance plots shown in this section are based on the specified engine parameters from the design analysis of Chapter 5. The equations used to generate the performance curves are found in Section 5.2.2.3.4. Note that all plots are made with different pressure ratios, r, and the turbine-inlet temperature is fixed.

Cycle Comparison

As previously mentioned, regenerators increase the cycle thermal efficiency. This can be illustrated with the following figure which plots thermal efficiency versus specific power (a dimensionless gas-turbine power output) for two cycles. CBE is the simple cycle (compressor, burner, and turbine), and CBEX is the regenerative cycle (compressor,

burner, turbine, heat exchanger). Note that the CBEX curve has the regenerator effectiveness equal to 0.95.

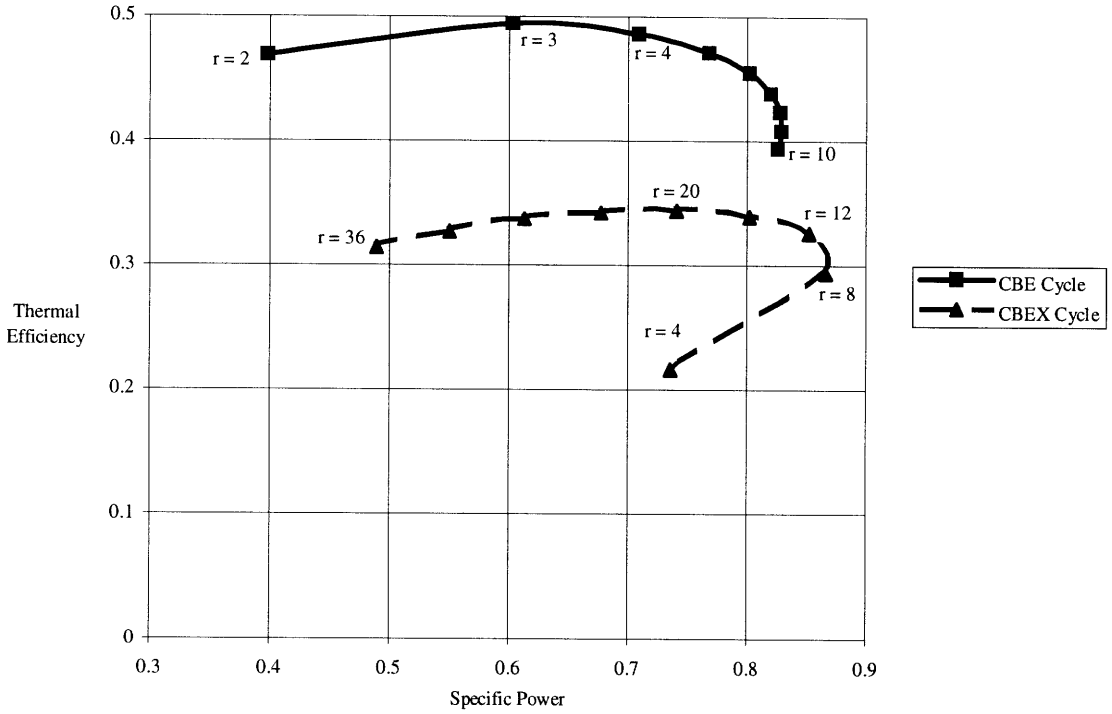

Figure 1.3 Plots of thermal efficiency versus specific power for simple cycle, CBE, and regenerative cycle, CBEX.

The figure shows that the regenerator increases the thermal efficiency approximately by 40 percent. Furthermore, with the introduction of a regenerator, the optimum compressor pressure ratio (where the thermal efficiency peaks) is much lower. From the plot, the thermal efficiency peaks at r=20 for CBE and at r=3 for CBEX. Operating at a lower pressure ratio has several benefits: reducing compressor blades stresses, increasing compressor efficiency because blade tip-clearance effects are reduced (since longer blade usage is allowed due to the lower air density), reducing losses since the compressor air flow can travel at subsonic speeds, and increasing the part-load efficiency [2].

Effectiveness

Effectiveness is a measure of the regenerator's thermal performance. Effectiveness is defined as the ratio of the actual heat transfer that occurs divided by the maximum possible amount of heat transfer. This can be written for a regenerative cycle as

$$\varepsilon = \frac{(\dot{m}\,\bar{c}_P)_{cold}\,(T_3 - T_2)}{(\dot{m}\,\bar{c}_P)_{min}\,(T_5 - T_2)} \tag{1.1}$$

or

$$\varepsilon = \frac{(\dot{m}\,\bar{c}_P)_{hot}\,(T_5 - T_6)}{(\dot{m}\,\bar{c}_P)_{min}\,(T_5 - T_2)} \tag{1.2}.$$

Limits do not exist (100 percent is the absolute limit) for effectiveness but the regenerator's size will increase as effectiveness increases [2]. Increasing effectiveness has several advantages which can be shown graphically in the next plot.

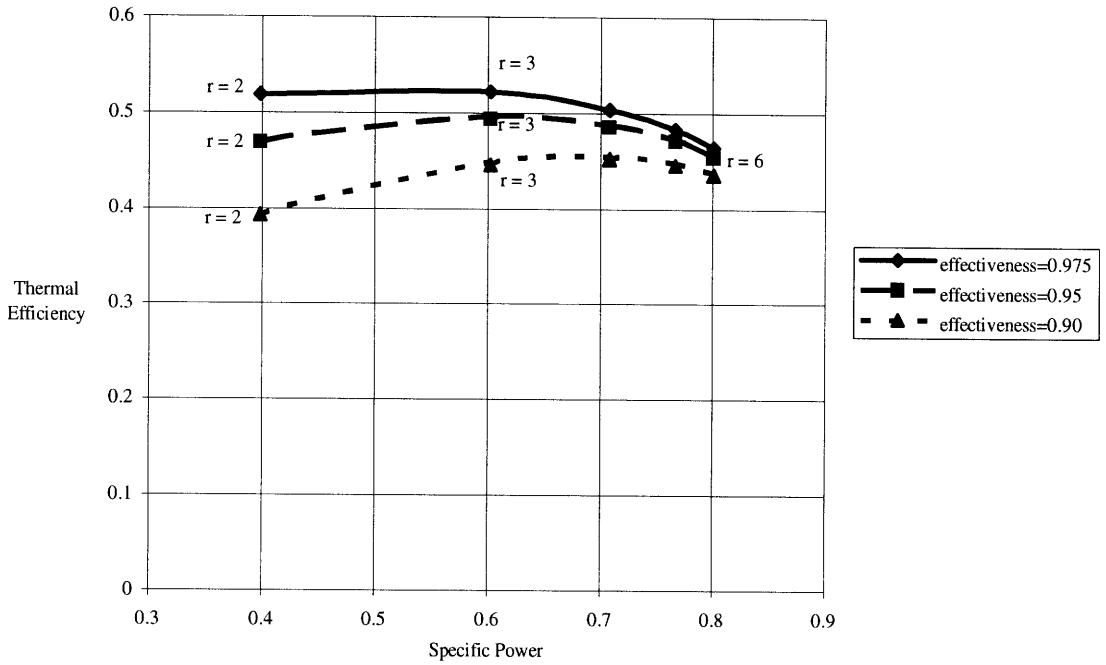

Figure 1.4 Consequence of changing regenerator effectiveness on thermal efficiency and specific power for a fixed turbine-inlet temperature.

Thus, when effectiveness increases, thermal efficiency increases (by a greater factor at pressure ratios), and the optimum compressor pressure ratio is decreased. Therefore, high-effectiveness regenerators are quite desirable.

Pressure Drop

A pressure drop occurs as the fluid flows through a regenerator and its ducting because of fluid friction. The larger the pressure drop, the more power required to move the fluid. The pressure drop can be controlled by changing the fluid velocities and the regenerator-passage areas. Other components of the gas turbine have pressure losses such as the combustor. The total pressure drop over a cycle is the sum of all component pressure drops and will influence the thermal efficiency as shown in the next figure.

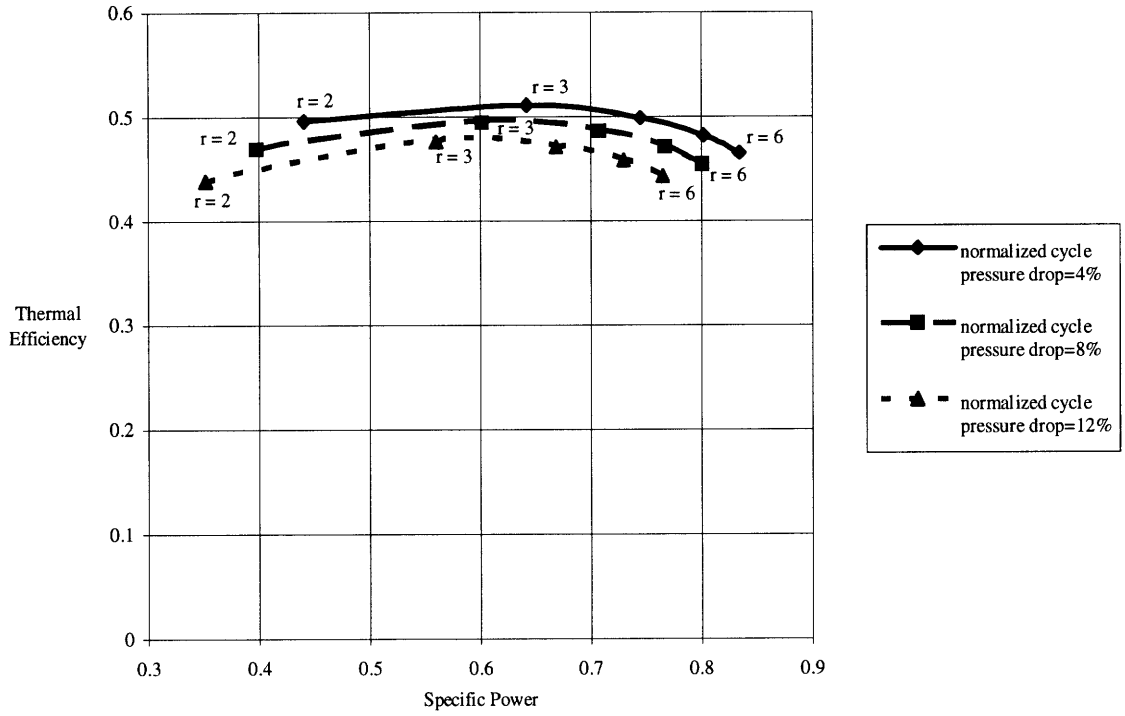

Figure 1.5 Consequence of changing cycle pressure drop on thermal efficiency and specific power for a fixed turbine-inlet temperature.

As the cycle pressure drop increases, the thermal efficiency and specific power decreases for a given pressure ratio. More power is required to overcome the pressure drop resulting in less power output and thus, a lower thermal efficiency. Since the regenerator pressure drops contribute to the cycle pressure drop, they should be kept low.

Leakage

A problem with regenerators is the leakage of compressed air along the seals. Some 4-14 percent of the compressor mass flow escapes for typical regenerator designs [2]. A high leakage rate has detrimental effects on gas-turbine performance as illustrated in the following figure.

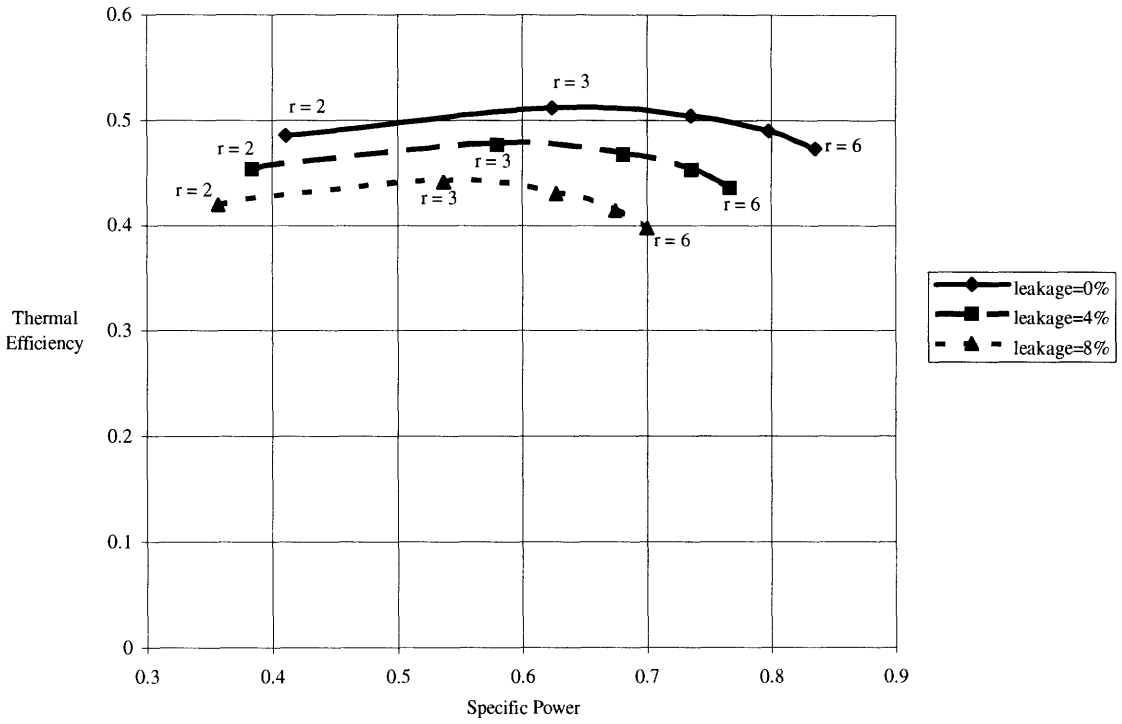

Figure 1.6 Consequence of changing regenerator seal leakage on thermal efficiency and specific power for a fixed turbine-inlet temperature.

As the leakage increases, drops in both thermal efficiency and specific power occur. As the compressor pressure ratio increases, leakage rates increase and reductions in thermal efficiency and specific power are more evident. Thus, the seal leakage should be reduced as much as possible to minimize such performance drops. Unlike effectiveness and pressure drop, leakage rates cannot easily be adjusted by changing some design parameters since much of the leakage is inherent to the design. This was the motivation in developing the modular regenerator.

1.2.2 Regenerator Concepts

The regenerators described in this section are termed periodic-flow heat exchangers because they consist of a heat-transfer surface (ceramic material containing small passages in a honeycomb arrangement called a matrix) that is periodically transferred

from the cold compressed-air flow to the hot exhaust flow. On the hot side, heat is transferred from the exhaust gases to the ceramic material as it flows through the passages. On the cold side, heat is transferred from the matrix material to the compressed-air flow.

1.2.2.1 Rotary Regenerators

Typical gas-turbine regenerators are rotary types which consist of a ceramic matrix disk. The hot exhaust flows through part of the disk and the cold compressed air flows through the rest in the opposite direction. This is shown in the following figure taken from Bathie [3]. The disk is rotated such that the hot portion is then exposed to the cold side and vice versa. Despite using a matrix with small passages, the passage blockage from exhaust particles is usually not a problem since the flow directions are reversed between the two streams. So any exhaust contaminants stuck in a passage are pushed out as the passage moves to the cold side. These particles then are burned up in the combustion chamber.

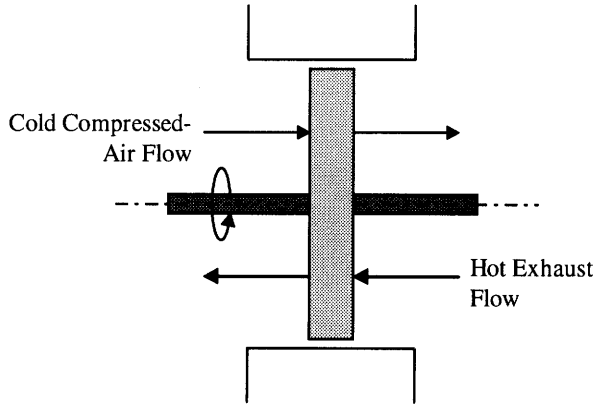

Figure 1.7 Cross-sectional view of a rotary regenerator.

1.2.2.1.1 Continuous-Rotation Regenerators

Continuous-rotation regenerators rotate at a constant rate to give a desired temperature distribution within the matrix. Face seals exist on both sides of the disk along the inner and outer circumference and along two radii to separate the compressed-air flow, exhaust-gas flow, and the surrounding atmosphere. The seals are pressed upon the matrix to minimized the leakage. As the disk rotates over time, the seals and matrix wear down which normally results in higher leakage rates. Current designs have yet to maintain seal leakage at acceptable levels over time.

1.2.2.1.2 Discontinuous-Rotation Regenerators

In addition to the patent for the modular regenerator, Wilson and MIT [1] have patented a sealing concept that reduces the seal leakage associated with rotary regenerators. This concept consists of rotating the matrix disk discontinuously. The face seals lift up by a small distance during matrix rotation over a finite angle (such as 30 degrees), then clamp down until the next rotation. This provides essentially zero leakage between rotations. The net result is a significant reduction in leakage and seal wear. Discontinuous-rotating regenerators have been investigated by Beck [4] and Pfahnl [5].

1.2.2.2 Modular Regenerators

This section gives the rationale made by Wilson [6] on how the modular-regenerator concept was conceived. Rotary concepts have long sealing distances (transverse length of the seals along the periphery of the high-pressure side). Reducing the sealing distance will reduce the leakage. Most of the leakage occurs over the radial seals. The radial sealing distance can be reduced by increasing the inner radius of the disk forming an annular matrix. The seals can then be relocated to encompass the cross-sectional area of the matrix, thus reducing the sealing distances considerably. The relocated seals are illustrated in the figure below.

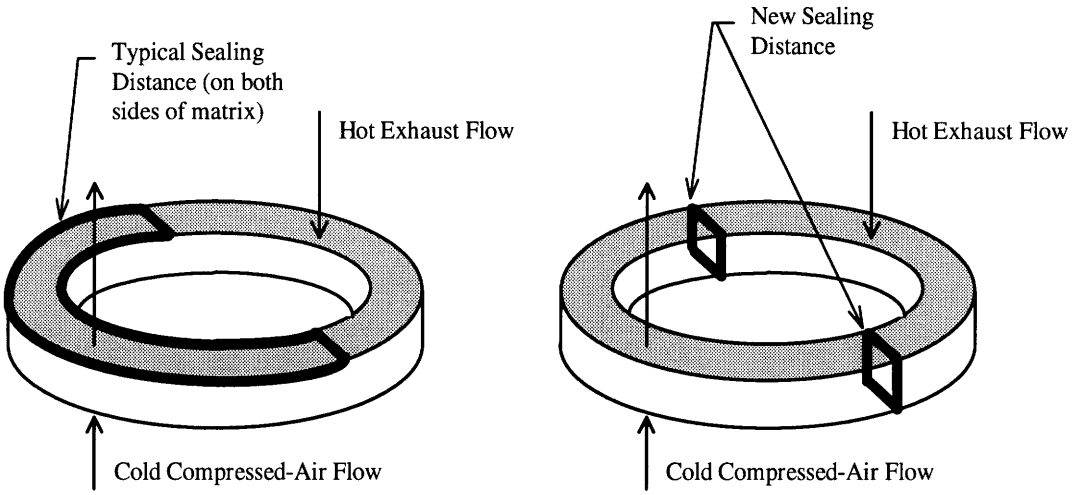

Figure 1.8 Relocation of sealing distances for an annular matrix.

Then the matrix can be broken up into smaller segments (called modules) and straightened to form blocks with rectangular flow passages as shown in the next figure. The modules are moved linearly within the passages such that modules exposed to one flow are moved to the other exposed area. A space of at least the volume of one module is needed to allow movement. In addition, the two exposed areas could be separated further than as shown below to eliminate any special ducting of the flow. The modular concept is also self-cleaning since the flow directions are reversed. Furthermore, removal of modules (that are not located within the exposed areas) from the regenerator for periodic maintenance or replacement is possible. This can be performed during regenerator operation which is not feasible with any other regenerator concepts.

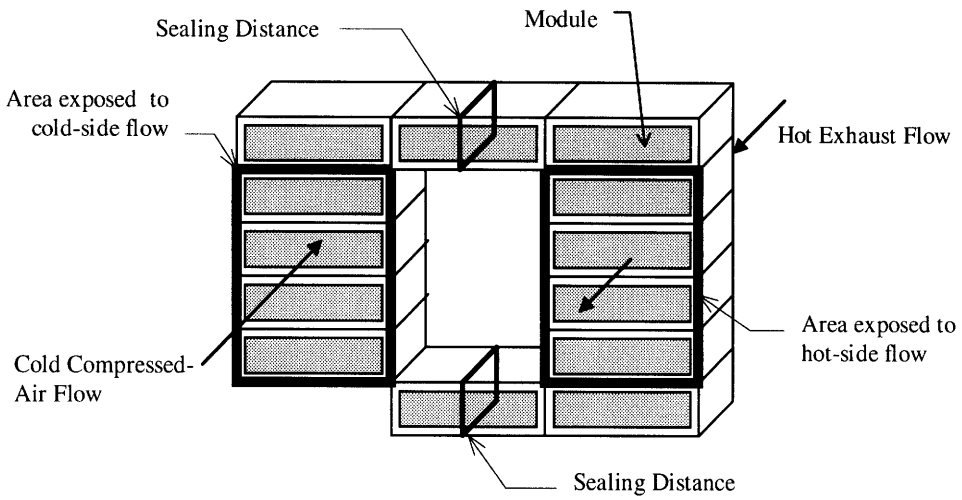

Figure 1.9 General arrangement of a modular regenerator.

Since the total sealing distance has dramatically decreased, the seal leakage should be much lower than conventional rotary types. The major consequence in making the transition to the modular case is an increase in mechanical complexity. Several devices, such as linear actuators, will be required for module movement.

1.2.2.3 Other Types

Other regenerator concepts exist but are not as commonly used. One example is the rotating drum which consists of the matrix in a cylindrical configuration, where the matrix is rotated along the cylinder axis. A cross section of a drum regenerator is shown below taken from Bathie [3]. Another regenerator type is the valved regenerator. This concept has a stationary matrix with valves that allow the matrix to be exposed to each stream periodically. Since these concepts are not as prevalent, they are not included in any comparative studies with modular designs.

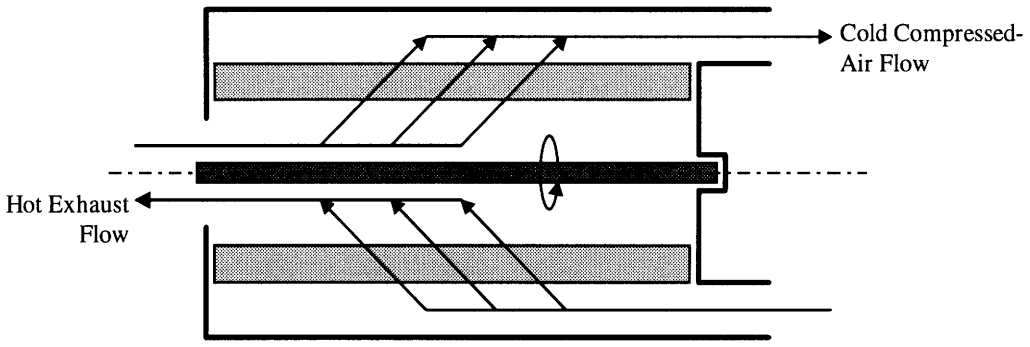

Figure 1.10 Cross-sectional view of a drum regenerator.

1.3 Regenerator Applications

1.3.1 Rotary

Rotary regenerators have been designed primarily for vehicular applications. The regenerator allows the gas-turbine to have high thermal efficiency at full and part load which is required for vehicular use. Many of the larger automobile manufacturers have developed experimental vehicles with regenerative gas-turbine engines in the past 30 years.

The size of the monolithic ceramic matrix disk is limited to a diameter of 1 m due to manufacturing and thermal-stress constraints [6]. Therefore, applications to larger gas-turbine engines are not generally possible.

1.3.2 Modular

Breaking up the matrix into modules allows the exposed flow areas to have virtually unlimited size. If a larger area is needed, the designer can just add more modules. In addition, two separate modular regenerators could be used when larger heat-transfer areas are required. This makes modular regenerators suitable for ground-based gas

turbines used in industrial power-generation units. Furthermore, the modular concept could be used in exhausted-heated cycles to burn coal, wood, and refused-derived fuels as proposed by Wilson [7]. These cycles burn "dirty" fuels in which combustion products can clog the matrix passages despite the inherent self cleaning of the matrix. Having the capability to replace the modules for cleaning during continuous engine operation makes the modular case attractive.

When competing with rotary applications, a modular regenerator's size might preclude their use on some small gas-turbine vehicles. The overall dimensions will be considerable greater than rotary designs due to the open space between the two sides. The size might be too large to fit in a vehicle's engine compartment. Furthermore, additional analysis is needed show that module movement can withstand the vehicular environment.

Finally, Wilson states that regenerator designs would require very low leakage at pressure ratios of 8:1 for aircraft-engine applications [6]. Rotary concepts have been unsuccessful thus far to provide this, but modular concepts (and discontinuous-rotation concepts) might be able to achieve such performance.

1.4 Conventions and Terminology

The following are some conventions and terms used throughout this study:

- The fluid flowing through stations 1 to 3 is called "air" since it is just the ambient air undergoing compression and heat addition. The fluid flowing through stations 3 to 6 is called a "gas" since it contains air, unburned fuel, and combustion products.
- The compressed air travels through the regenerator from station 2 to 3. This is called the cold or high-pressure side.
- The exhaust gas travels through the regenerator from station 5 to 6. This is called the hot or low-pressure side.

- The terms "core", "matrix", and "core matrix" are used interchangeably to represent the ceramic-honeycomb matrix material.
- When assigning dimensions to regenerator objects in 2-D, generally, the terms "length" and "width" refer to the longer and shorter dimensions respectively. There is one exception to this convention. This occurs when defining the channel areas in Section 4.2.2.3.
- For all modular configurations, the cold side is located on the left with the flow going into the paper, and the hot side is on the right with the flow going out of the paper. The seals are located between the two sides.
- Module movement occurs in a clockwise direction.
- Sealing distance refers to the transverse length of the seal where leakage can occur. Seal length refers to the longitudinal length of the seal in the direction of leakage flow. This is not a standard nomenclature convention when describing regenerator seals. Typically, "sealing distance" is referred as "sealing length." The convention used is made to eliminate any possible confusion between the two seal parameters.

1.5 Summary

Modular regenerators should provide less leakage than other designs due to a large reduction in sealing distance. Nevertheless, this type of heat-exchanger is more mechanically complex since several devices are needed to move the modules. By separating the matrix into rectangular entities, the range of regenerator applications is increased because larger matrix sizes are conceivable. The following chapters are devoted for additional design descriptions along with design and performance calculations.

2. Modular Regenerators

2.1 Introduction

The section presents the various modular concepts. Basically, two different types exist. Both concepts are similar except in the type of sealing technique used. The first concept has a module acting as the seal. The second uses partitions to seal off the compressed air.

2.2 Modular Concepts

2.2.1 Module-Seal Concept

The module-seal concept consists of separating the hot and cold sides with two rectangular passages containing seals that are surrounding the modules located within these passages. This passage area is called the seal section. The modules must always be present in the seal section to seal off the high-pressure air. The following figure illustrates

the general layout. This concept provides the simplest modular configuration from a mechanical standpoint.

With the short sealing distances and the long seal length, this option should provide very low leakage. The seal length could be increased as shown in Figure 2.2. Increasing the seal length could also reduce any special ducting of the flow. Consequently, as the seal length gets larger, the time for a module to travel from one side to the other will increase (if the speed of the modules remains constant). This may cause a reduction in effectiveness due to heat conduction within the matrix material. Such effects are analyzed in Chapter 5.

The large pressure forces must be accounted for on the modules located within the seal section. These forces push the modules toward the low-pressure side. This will be advantageous for modules traveling in the direction of the pressure force; however, these forces must be overcome when modules are traveling towards the high-pressure side. Several mechanisms could be used to move the modules through the seal section and within the hot and cold sides. Detailed techniques on the methods chosen for module movement are described in Section 4.2.

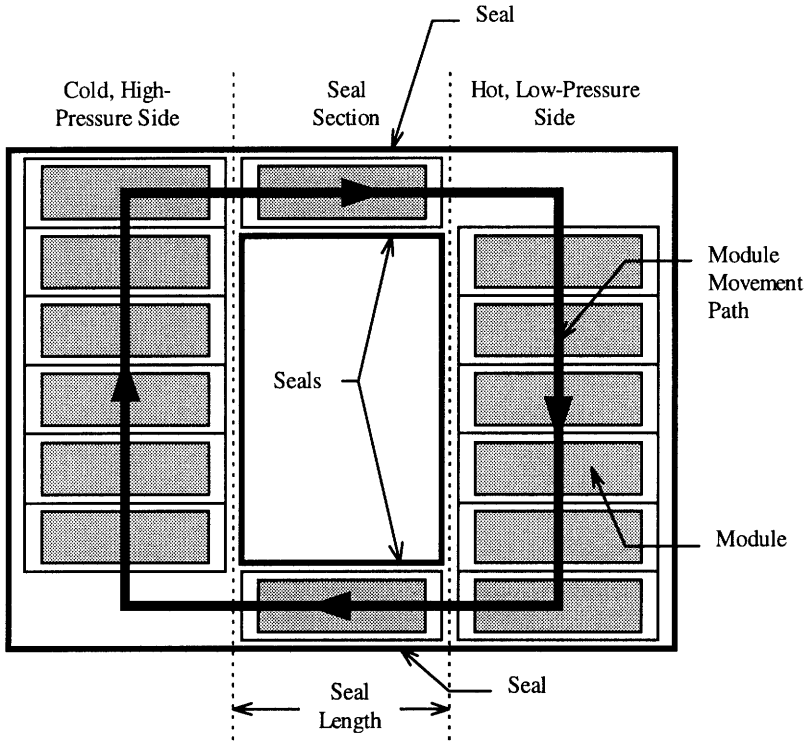

Figure 2.1 General layout of the module-seal concept with a seal length of one module.

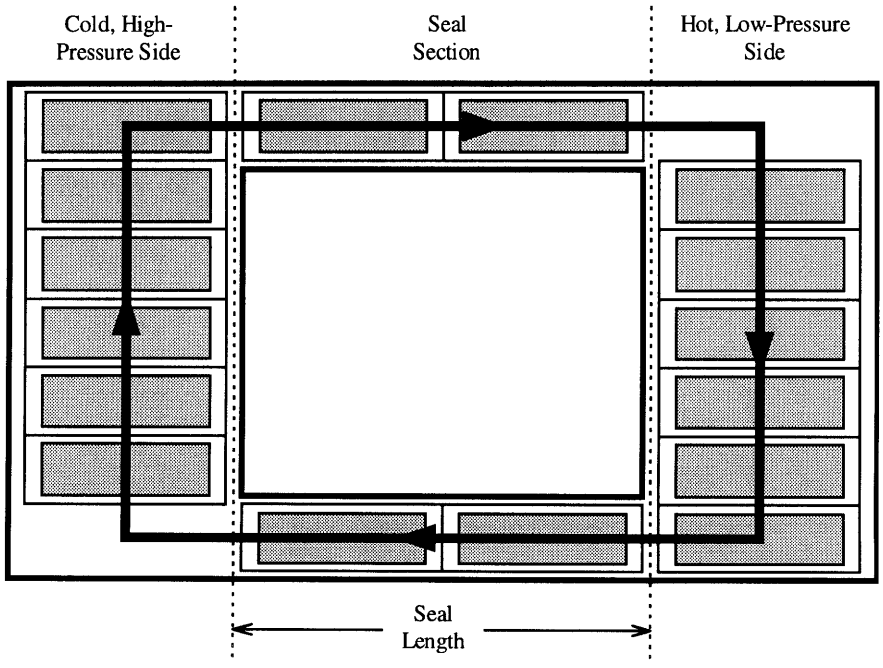

Figure 2.2 Module-seal concept with a seal length of two modules.

2.2.2 Gate-Seal Concept

Wilson's first proposal for sealing the modules in the regenerator was to partition the hot side, cold side, and seal section using gate-seal doors (also called gate valves) [1]. These doors open and close to allow module movement. This concept is termed the gate-seal concept. The basic layout has the seal section containing two chambers with gate-seal doors on either side. The general arrangement is shown in the next figure. Module movement through a seal section occurs when one of the two gate-seal doors opens for each chamber, thus letting modules in and out. This movement scheme is described in more detail in Section 4.3.

For this concept, the leakage consists of the transfer of compressed air when the door opens to the low-pressure side. This differs for each chamber where the upper chamber has less leakage than the lower chamber. This occurs because the upper-chamber door on the right opens to move a module out of the chamber to the low-pressure side, and the lower-chamber right door opens to let a module enter. Thus, part of the upper chamber's volume is occupied by a module, and the rest is air that is transferred as leakage. For the other chamber, it is empty as the right door opens, therefore, the entire volume of air within the chamber is transferred as leakage.

Mechanisms are require to move the modules within the hot and cold sides and in and out of each chamber. This concept will probably require more mechanisms than the module-seal concept because more steps are made during module movement (with the addition of the gate-seal doors). Furthermore, like the module-seal concept, the gate-seal regenerators can have a longer seal section by adding more chambers as shown in Figure 2.4.

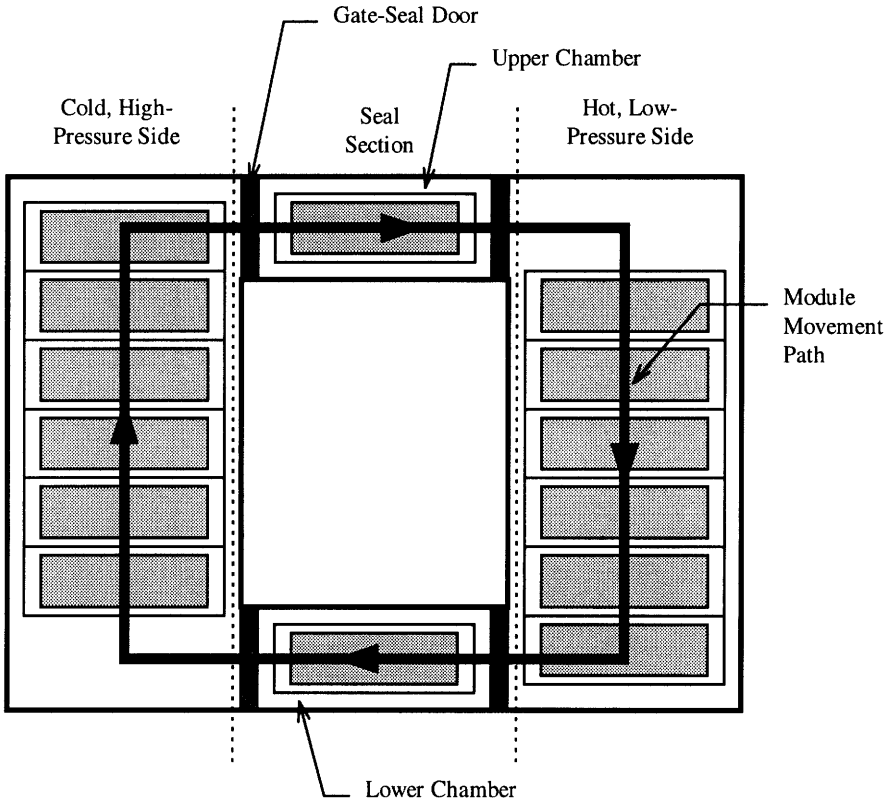

Figure 2.3 General layout of the gate-seal concept with a chamber length of one module length.

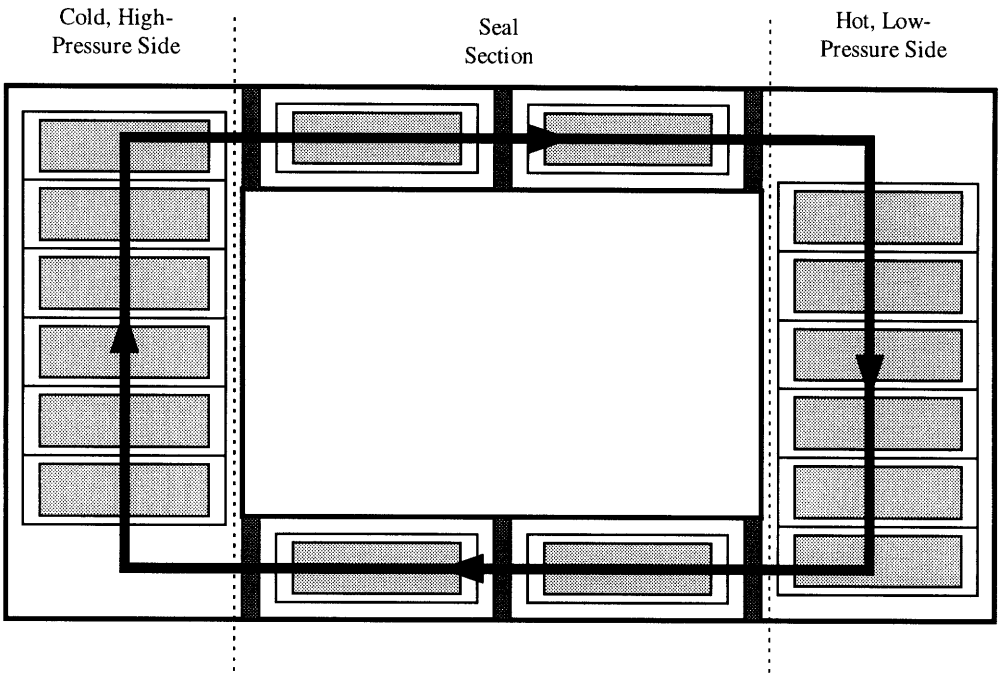

Figure 2.4 Gate-seal concept with a chamber length of two module lengths.

2.3 Summary and Conclusions

Two modular concepts were presented: the module-seal concept and the gate-seal concept. These concepts reduce the sealing distances for leakage reduction. The module-seal concept is the simplest concept and should require the least amount of module-movement devices. Since modular regenerators have additional mechanical complexity than rotary regenerators, a logical step is to design a modular regenerator with the least complex concept. Therefore, the majority of the mechanical design and analysis will focus on the module-seal concept.

3. Module/Matrix Design

3.1 Introduction

One major aspect of designing a modular regenerator is the design of the ceramic module. Modules have yet to be manufactured but current ceramic technology should be sufficient for preliminary development. Corning Incorporated is currently developing ceramic matrices for gas-turbine regenerators under the Automotive Turbine Technology Applications Project (ATTAP), sponsored by the U.S. Department of Energy. Fortunately, much of their work has direct applications for module development. This section will discuss Corning's research, its applications for module development, and other aspects required for module design.

3.2 Regenerator Development at Corning

3.2.1 Summary of Research

Corning Incorporated is currently conducting research with Allison Engine Company to develop a cost-effective process for the manufacture of ceramic rotary regenerators. Their investigation concerns the development of ceramic matrix materials that are low in cost and provide adequate temperature capability, chemical durability, dimensional stability, thermal shock, stress resistance, leakage from material porosity, and strength [8].

Corning has determined that one way to reduce cost is to use extrusion as the manufacturing process. The earlier method for fabricating regenerator cores is by wrapping thin paper coated with lithium-aluminosilicate (LAS) material in a coil, a very expensive process. This technique was used on the first glass-ceramic gas-turbine regenerators in the 1960s. The process consists of applying glass and ceramic binders to two sheets of tea-bag paper. One sheet is crimped to form a sinusoidal shape and the other remains flat. The two sheets are joined and then wrapped in a spiral to form a core matrix with near-triangular passages. Then the matrix is fired and machined to become the final product. On the other hand, extrusion consists of forcing the ceramic material through dies. Afterwards, it is fired and machined. This process is considerable less expensive because Corning has been manufacturing millions of automotive catalyst supports using extrusion for the past twenty years [9].

The candidate materials first consisted of LAS, aluminosilicate (AS), magnesium-aluminosilicate (MAS), mullite-aluminum titanate (MAT), and sodium-zirconium phosphates (NZP). MAT was dropped from the project based on initial assessments. NZP was also dropped because of extremely high cost [9]. LAS, the standard regenerator material, has been plagued with chemical durability problems in the past, and is relatively high in cost. AS, a derivative of LAS, was developed to ameliorate the LAS chemical

problems by refiring the material to remove the hydrogen. This additional process makes AS production more expensive than LAS. MAS materials, generally known as cordierite, is the least expensive since this material was developed for use in catalyst supports. Recently, Corning has settled on two compositions, LAS and MAS. LAS's main problem now is high cost. MAS materials that have been developed show promise in all areas except maintaining strength under thermal cycling [8]. Corning is currently testing MAS cores at Allison and investigating ways to improve the MAS strength and reduce the LAS cost.

The other aspect of Corning's work concerns extrusion-die development. Corning has been able to extrude ceramics at 170 rectangular cells per square centimeter with a diameter of 0.27 m [8]. This falls short of their 0.3 m goal, and further research is ongoing.

Work on this project will probably continue until a material developed meets all design requirements. Cordierite (MAS) appears headed towards satisfying the requirements mainly because its hurdles are easier to overcome.

3.2.2 Applications for Module Development

Since the modules are rectangular in shape, manufacturing rectangular matrices by extrusion will obviously be a better (and cheaper) process. Therefore, the results of Corning's research should be directly applicable toward module design. Additional work will be required in developing a die for rectangular extrusions since Corning is making only circular dies. Considering the size of current dies, rectangular extrusions will probably be no larger that 0.3 m square in cross section [10].

3.3 Matrix Construction and Design

3.3.1 Matrix Materials

Based on Corning's research, extruded cordierite will be the preferred material in this design study. Even though cordierite has not met all of Corning's requirements, current compositions should be satisfactory for module prototypes.

A typical module is shown in the next figure (matrix passages are not to scale). Notice that core matrix is surrounded by a solid rim. This gives protection to the core during module transit. The rim material should probably be composed of the same material as the matrix to avoid potential thermal-expansion problems. Nevertheless, the potential exists to use other rim materials such as metals, alloys, or composites (neglecting current temperature limitations) that have quite different thermal-expansion properties. Such possibilities exist by using a mat mount along the core/rim interface. Mat mounts such as the Carborundum Company's Expanding Paper is a material used in catalytic converters to support ceramic monoliths within steel frames. The current drawback is the limited maximum operating temperature of 800°C. If temperatures exceed 800°C, then thermal degradation of the material occurs [11]. Therefore, further development is required to use mat mounts with modular-regenerator applications.

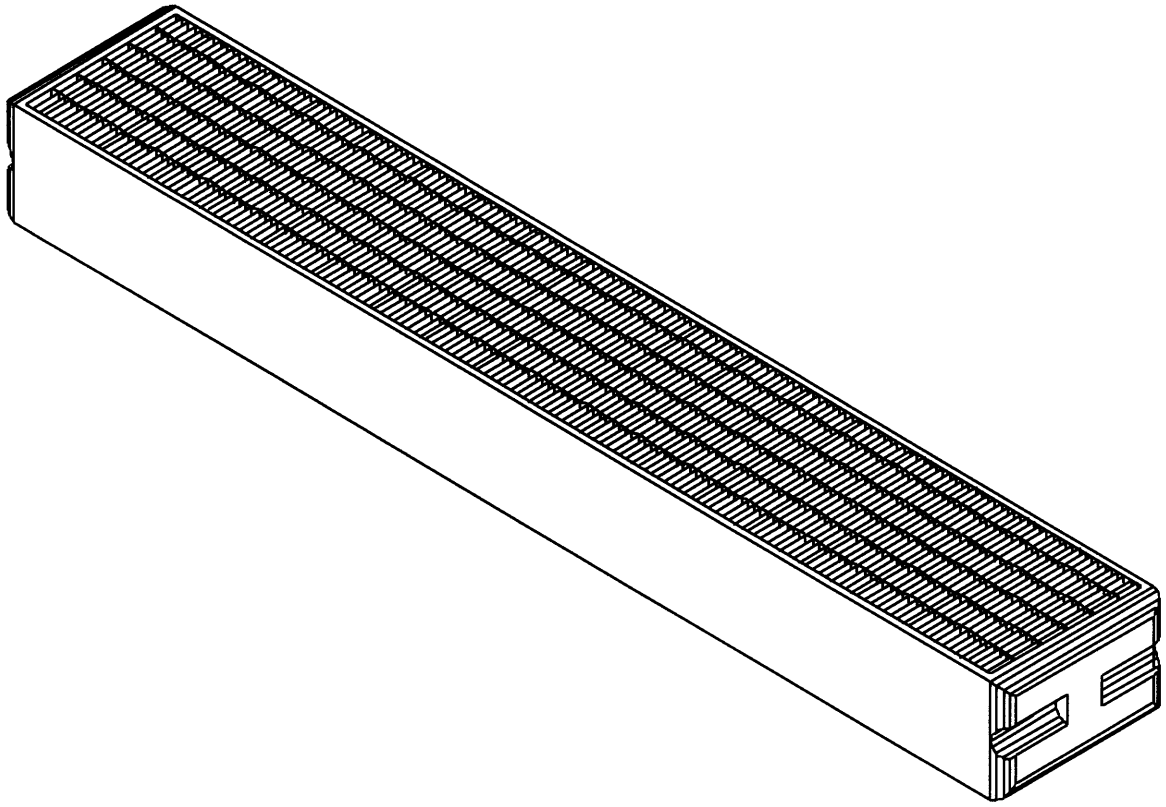

Figure 3.1 Representation of a typical ceramic module.

3.3.2 Matrix/Rim Integration

From the design results of Chapter 5, typical modules for a small gas-turbine engine will have dimensions around 0.75 m by 0.1 m. If the maximum size limit for an extruded ceramic matrix is 0.3 m square, several matrices will have to be mated to each other to form a complete module. Furthermore, these matrices will have to be integrated with the module rims. A cement will be needed at all matrix/matrix and matrix/rim interfaces. The cement will have to maintain its bonding strength under the intense thermal environment of the regenerator. This analysis does not address this issue and is left for future work. A diagram showing the typical individual parts of a module is given below. The rim is composed of 4 parts (one for each module face) and the core is made up of 3 separate matrix blocks.

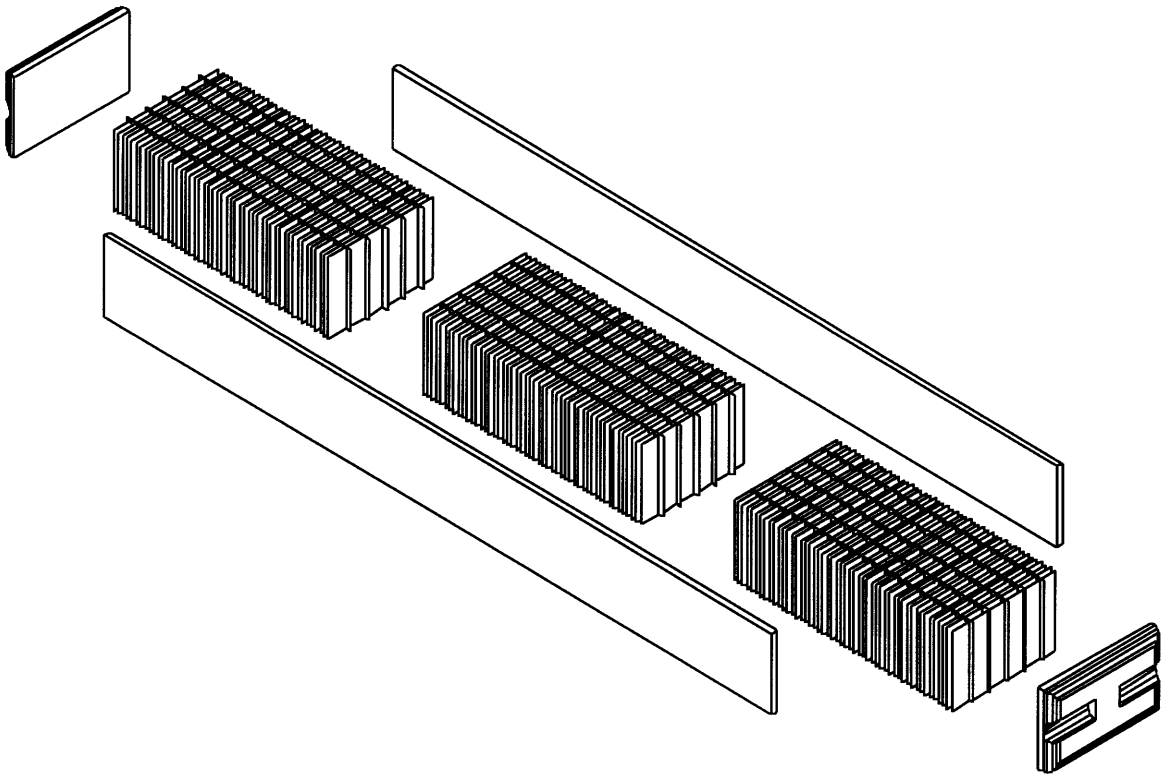

Figure 3.2 Representation of typical rim and matrix components that comprise a ceramic module (matrix passages are not to scale).

3.3.3 Matrix Passage Geometry

When designing the module, selecting the type of matrix passage geometry is critical since this can dictate the performance of the regenerator. When comparing the Nusselt numbers for various passage geometries for laminar flow, rectangular passages have the highest value. The Nusselt number is a non-dimensional heat-transfer coefficient; therefore, a rectangular geometry appears to be favorable choice. Furthermore, Hagler [12] concluded that the rectangular passages offer the best heat-transfer performance and recommended using such a geometry. Therefore, a rectangular geometry is preferred and will be used throughout this design study.

The Nusselt number also increases as the passage aspect ratio so one would infer on using a high aspect ratio. The following will show that a higher aspect ratio does

correlate to better heat-transfer performance for rectangular passages. This analysis assumes that only the passage aspect ratio is varied and all other parameters are held constant.

The passage aspect ratio is defined as

$$AR_{pass} \equiv \frac{l_{pass}}{w_{pass}} \tag{3.1}$$

where l_{pass} is the greater passage distance. The matrix dimensions are shown graphically in the next figure.

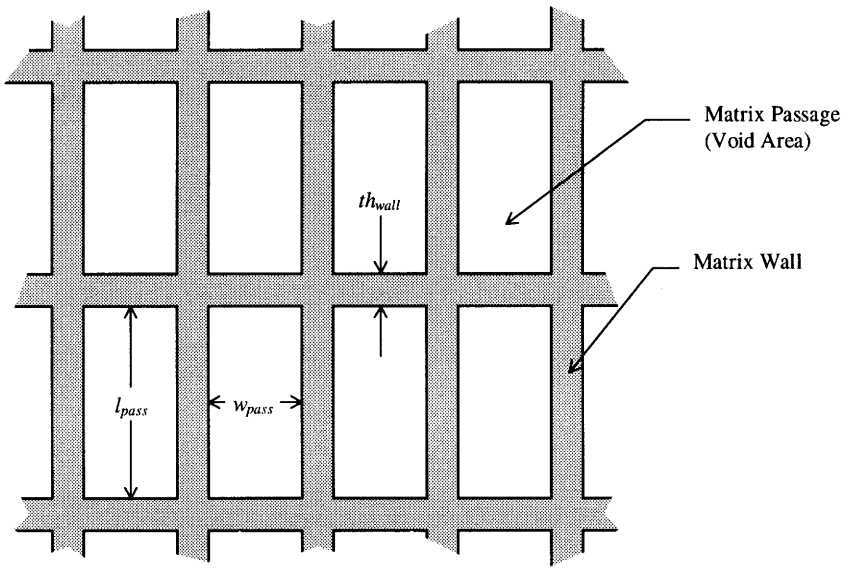

Figure 3.3 Ceramic matrix with rectangular passages with relevant dimensions.

Another parameter required when defining the geometry is the hydraulic diameter, d_h, defined as

$$d_h \equiv \frac{4(\text{cross sectional area})}{\text{periphery}} \tag{3.2}.$$

For rectangular passages, the hydraulic diameter can be rewritten as

$$d_h = \frac{4 w_{pass} l_{pass}}{2\left(w_{pass} + l_{pass}\right)} = \frac{2 AR_{pass} w_{pass}}{1 + AR_{pass}} \tag{3.3}.$$

The passage width and length can be expressed by combining the equations for hydraulic diameter and passage aspect ratio:

$$w_{pass} = \frac{\left(1 + AR_{pass}\right) d_h}{2 AR_{pass}} \tag{3.4}$$

$$l_{pass} = \frac{\left(1 + AR_{pass}\right) d_h}{2} \tag{3.5}.$$

The heat-transfer area, A_h, is the matrix surface area available for heat transfer which is

$$A_h = 2\left(w_{pass} + l_{pass}\right) th_{mat}\, Z \tag{3.6},$$

where th_{mod} is the passage length in the direction of the flow (module/matrix thickness) and Z is the number of passages. Plugging in the equations for the passage length and width simplifies to

$$A_h = \frac{\left(1 + AR_{pass}\right)^2 d_h\, th_{mat}\, Z}{AR_{pass}} \tag{3.7}.$$

Porosity is a measure of how open the passages are in relation to the matrix. Porosity is defined by

$$\Psi_{mat} \equiv \frac{\text{total void area}}{\text{total void area} + \text{total solid area}} \tag{3.8}$$

and can also can be written as

$$\Psi_{mat} = \frac{A_{ff}}{A_f} \tag{3.9},$$

where A_{ff} is the free face area (void area) and A_f is the face area (void + solid area).
The free face area can be expressed as

$$A_{ff} = w_{pass}\, l_{pass}\, Z \tag{3.10}.$$

Substituting in equations (3.4), (3.5), and (3.10) into equation (3.9) and solving for the face area gives

$$A_f = \frac{\left(1 + AR_{pass}\right)^2 d_h{}^2\, Z}{4\, AR_{pass}\, \Psi_{mat}} \tag{3.11}.$$

The Nusselt is the dimensionless temperature gradient at the surface defined as

$$Nu = \frac{h_t\, d_h}{k} \tag{3.12},$$

where h_t is the heat-transfer coefficient and k the thermal conductivity.
Now, the heat transfer per volume can be expressed as

$$\frac{\dot{Q}}{V} = \frac{h_t\, A_h\, \Delta T}{A_f\, th_{mod}} \tag{3.13},$$

where ΔT is the temperature difference.
Substituting in the equations for heat-transfer area, face area, and heat-transfer coefficient (from the Nusselt equation) reduces to

$$\frac{\dot{Q}}{V} = \frac{4\, Nu\, k\, \Delta T\, \Psi_{mat}}{d_h{}^2} \tag{3.14}$$

If the thermal conductivity, temperature difference, porosity, and hydraulic diameter are all held constant, they can be placed on the left hand side as shown:

$$\left(\frac{\dot{Q}}{V} \frac{d_h^{\,2}}{4\,k\,\Delta T\,\Psi_{mat}} \right) = Nu \tag{3.15}$$

Therefore, the heat transfer per unit volume is a function only of Nusselt number. Since *Nu* increases with passage aspect ratio, higher aspect ratios will give better heat-transfer performance. In Chapter 5, the passage aspect ratio will be varied to understand its influence on other regenerator parameters.

3.4 Summary

This section presented a summary of Corning's research for the development of low-cost extruded matrix cores. The results can be carried over to module design. Based on Corning's current findings, the module-core material chosen for this study consists of cordierite (MAS) material. Several core blocks will constitute one module with a solid ceramic rim along the perimeter. The matrix passages used for the design are rectangular since this offers the best heat-transfer performance.

4. Configuration and Mechanical Design

4.1 Introduction

This section will describe in detail the modular-regenerator configuration and mechanical design. The majority of the work in this chapter is devoted to the module-seal concept since this type of regenerator is preferred based on conclusions drawn from Chapter 2. Some of the sections contain design drawings to illustrate the configuration and mechanical concepts for a possible regenerator prototype.

First, the overall regenerator configuration is described. Then, module movement is discussed including the descriptions of specific movement scenarios. Several movement options are considered and recommendations are given. Afterwards, a discussion is made to address the mechanisms used to provide module movement. Then, other specific aspects pertaining to the mechanical design and layout are presented including the seals and module replacement. Finally, mechanical aspects associated with the gate-seal concept are briefly discussed.

4.2 Module-Seal Concept

4.2.1 Overall Configuration

This section provides the design drawings showing the overall configuration of a possible regenerator prototype. Specific discussions of the configuration are made in subsequent sections. The design drawings use pneumatic/hydraulic cylinders for module movement, but they do not include the supporting structure and equipment for the cylinders. In addition, the regenerator headers are not included. The drawings were made to give the reader a general view of the overall regenerator size and layout. These drawings reflect the final design results given in Chapter 5 but some items were not drawn to scale for clarity. For example, the matrix surface is not to scale since the passages are quite small and would appear as a solid surface from a distance.

The first figure displays the overall structure showing the exposed matrix areas. Figure 4.2 has the casing covers removed to show the internal structure and module organization. The casing structure is shown in Figure 4.3. Notice that the casing sides consist of a double-walled support structure. This was incorporated to withstand the cold-side pressure loading on the casing walls. The hot side does not require this double-walled support since its internal pressure is near atmospheric. The casing has the double-walled support on both sides to give it symmetry for proper weight distribution and manufacturing ease.

Further analysis will be required for casing design such as selecting the material composition. Candidate materials should provide limited thermal expansions within the seal section to give adequate seal clearances to allow module movement, since clearances could be as small as 0.1 mm.

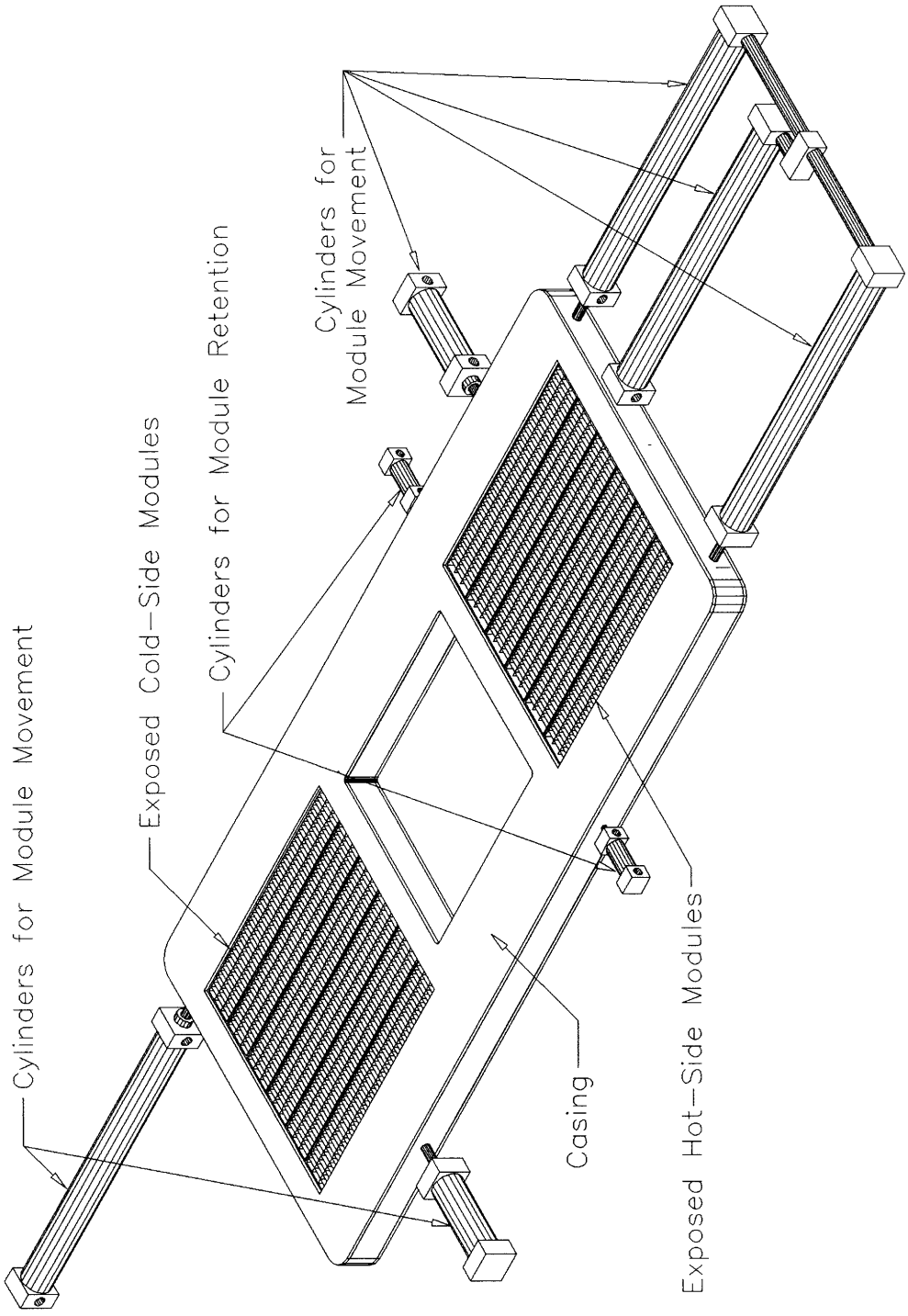

Figure 4.1 Design drawing of overall configuration.

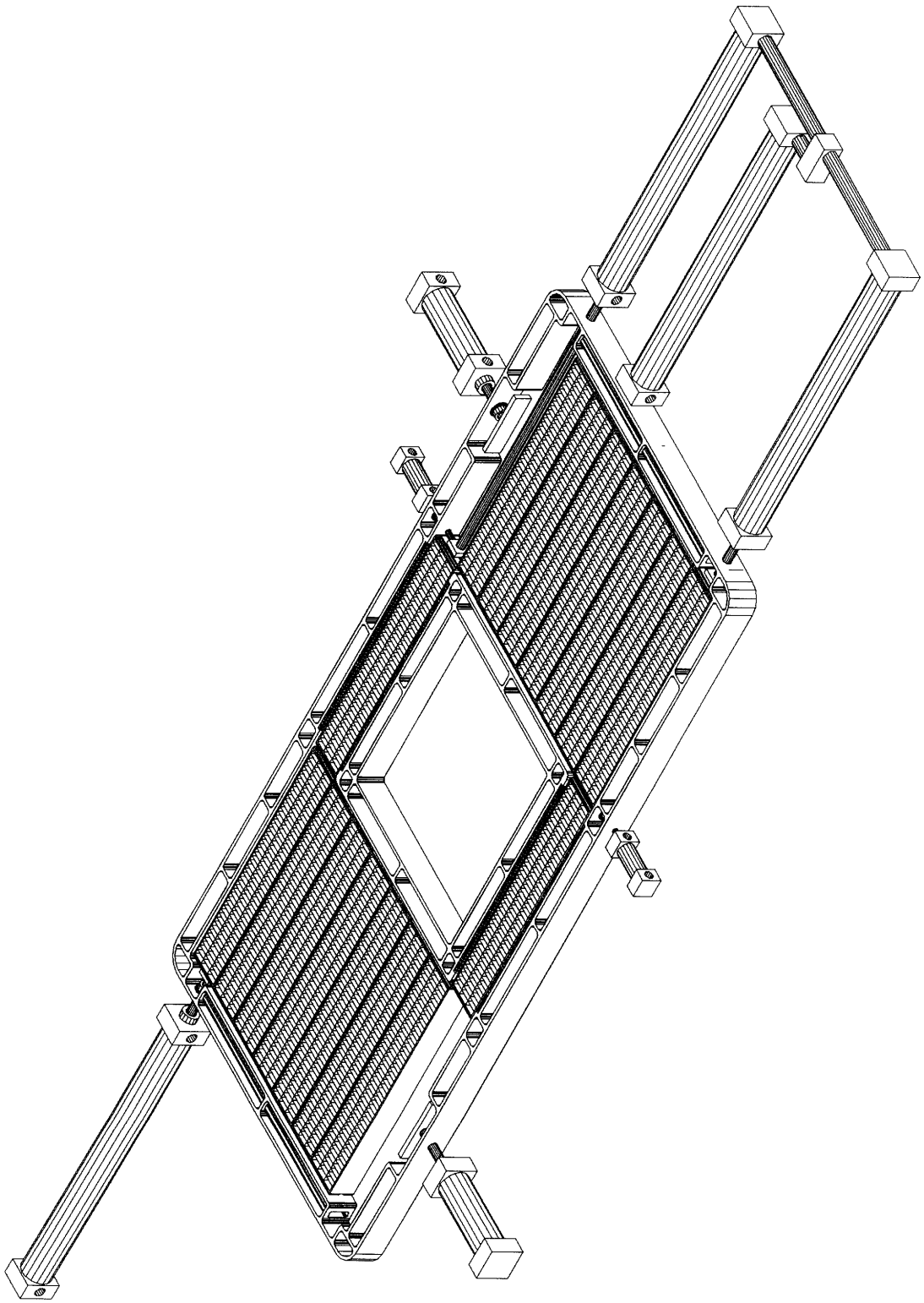

Figure 4.2 Design drawing of overall configuration without casing cover.

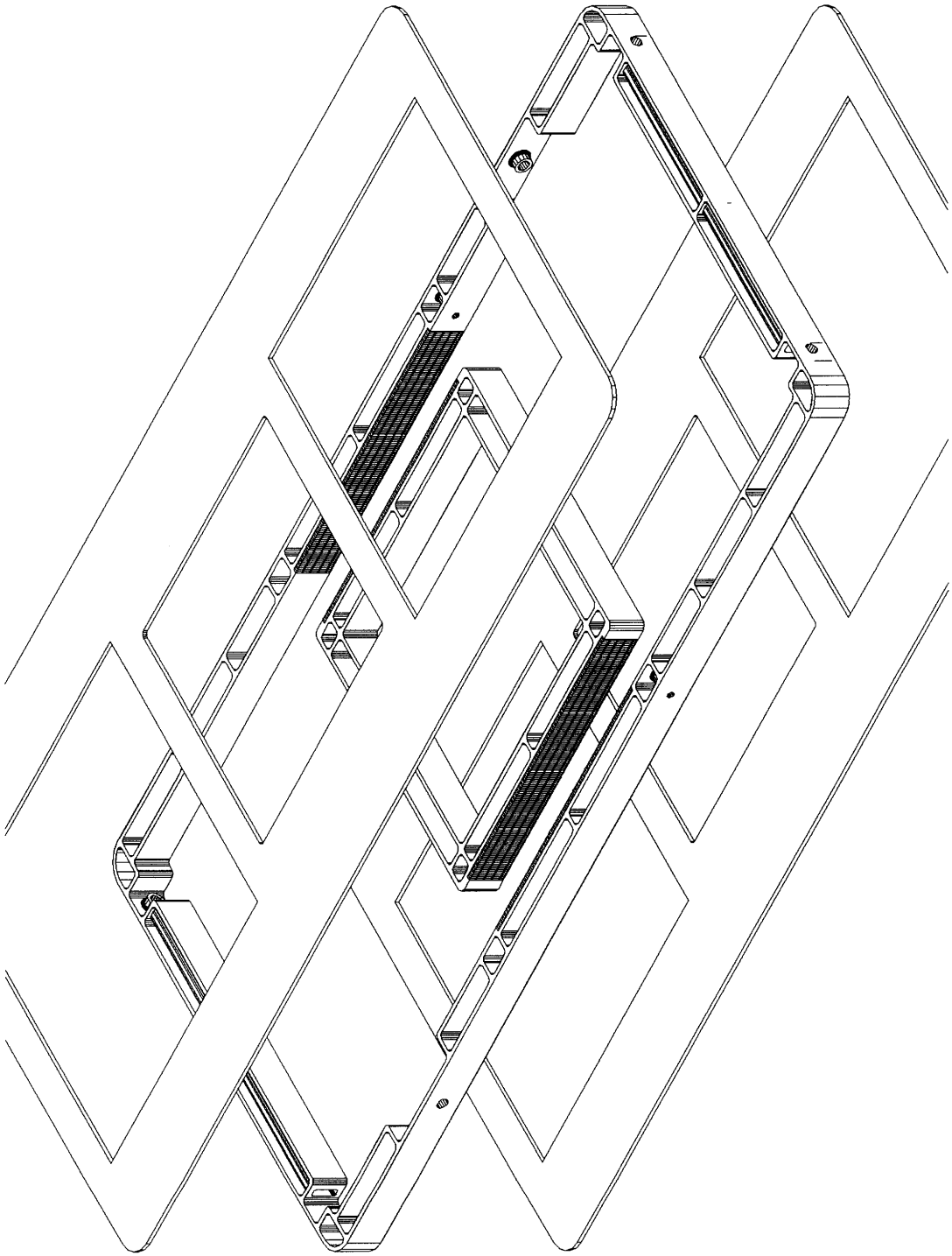

Figure 4.3 Design drawing of regenerator casing including the covers.

4.2.2 General Module Movement

Module movement from one module location to an adjacent one is performed in steps. Open spaces, called module voids, are needed to allow movement. When modules move into a void, the void obviously disappears, but a new void is created behind the last trailing module. The figure below depicts this with an example of module movement on the cold side. After this step, another set of modules (from the seal section and the hot side) can move into the new void. This repeats until the first module that moved into the original void has a new void to move into, thus completing a "one-module-movement cycle." The number of module voids dictates the number of steps required for a module-movement cycle. The number of module voids can be slightly varied depending on the module layout.

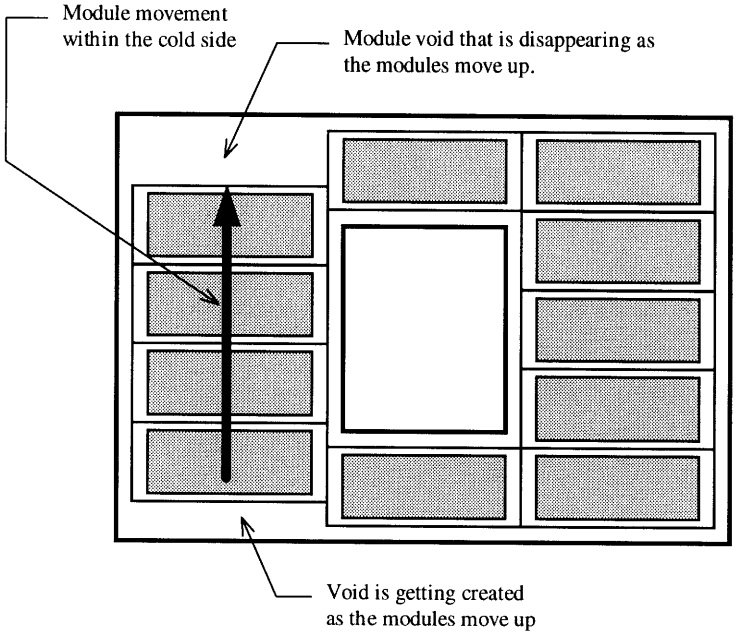

Figure 4.4 Example of module movement on the cold side.

4.2.2.1 Four-Step Module-Movement Process

With only one module void, a one-module-movement cycle occurs in four steps. Steps are required to move the modules through the cold side, a seal, the hot side, and the other seal. This is shown in the next figure. The arrows within the regenerator represent the modules that are just about to move for a particular step.

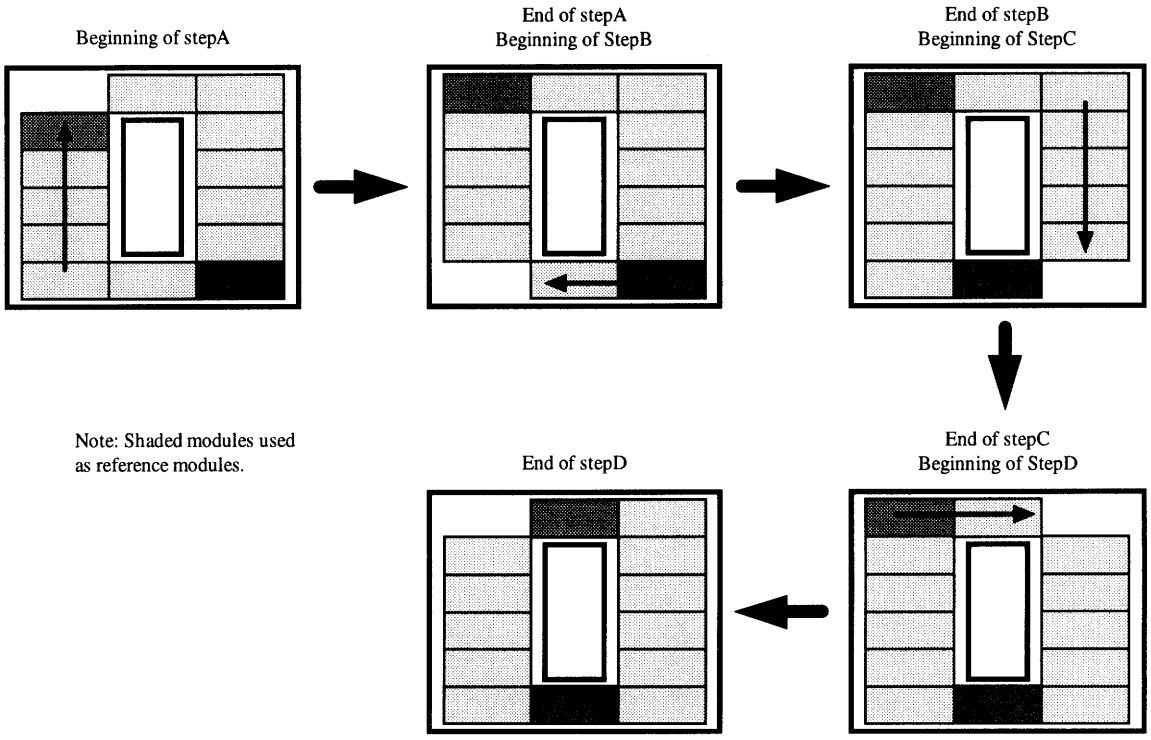

Figure 4.5 Diagram of the four-step one-module-movement cycle when one module void exists.

4.2.2.2 Two-Step Module-Movement Process

By providing two module voids, module movement occurs in two steps, step1 and step2. Step1 is simultaneous module movement through the seal section. Step2 is simultaneous movement though the hot and cold sides. So four steps actually occur but is reduced to two steps with simultaneous movement. The movement process is illustrated in

the following figure. Again, the arrows within the regenerator represent the direction of module movement at the beginning of particular step.

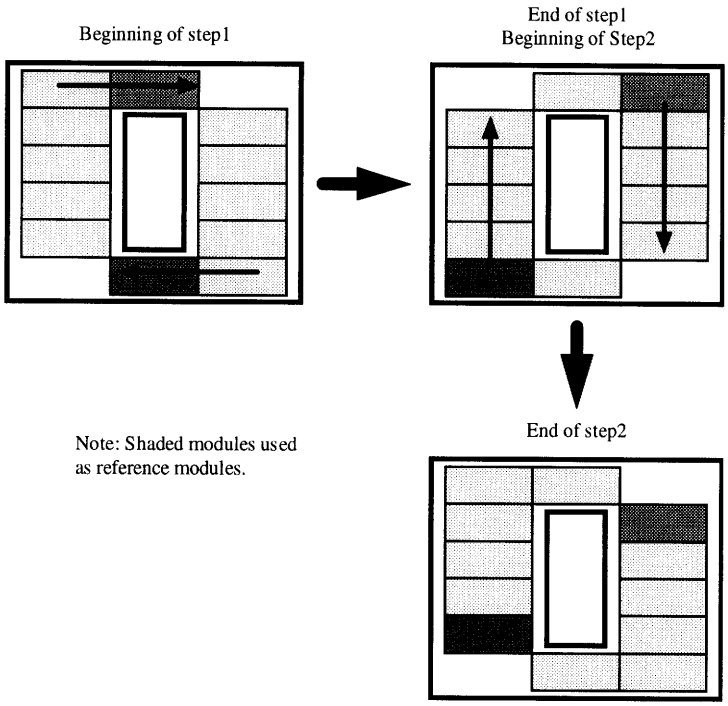

Figure 4.6 Diagram of the two-step one-module-movement cycle when two module voids exists.

Since each step contains simultaneous movements, step1 and step2 can be classified into two sub-steps. For step1, the two sub-steps are positive module movement and negative module movement. Positive movement is defined as the movement through the seal section from the cold side to the hot side. Positive movement is named as such to correspond with movement in the positive x-direction using the coordinate system from the seal-leakage calculations of Chapter 5. Negative module movement is defined as the movement through the other seal section where modules travel from the hot side to the cold side. Step2's two sub-steps consists of module movement within the hot and cold sides. The various sub-steps are summarized in the next figure.

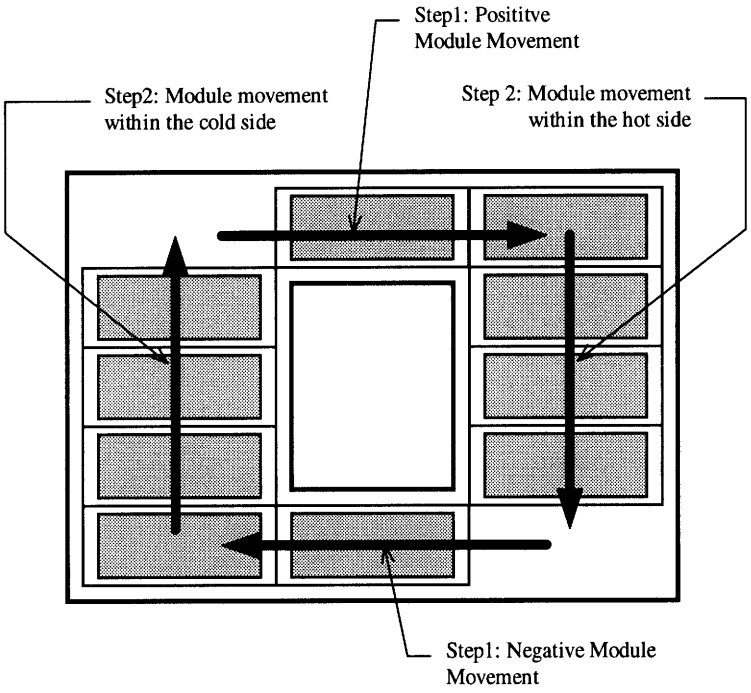

Figure 4.7 Diagram of the sub-steps used in two-step module movement.

4.2.2.3 Module Movement With Different Exposed-Matrix Areas

For some regenerator applications, having a larger exposed matrix area (channel area) on the hot side might be desirable. This could result in complications for module movement. Two options are introduced to define the geometry of the hot-side exposed area (hot-side channel) based on a chosen cold-side geometry. The first option, option A, is when both channels share identical channel lengths. The second option, option B, is when both channels share identical channel widths. Note that the nomenclature used to define the channel dimensions deviates from the standard convention that "length" refers to the longer of the two dimensions. The following two figures illustrate the two options with an example when the hot-side channel area is twice the cold-side channel area.

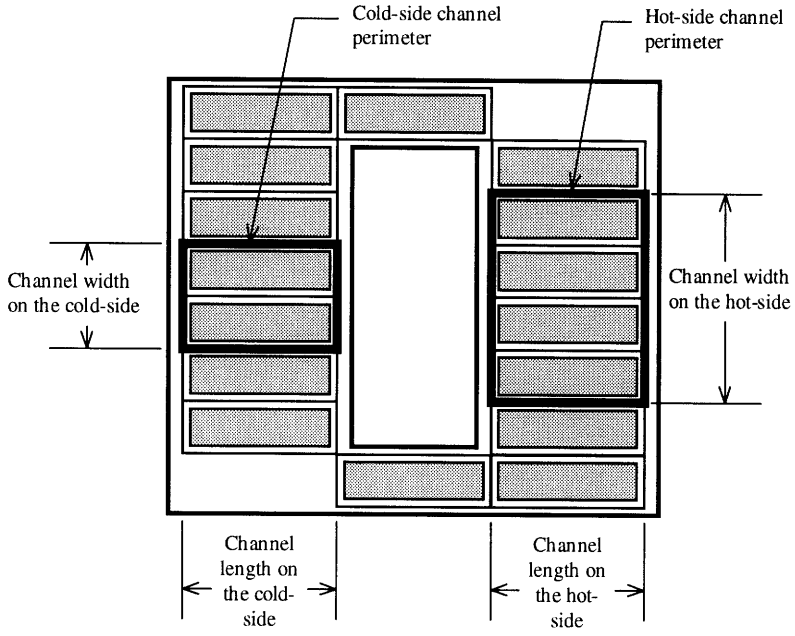

Figure 4.8 Channel-geometry option A where both sides have the same channel length.

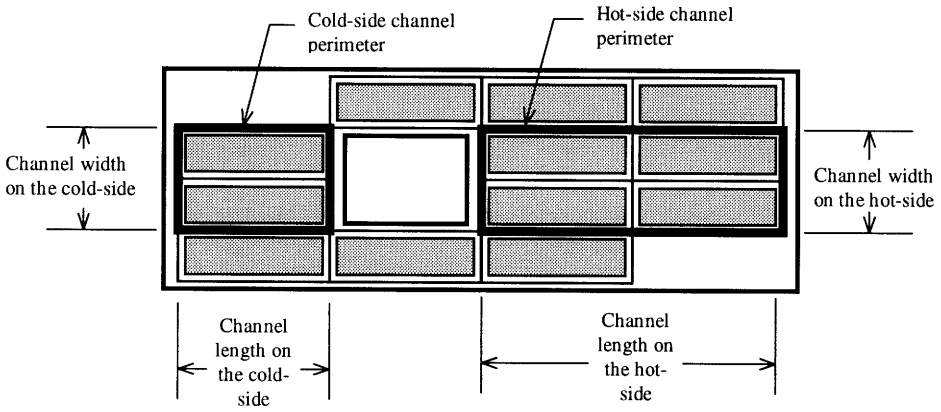

Figure 4.9 Channel-geometry option B where both sides have the same channel width.

By comparing the two figures, one can see that Option B's hot-side channel area must be a multiple of the cold-side channel area. Option A offers the advantage that the ratio of the two areas can take on any value. In addition, option A has a simpler movement scheme described next.

Option A can move with a 2-step or 4-step process previously described (depending if one or two module voids are chosen). Option B requires more complicated movement schemes. In addition, the number of possible movement schemes is proportional to the chosen number of module voids. Up to 4 module voids can be chosen in the example; however, if the area ratio is larger than two, the number of possible module voids increases. Due to the larger number of possible movement scenarios, examples are not given for option B.

4.2.2.4 Conclusions

The two-step movement process is more efficient than the four-step process since simultaneous movement occurs with the two-step process. Having two movement steps occurring within a one-module-movement cycle instead of four will allow slower module movement, lower accelerations, and a lower power requirement. Therefore, the two-step process is recommended for all modular designs and is used in this entire analysis.

Decreasing the mechanical complexity of a modular regenerator should reduce the potential for mechanical problems and failures. In light of this, channel-geometry option A is preferred due to the complexity of the movement schemes of option B (since option A provides the simple two or four-step movement process, whereas option B requires more complicated movement scenarios). In addition, option A has the capability of using non-integer channel-area ratios. A disadvantage with option A is that more modules can exist between the exposed face areas. This will increase the time for module movement from one exposed side to the other. A long time period may decrease the regenerator effectiveness due to conduction within the matrix (axial conduction) which is discussed in the next chapter. Nevertheless, preliminary calculations have shown axial conduction is not a factor. Hence, option A is recommended for all regenerator designs and is used throughout this design study.

4.2.3 Movement Mechanisms

Mechanisms are required to move the modules along linear paths through the seal section and the hot and cold sides. Pneumatic/hydraulic cylinders provide a simple, low-cost system to provide the necessary controlled linear actuation. These devices typically consist of a cylindrical rod connected to a piston within a cylinder. The piston's movement is controlled by adjusting the fluid pressures across both piston sides. The fluid is usually air or an incompressible hydraulic fluid, depending on the application. The cylinders can be double acting in which two ports exist at the end of the cylinder. Others can be single acting, with only one port, using a spring to provide the return force to bring the piston to its original position. Single-acting cylinders are longer than double-acting in order to accommodate the spring. The next figure gives a graphical description of a typical double-acting cylinder.

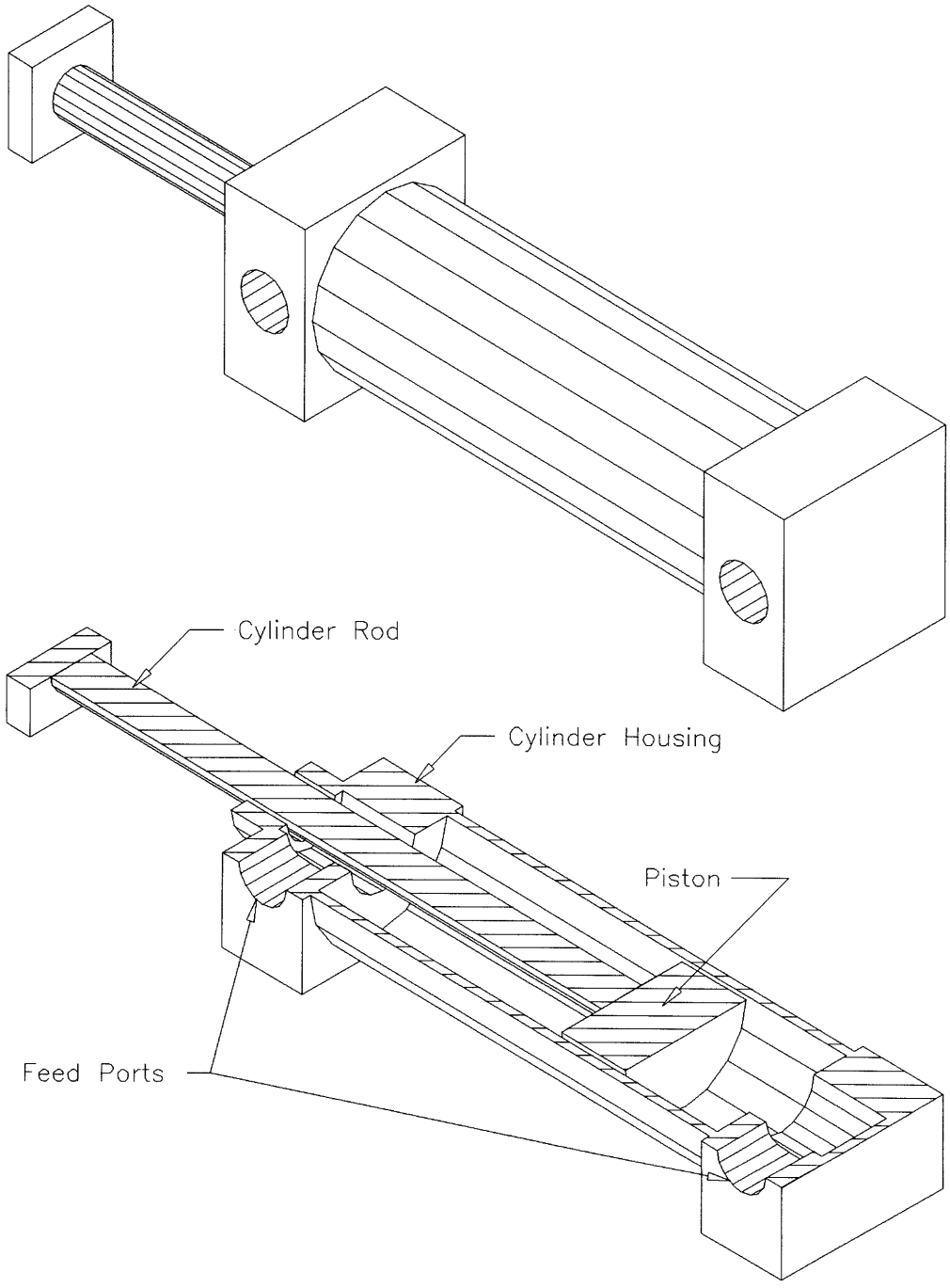

Figure 4.10 Typical pneumatic/hydraulic double-acting cylinder used for module movement including a cross-sectional view.

When sizing the cylinders, two basic dimensions are needed, the stroke length and the bore diameter. The stroke length is the linear distance the piston can travel within the cylinder. The bore size is the inside diameter of the cylinder. This parameter is required when determining the pressures and forces on the piston. The cylinder system requires additional equipment such as an air compressor, filters, regulators, valves and fluid connecting lines. This equipment has not been specifically designated in this design analysis. The design drawings depict cylinders with only representative stroke lengths and bore diameters. Cylinder sizing is discussed in the next chapter.

Typical module movement occurs when a cylinder rod is first pressed against a module. The feed pressure is increased on one piston side to provide the necessary force for movement. So the piston rod is extended which moves the module. After the module is displaced to a specified distance, the feed pressures are adjusted to return the piston and rod back to their original position. All cylinders use air as the fluid medium except for a special cylinder configuration for step1 movement discussed in the next section.

The figure below shows a close up of the casing as designed to accommodate the end to the cylinder rod. Part of the double-walled structure is removed so that the cylinder-rod end can retract past the wall. This should eliminate any possible problems as the modules contact the wall during movement.

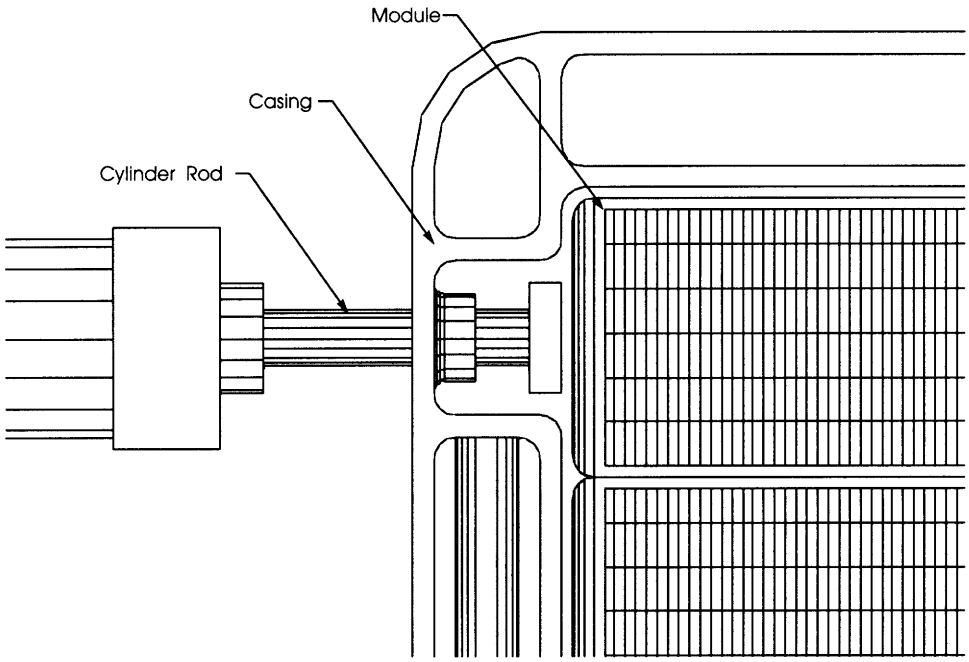

Figure 4.11 Accommodation in the regenerator casing for the cylinder rod end.

4.2.4 Step1 Module Movement

This section presents the mechanical configuration required for movement through the seal section. Two options are presented which use different cylinder arrangements to tackle the large pressure forces resisting module movement. The first, cylinder-configuration #1, is an arrangement where a cylinder has a large enough bore and piston feed pressure to overcome the pressure forces. The second, cylinder-configuration #2, is a novel arrangement where the resistive pressure forces are practically eliminated.

4.2.4.1 Cylinder Configuration #1

Cylinder configuration #1 uses a cylinder that overcomes the high-pressure forces resisting negative module movement. For positive module movement, the pressure force is acting the direction of movement. As a result, a cylinder is not needed for movement but a deceleration device (such as an industrial shock absorber) is required to slow the modules

to a complete stop. A small cylinder on the cold side (for positive module movement) should be used to ensure that the module enters the seal properly so that the pressure forces can propel the module into the hot side. This cylinder may not be necessary, but should be implemented as a safeguard.

The movement sequence for the modules and cylinder rods is shown in Figure 4.12. The movement sequence begins when the cylinder extends to move the modules into the cold side and the deceleration device is compressed (first two pictures). The cylinder rod retracts to allow step2 movement, and then the deceleration device extends (third and fourth pictures). Note that when step2 movement occurs in the third and fourth pictures, the modules within the seals must remain stationary. Devices that provide this are described in later in this chapter.

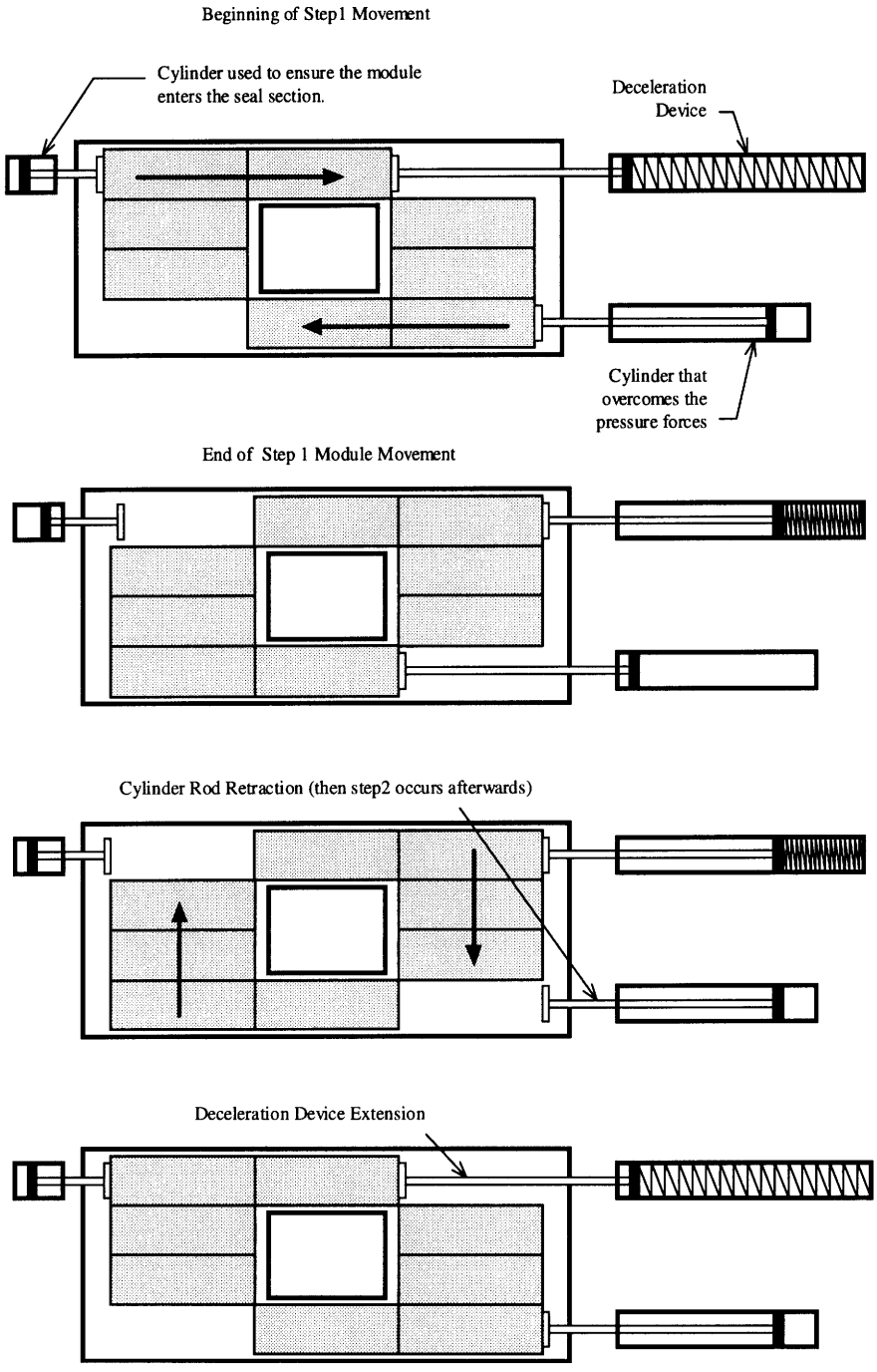

Figure 4.12 Module and cylinder-rod movement sequence for cylinder configuration #1.

4.2.4.2 Cylinder Configuration #2

This configuration uses a novel cylinder system that transfers the strong pressure forces resisting step1 module movement such that the work required is reduced dramatically. This concept transfers the forces during positive module movement to the forces for negative module movement. This is performed using two hydraulically-linked cylinders. Basically, two double-acting cylinders are connected to each other at one port containing an incompressible hydraulic fluid. When a piston for one cylinder moves in one direction, the other cylinder's piston moves exactly in the opposite direction at the same rate. So the pressure force on the modules for positive module movement is transferred through the two cylinders and finally to the modules for negative movement. Therefore, the pressure forces are almost completely balanced. A small net force exists since the module entering the cold side for negative movement does not have a cylinder rod acting on it. So the pressure has a slightly larger area to act on than with other modules. The overall mechanical configuration for this movement is shown in Figure 4.13.

The linked-hydraulic system consists of 3 cylinders. Two of the cylinders have rods that move the modules. The third cylinder is rod-less and acts as a reservoir to permit the other two cylinder rods to return to their original position for the next movement cycle. The cylinder-rod movement sequence is illustrated in Figure 4.14. The sequence starts when the rod for cylinder A is extended which pushes two modules through the seal for positive module movement (first picture). This forces the hydraulic fluid in cylinder B to be displaced to cylinder C which initiates negative module movement (second picture). Now cylinder C's rod must be retracted to allow step2 movement (third picture). During this retraction, cylinder B's piston cannot move since a module is in contact with the cylinder rod. Therefore, the rod-less cylinder (reservoir) allows cylinder C's hydraulic fluid to enter, thus cylinders C's rod retracts. After step2 movement (fourth picture), cylinder B's rod is extended to start the next cycle (fifth picture). Note that the third and fourth pictures show instances where the modules within the seal must be restrained from entering the hot side during step2 movement.

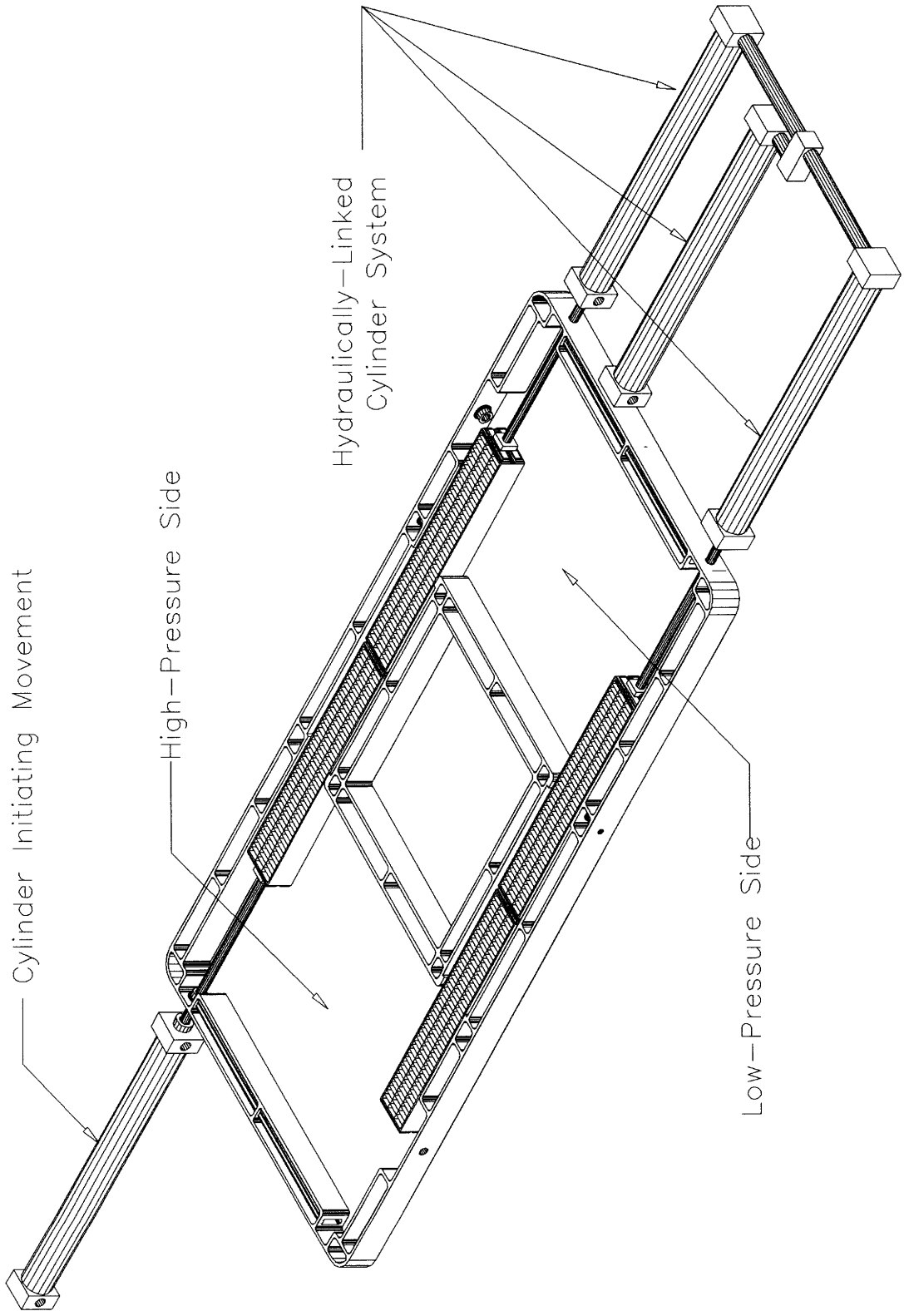

Figure 4.13 Cylinder configuration #2 for step1 module movement

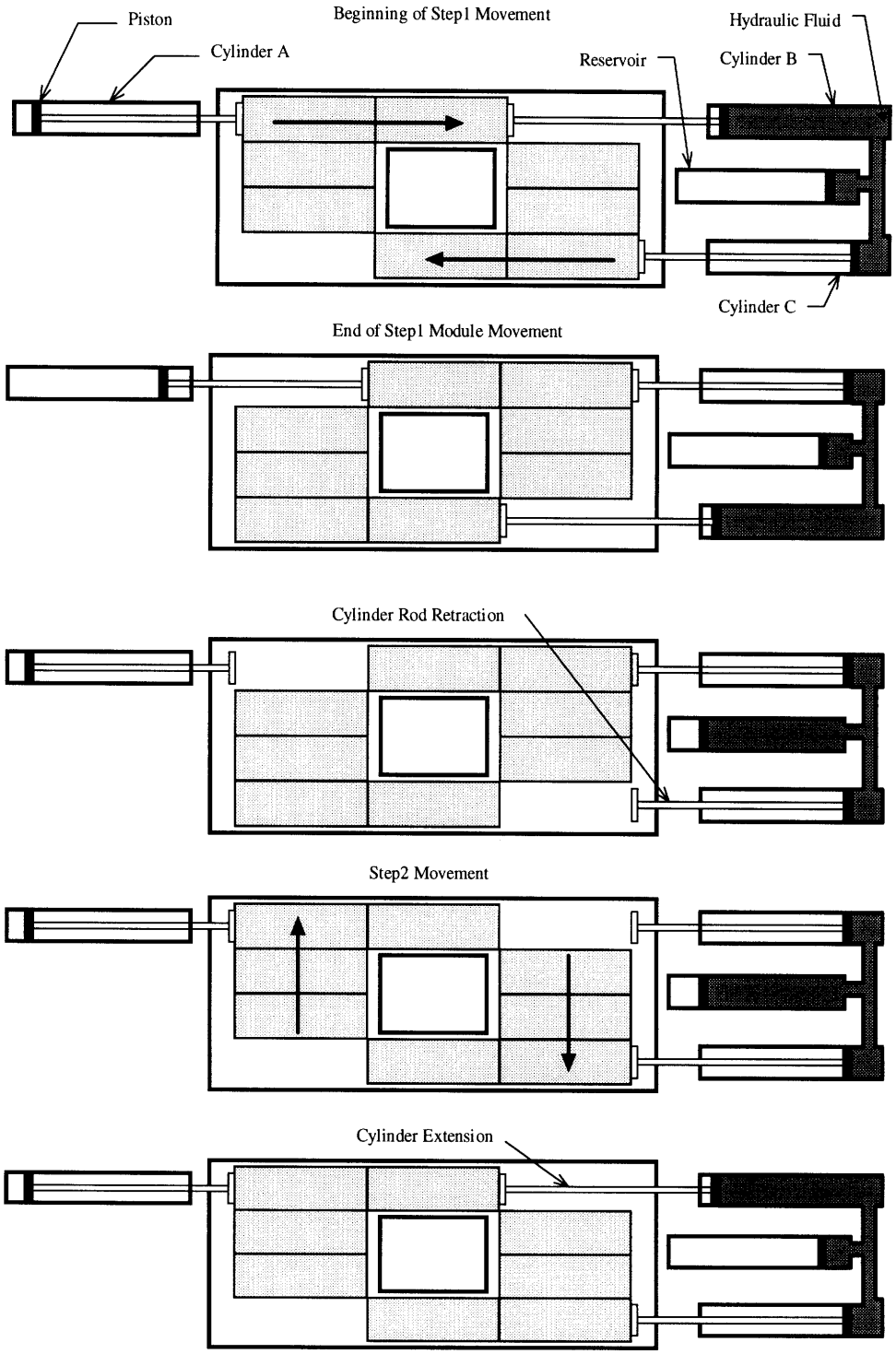

Figure 4.14 Module and cylinder-rod movement sequence for cylinder configuration #2.

4.2.4.3 Conclusions

Configuration #2's movement scheme is slightly more complex but this disadvantage is far outweighed by the near balance of the pressure forces that reduce the work required for movement. The lower work requirement should translate to a dramatic reduction in the power required for movement. This will be shown later in Chapter 5. Thus, configuration #2 is the preferred option.

4.2.5 Step2 Module Movement

This section presents the mechanical configuration required for movement through the hot and cold sides. Two options are presented which use different regenerator orientations to dictate the influence of gravitational and frictional forces (no resistive pressure forces exist for step2). The first option, regenerator orientation #1, minimizes the gravitational forces by placing the regenerator in a horizontal plane. The second option, regenerator, orientation #2, minimizes the frictional force by placing the regenerator in a vertical plane. Different mechanical devices are needed for each orientation. Other orientations could exist, but the two presented represent the extreme cases.

4.2.5.1 Orientation #1

Orientation #1 places the regenerator in a horizontal plane. As a result, the gravitational force is normal to module movement. Thus, friction is the main resistive force. Two cylinders are needed to move the modules, one for each side. The mechanical configuration for this orientation is shown in Figure 4.15. The movement sequence is given in the Figure 4.16. The sequence is quite simple: the two cylinders simultaneously extend to move the modules, then they both retract to permit step1 movement to occur.

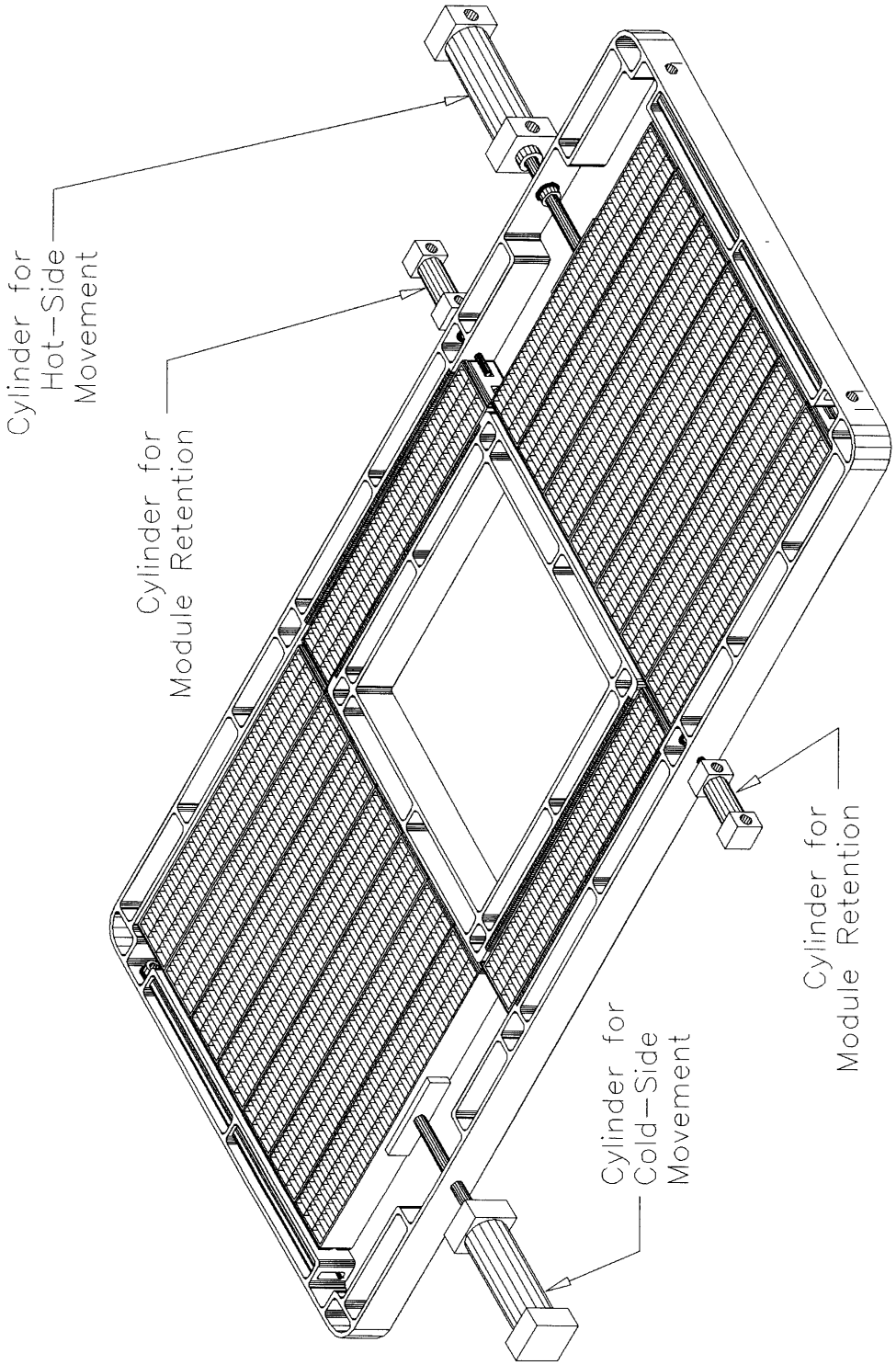

Figure 4.15 Module-movement mechanisms for regenerator orientation #1.

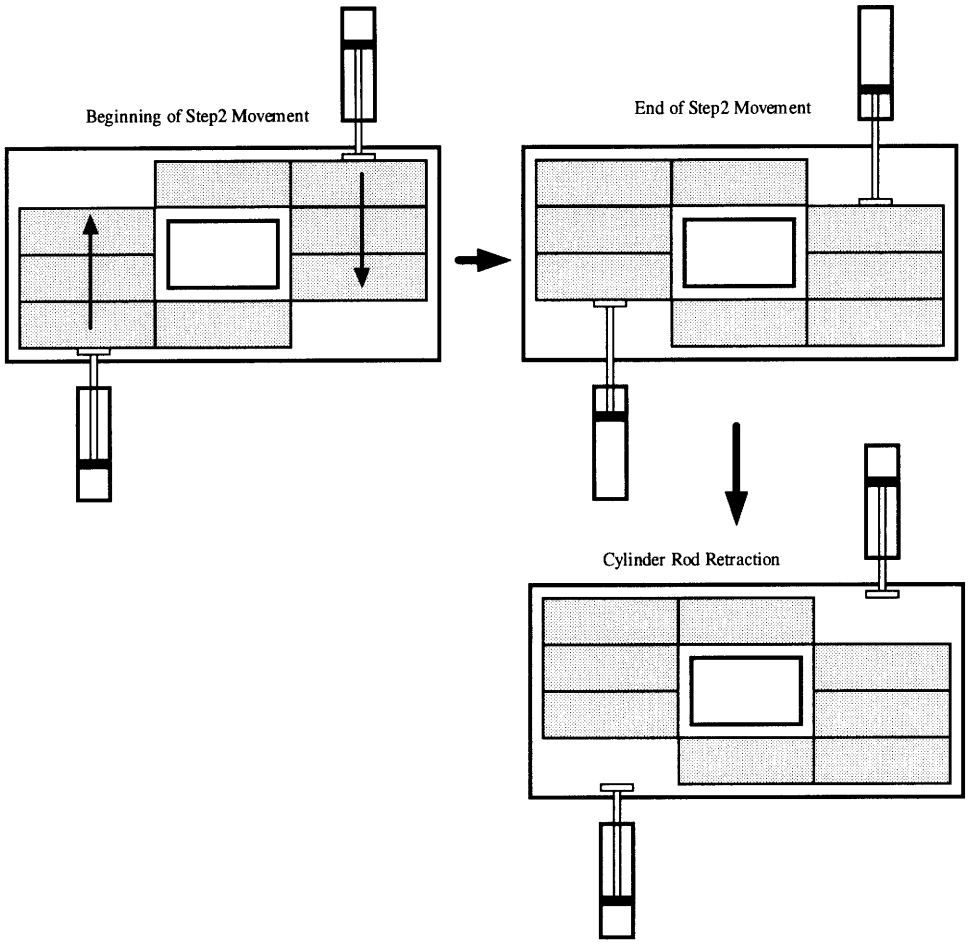

Figure 4.16 Module and cylinder-rod movement sequence for regenerator orientation #1.

4.2.5.2 Orientation #2

Orientation #2 place the regenerator in a vertical position. With the conventions used, the gravitational force is in the same direction as hot-side module movement (and opposes movement on the cold side). Therefore, a cylinder is needed to overcome the gravitational force during only cold-side movement. On the hot side, a deceleration device is required. A small cylinder can be added to the hot side at the opposite end to ensure that the gravitational force will initiate movement (not shown in the next figure).

The movement sequence is shown in the next figure. It starts with extension of the cold-side cylinder rod and retraction of the deceleration device (the first and second pictures). Then the bottom module on the cold side must remain stationary as the cylinder-rod retracts to allow step1 movement to occur (third picture). Then the deceleration device is extended to begin the next cycle.

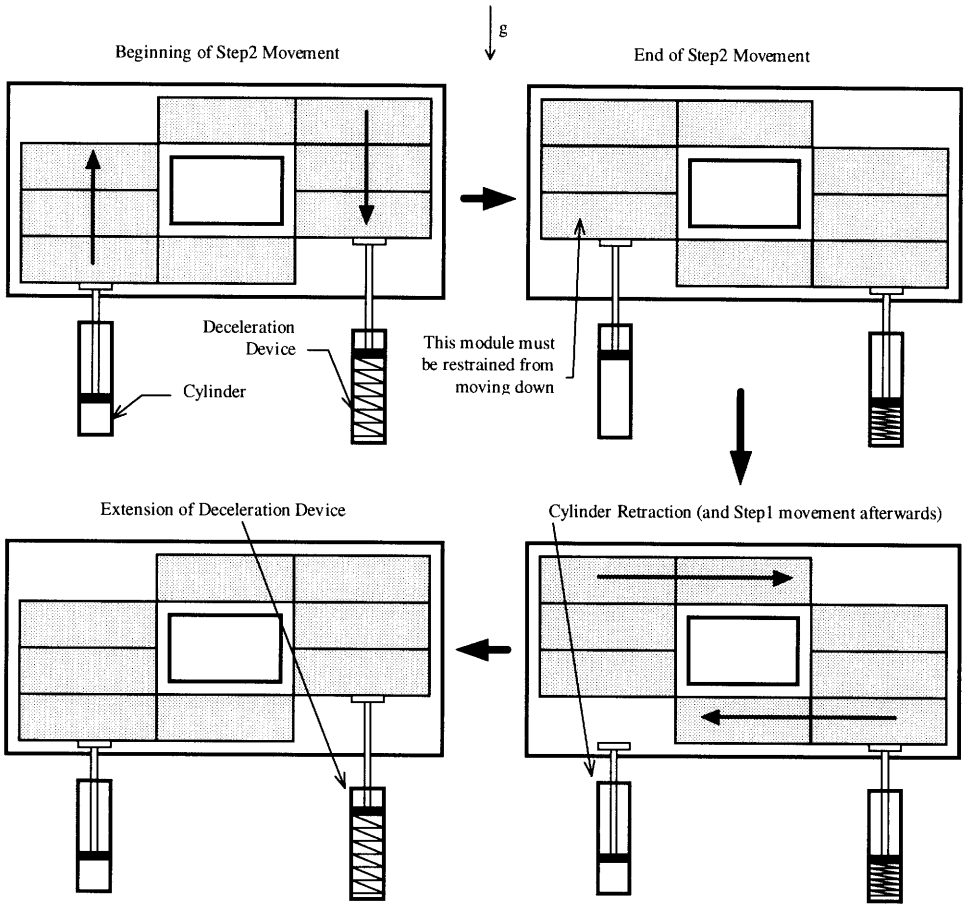

Figure 4.17 Module and cylinder-rod movement sequence for regenerator orientation #2.

4.2.5.3 Conclusions

Orientation #2 has several disadvantages when compared with #1. First, step2 movement requires synchronous module movement to occur for both sides. Therefore, the deceleration device must provide identical movement as the cylinder but in the opposite

direction. This may be difficult to achieve since they are two completely different devices. Orientation #1 has identical configurations for both sides so synchronous movement should be easy to accomplish. Another disadvantage for #2 is that a module on the cold side must be restrained from moving down as the cylinder retracts. A mechanism to provide this is not needed for orientation #1. Therefore, orientation #1 is the preferred option.

4.2.6 Air-Transfer Ducting

Using a two-step module-movement process, one module void is located in each side. Considering only one side during either step1 or step2 movement, the one module void is decreasing in volume and a new one is being created during module movement (see Figure 4.4). For the void that is decreasing, the air pressure will increase unless the void air is routed to the area where the new void is being created. A solution to this is to create a duct connecting the partial module voids for one side. This ducting and the corresponding air flow within it for each module-movement step is shown in the next two figures.

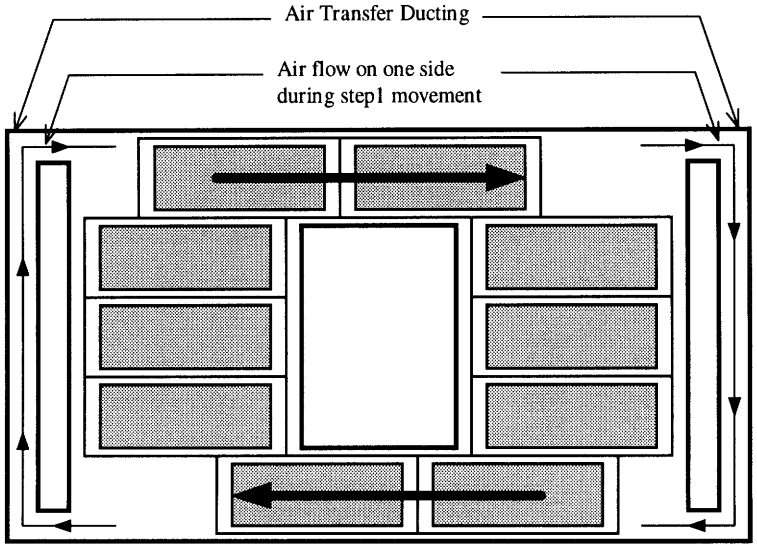

Figure 4.18 Air flow with the air-transfer ducting during step1 module movement.

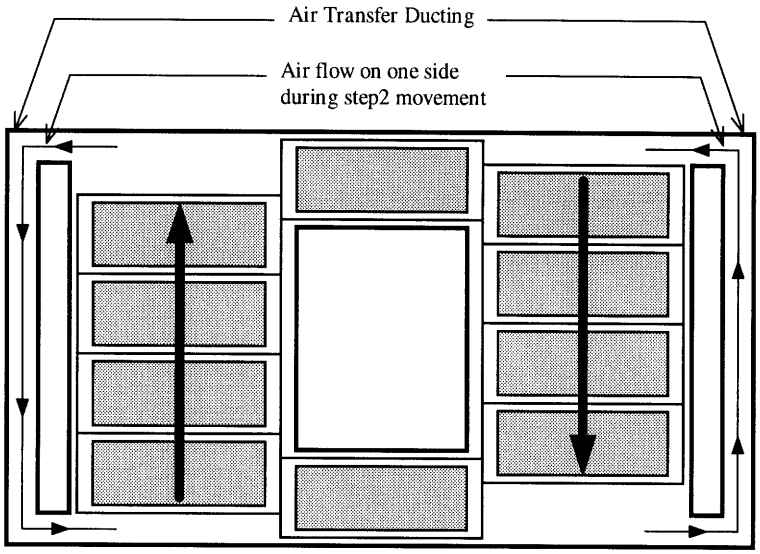

Figure 4.19 Air flow with the air-transfer ducting during step2 module movement.

The prototype design depicted in the drawings has the ducting incorporated into the casing between the double-wall support structure. This eliminated the need to provide external ducting. The next figure shows the air-transfer ducting within the casing.

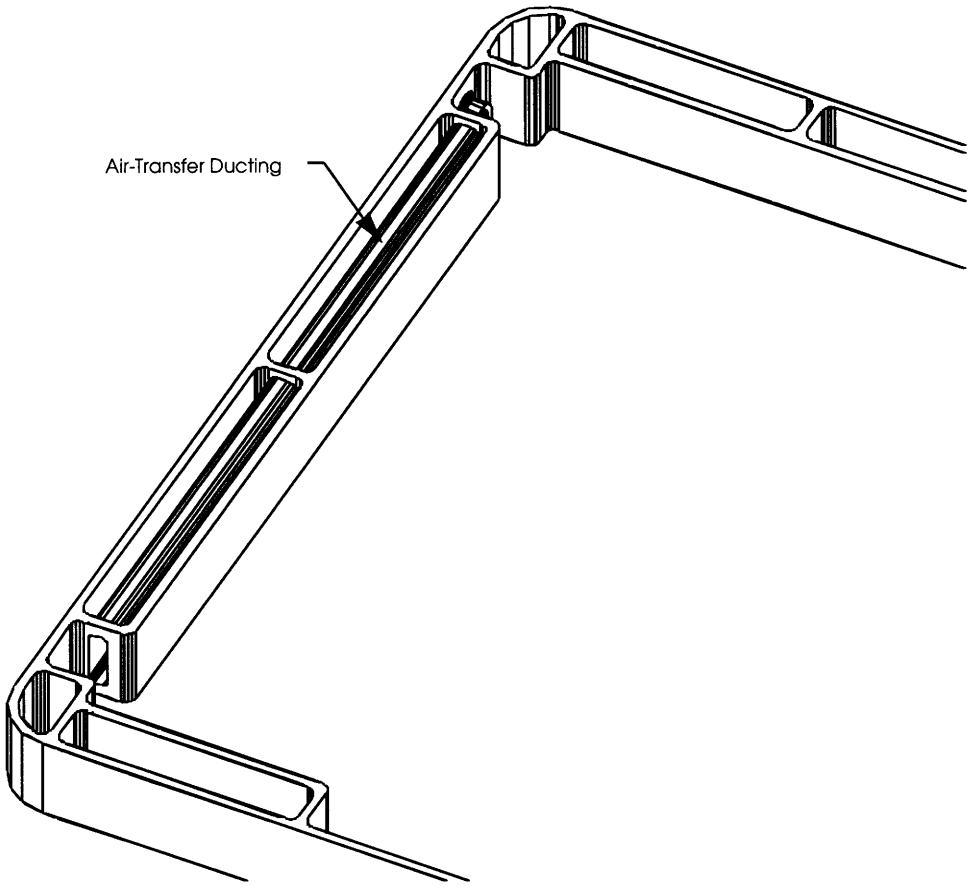

Figure 4.20 Air-transfer ducting incorporated into the regenerator casing.

4.2.7 Module-Retention Mechanism

During step2 movement, the modules within the seal section must remain stationary; however, net pressure forces are pushing the modules towards the hot side. At the beginning and end of step2 movement, one of the modules within a seal does not have a hot-side module adjacent to it. This is shown in the next figure. Thus a mechanism is needed to prevent such modules within the seals from entering the hot side prematurely.

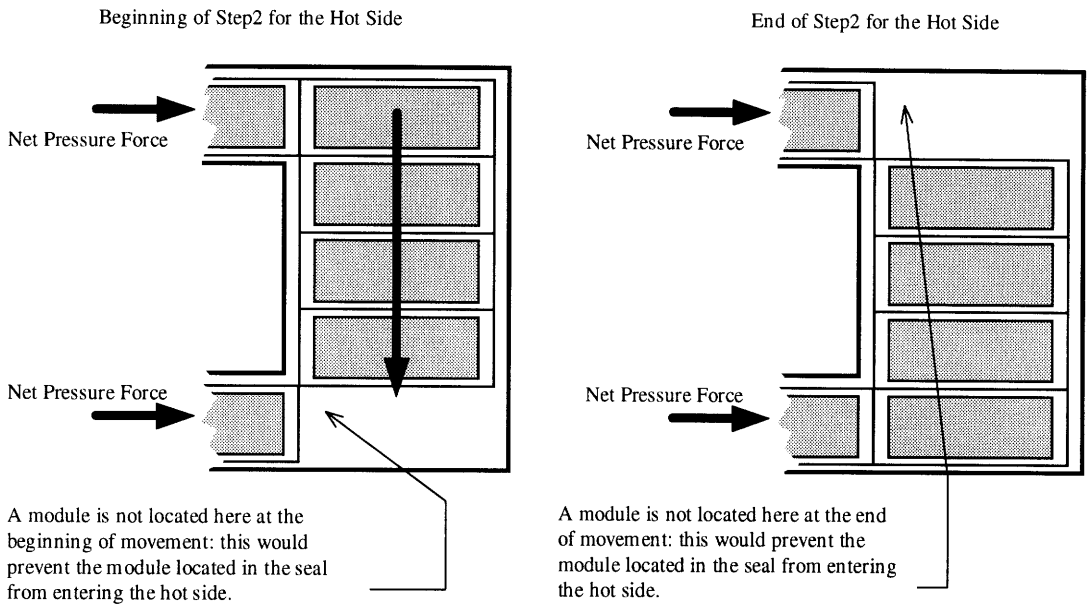

Figure 4.21 Diagram of how the modules within the seals can move into the hot side due to the net pressure forces.

Two types of retention mechanisms have been considered. One type is to have part of the seals clamp down across a module along its rim. Since the pressure forces on a module will be significant, the clamping forces will have to be large. Actuators such as pneumatic cylinders could be used to clamp the seal on the module. Two cylinders will then be needed for each module (to clamp down across a module), thus requiring a total of 4 cylinders for the regenerator. One major problem with this concept is that a module could slip as it is clamped. If this occurred, the module would enter the hot side prematurely thus halting further module movement. This failure could cause the regenerator to shut down completely. In addition, the clamping mechanism may produce some wear on the seal and the module rims.

Another concept uses a pin that is inserted into the module passage at the seal-section/hot-side interface. The pin comes in contact with a module located within the seal, thus preventing it from entering the hot side (until the pin is retracted). In order to allow the pin to enter through the casing to contact the modules, the module rims have a semi-cylindrical slot cut out of its end rims. These slots can be seen on a module in Figure 3.1.

The slots are located on both ends of a module so when two modules are along side each other, the two slots create a cylindrical hole for pin insertion. Furthermore, sometimes the hot-side cylinder rods are in full extension (where the rod contacts the modules located within the seal) when a pin is extended into the passage. Therefore, the ends of the cylinder-rod will need similar slots to allow the pin to extend into the passage. The module-retention mechanism for the design is shown in the following figure. The figure shows a cross-sectional view of the casing in order to view casing's pin-support structure. This particular mechanism uses an air cylinder to extend and retract the pin.

This concept has several advantages over the clamping-seal concept. First, the cylinder will not require a large force to move the pin since no resistive force exist during extension. Second, the module cannot enter the hot side until the pin is retracted, thereby eliminating possible module movement failures associated with the clamping-seal mechanism. Finally, only two cylinders are required, one for each seal (as opposed to four for clamping seals). The location of both cylinders is shown in Figure 4.1. The module-pin design must ensure that the pin can withstand the loading on it from the pressure forces. Detailed stress analysis should be made on the pin mechanism to prevent it from fracturing during operation. As a result, the module-pin mechanism is recommended for most modular designs.

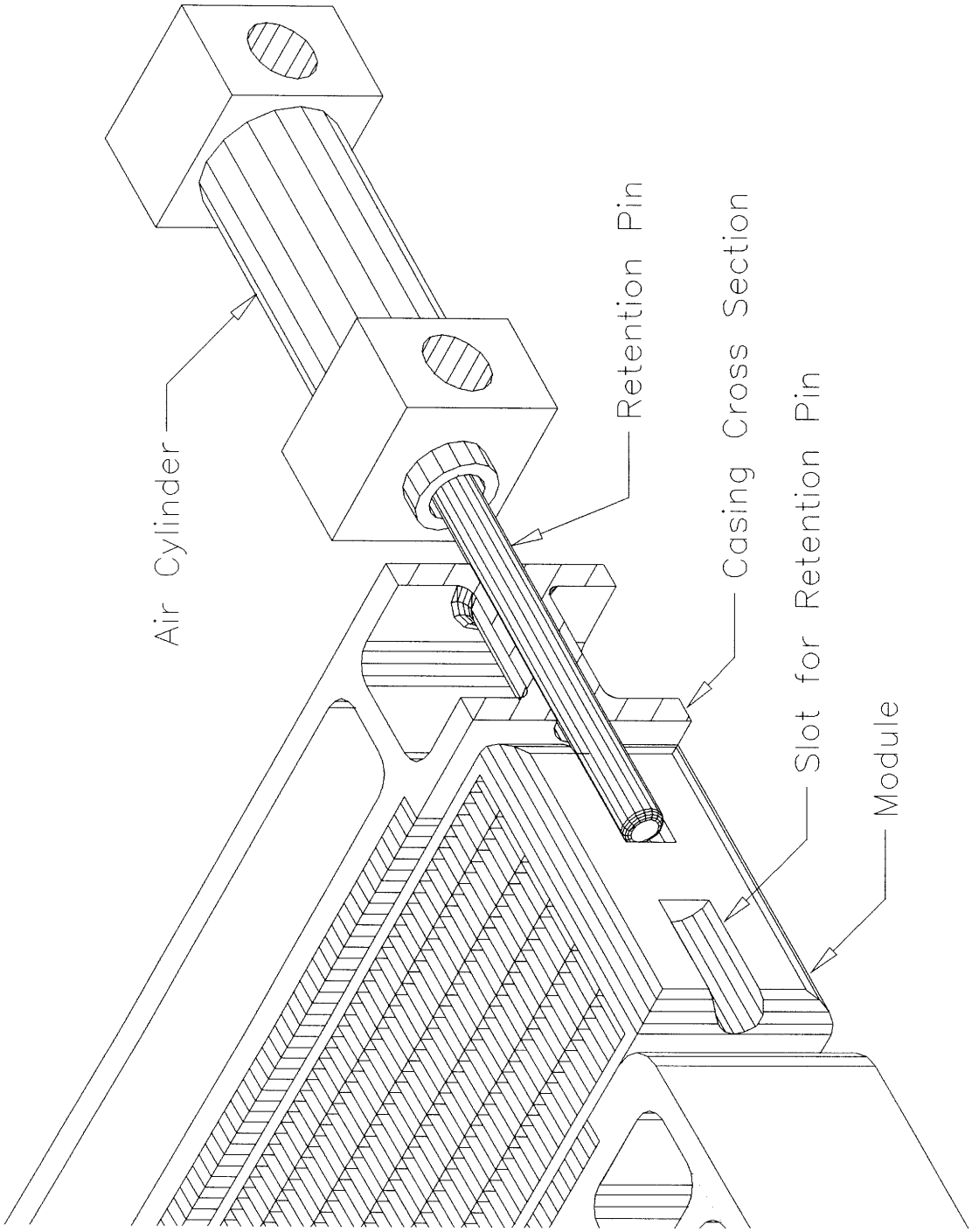

Figure 4.22 Module-Retention Mechanism

4.2.8 Sealing Description

This section presents the types of seals needed and its locations to contain the high-pressure air within the cold side. Leakage can occur in two locations on the cold side: around the modules in the seal section and around interface between the cylinder rods and the regenerator casing.

4.2.8.1 Labyrinth Seals

Most of the leakage will occur through the seal section to the hot, low-pressure side. To reduce this leakage, labyrinth seals are used around all module faces located within the seal section. Each module contains a matrix surface on two faces. When these faces are in close contact with the regenerator casing, a labyrinth seal inherently exists due to the matrix surface. The other two faces are along the smooth module rims. A matrix-like surface has been incorporated into the casing to provide the labyrinth seal. The following figure depicts the seal section showing the labyrinth seal structure built in the casing (the module has been removed for clarity).

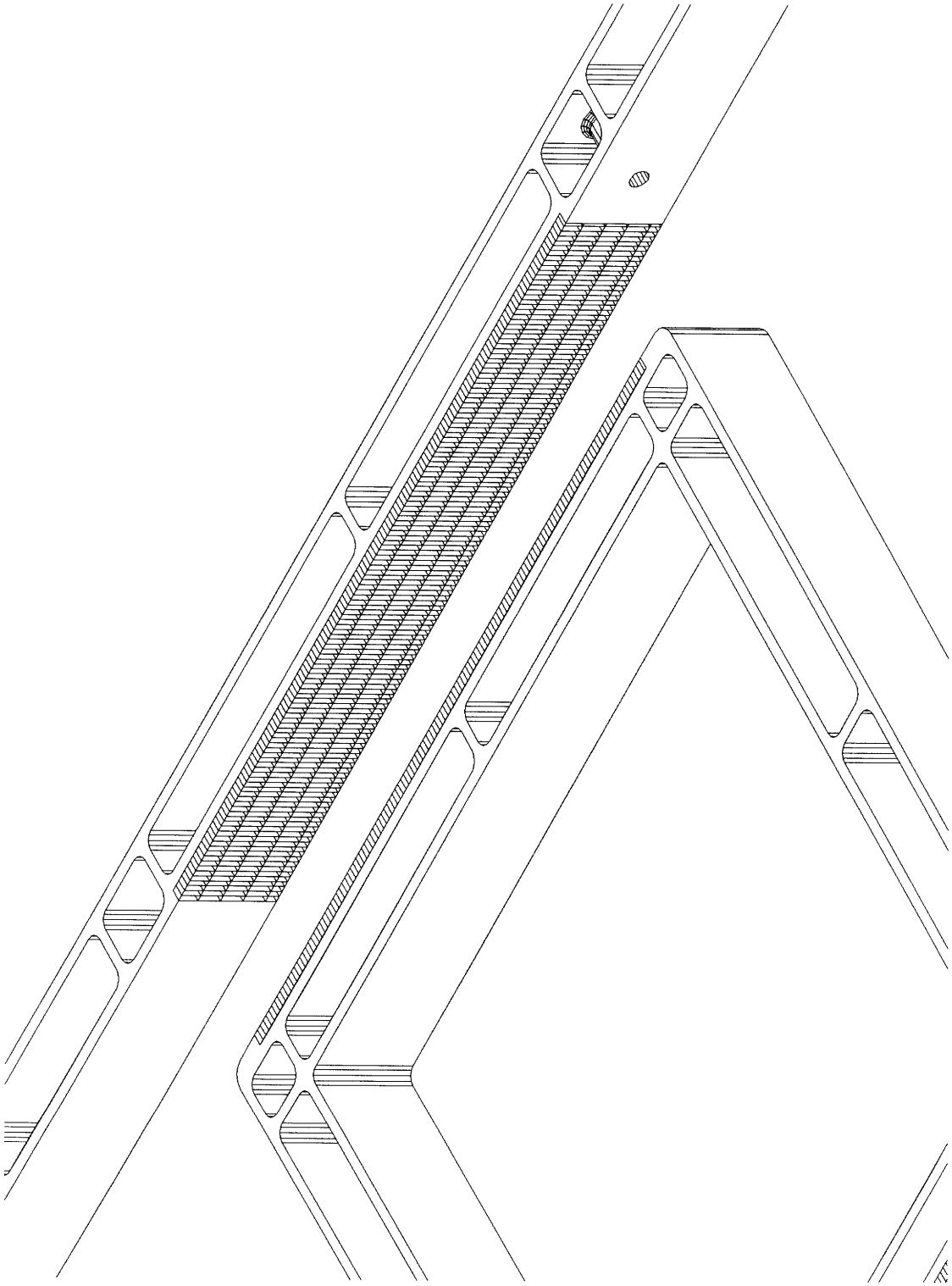

Figure 4.23 Seal section for the module-seal concept.

4.2.8.2 Cylinder Rod Seals

Two cylinders located on the cold side are used for module movement. The cylinder rods enter the cold side area through the casing walls. Seals should be used at these interfaces to prevent leakage to the atmosphere. The seals could consist of ones similar to piston seals for pneumatic cylinders; however, actual seal design has not been investigated and is left for future work.

4.2.9 Module Replacement During Operation

As previously stated, modular regenerators have the capability to switch out modules during operation. This can be performed for periodic maintenance or replacement of damaged modules. Unfortunately due to time constraints, this study does not encompass the design of the module replacement-mechanism.

Module replacement should probably occur with the unexposed modules traveling from the cold side to the hot side. New modules inserted in the regenerator are probably cold and at uniform temperature, replacing modules that just leave the cold side will give the least amount of reduction in regenerator effectiveness (since the modules leaving the cold side are at the lowest mean temperatures). An alternative is to divert some of the exhaust gas to the module just prior to insertion into the regenerator. This should provide minimal effectiveness reductions and allow module replacement to occur in more locations.

Wilson suggests that a possible location for module replacement is to incorporate the replacement mechanism within the seal section [6]. This can be done by extending the seal section by a module length as shown in the figure below.

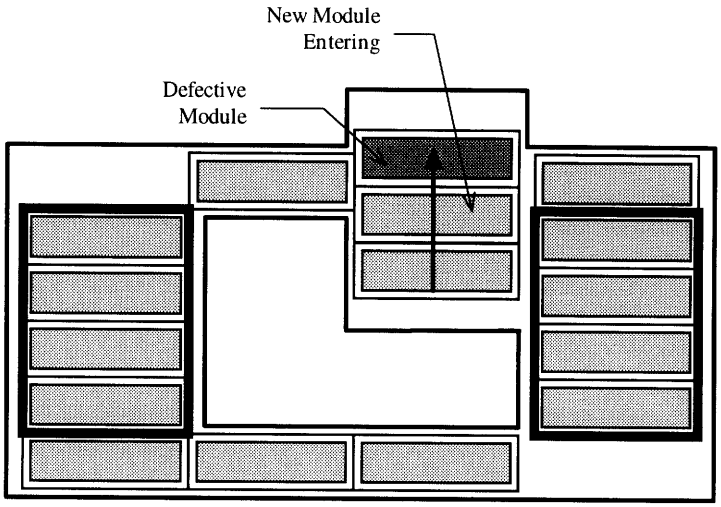

Figure 4.24 Module replacement during regenerator operation.

4.3 Gate-Seal Concept

The gate seal concept uses partitions (gate seal doors) to separate the hot and cold sides. The movement scheme is illustrated in the figure below. Basically, a gate-seal door opens to allow a module to enter and then closes (first two pictures) . Then the door on the other side of the chamber opens so the module can exit (third picture). This concept can easily accommodate a module replacement mechanism by adding another chamber within the seal section. Then module replacement would occur in the chamber just adjacent to the hot side.

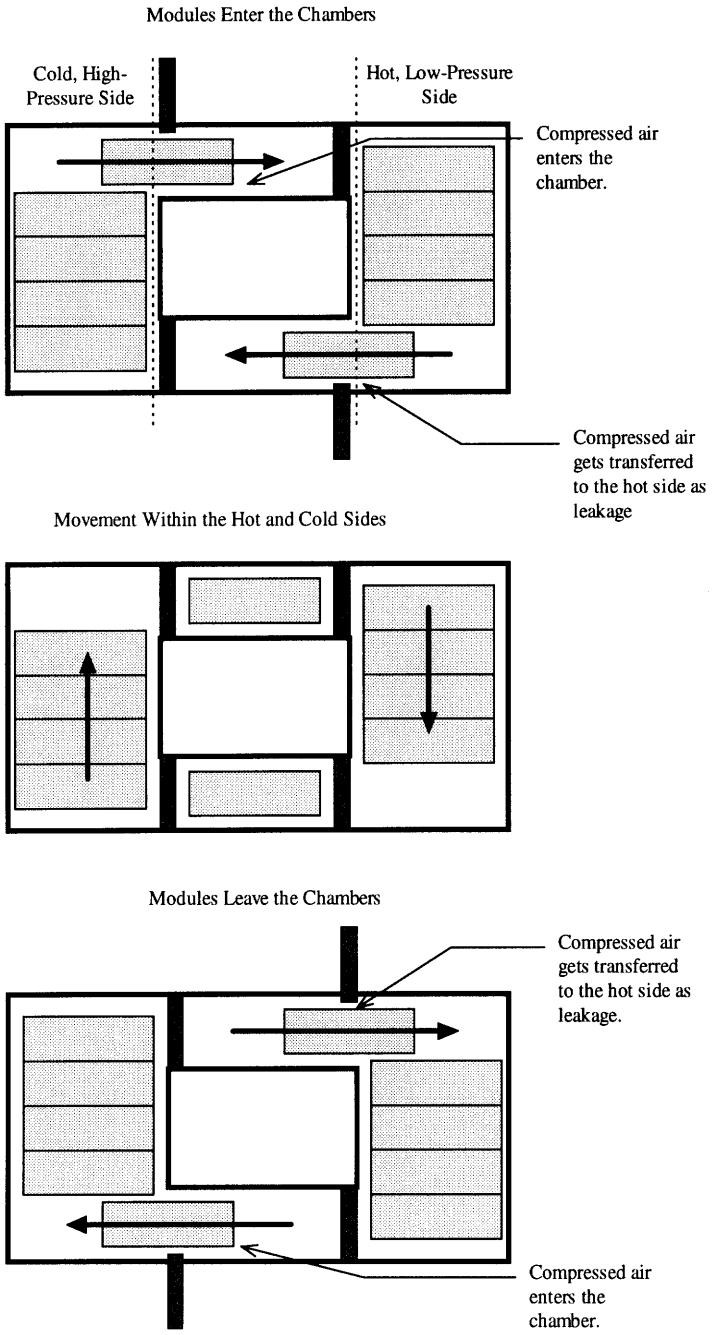

4.4 Summary and Conclusions

This chapter presented the mechanical design associated with the module-seal concept. Design drawings of a possible prototype regenerator were presented. Several

types of module-movement schemes were discussed including various regenerator configurations and orientations. The two-step module-movement process using cylinder configuration #2 and regenerator orientation #1 is recommended for most regenerator designs. If unequal exposed matrix areas are needed, then having identical hot and cold-side channel lengths is preferred. In addition, module retention (within the seals) using a pin inserted into the seal passage is preferred. Finally, the module movement using the gate-seal concept was briefly discussed. This type of regenerator might yield satisfactory results but its mechanical design is not investigated in this study. With the understanding of how the modular regenerator works mechanically, the next step is to design a regenerator by sizing it and calculating various performance aspects, which leads to the next chapter.

5. Design/Performance Calculations

5.1 Introduction

This chapter addresses a modular regenerator's detailed design. First, a method for determining a regenerator's size and performance is presented. Afterwards, design optimization is discussed by investigating the effects on the design when changing some chosen parameters. The chosen parameters are then finalized and substituted into the sizing and performance method to get the numerical results for the final regenerator design. Thereupon, seal leakage for the final design is discussed and compared with other regenerator concepts. Then, pressure calculations within the seals are made. Finally, leakage reduction techniques are discussed.

Many dimensional variables are introduced in this chapter describing the configuration of the regenerator and modules. The following figures display most of the relevant dimensions used.

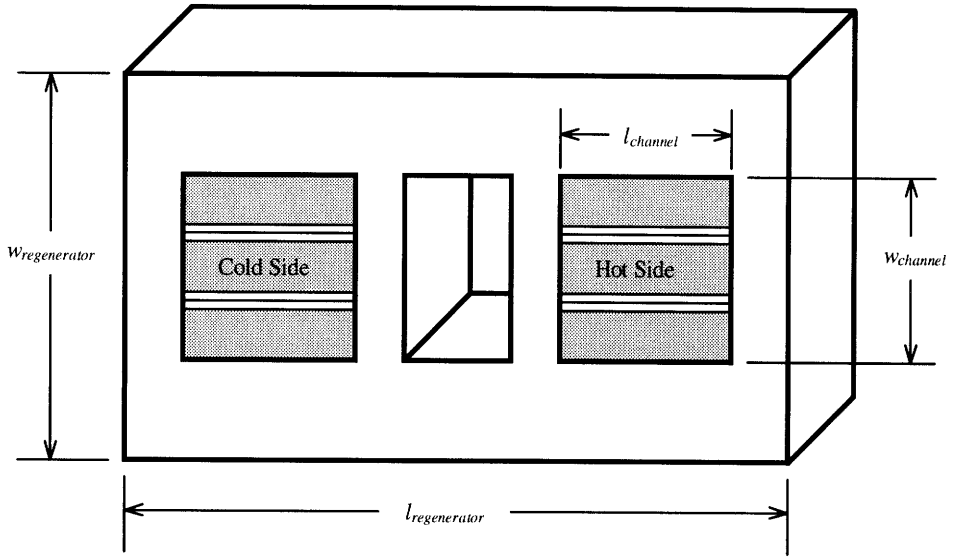

Figure 5.1 Regenerator Dimensions

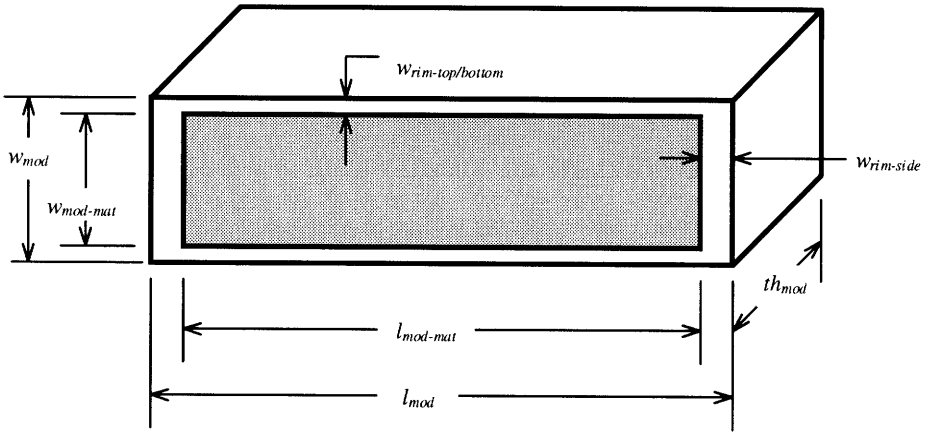

Figure 5.2 Module Dimensions

5.2 Regenerator Sizing and Performance

5.2.1 Introduction

The following sections present a method for sizing the regenerator and calculating its general performance. The sizing methods will determine the module and total matrix size. Performance calculations will determine the heat-transfer and fluid-mechanical performance. In addition, the power requirement for module movement is discussed.

The method presented contains calculations that are performed sequentially. Thus, parameters used in later portions sometimes require earlier derivations and computations. The following are some notes and assumptions that apply to the entire analysis presented in this chapter.

- The regenerator uses the module-seal concept with the two-step module-movement process.
- The ceramic honeycomb matrix consists of rectangular passages. The choice for this particular passage geometry is based on the results from Chapter 3.
- Air is assumed to be the fluid medium within all sections of the gas turbine. In reality, the fluid after the combustor (stations 4 to 6) is a gas comprised of air, fuel, and combustion products. This assumption is used because the properties of the gas would be difficult to determine since the gas composition can vary with time and location.

5.2.2 Method of Calculation

The method presented is initially based on the rotary-regenerator design example given in Wilson [13]. Wilson's example is derived from the regenerator design method pioneered by Kays and London [14]. This method uses mean values across the hot and cold sides of the regenerator to calculate its design and performance.

The method begins by first designating what parameters are needed initially to begin the design calculations. Then equations for the method are given or derived.

Example calculations are not supplied but numerical results of the calculations are shown later after the initial parameters have been optimized.

5.2.2.1.1 Engine Parameters

The design method assumes that a gas-turbine engine has already been specified. The heat-exchanger will be designed to corresponds to this particular engine. The engine parameters listed in Table 5.1 are sufficient to provide all the required cycle conditions needed for subsequent calculations. This analysis is set up so that the designer can modify the regenerator design to other gas turbines if the parameters in Table 5.1 are given.

Engine Parameter
compressor-inlet temperature, T_1
compressor-inlet pressure, P_1
compressor pressure ratio, r
compressor total-to-total polytropic efficiency, $\eta_{poly,1\text{-}2}$
turbine inlet temperature, T_4
heat-exchanger outlet pressure, P_6
turbine total-to-total polytropic efficiency, $\eta_{poly,4\text{-}5}$
compressor mass-flow rate, $\dot{m}_{1\text{-}2}$
$\sum\left(\frac{\Delta P}{P}\right)_{cycle}$, normalized pressure drops in cycle

Table 5.1 Specified gas-turbine engine parameters.

5.2.2.2 Chosen Parameter Designation

The design of any heat exchanger for a specified gas turbine requires several parameters to be chosen by the designer. Generally, choices consist of selecting parameters that specify the following: regenerator performance, a ceramic-matrix type, and regenerator configuration. Selecting which parameters are specified initially, instead of derived later, can vary depending on the preferred outcome.

This section presents those parameters needed for this particular design analysis. Section 5.3.2 assigns actual values for chosen parameters and then gives insight in optimizing those choices.

5.2.2.2.1 Regenerator-Performance Parameters

Certain parameters must be initially specified to design a regenerator with the intended performance. The designated performance parameters are listed in Table 5.2.

Effectiveness, core pressure drop, and leakage are important parameters because they affect the performance of the overall cycle (see Section 1.2.1).

C_{rot} is a non-dimensional measure of the matrix speed defined as

$$C_{rot} \equiv \frac{\left(\dot{m}\bar{c}_p\right)_{mat}}{\left(\dot{m}\bar{c}_p\right)_{min}} \tag{5.1}.$$

This parameter will later be used to determine the speed of the modules.

Specifying the pressure drop as an initial design criterion was suggested by Wilson [15] and is not conventionally done in regenerator design. Usually, the pressure drop is determined after first specifying either the hot or cold-side flow velocity. The parameters are then adjusted to give an adequate pressure drop.

Wilson's approach is to specify the pressure drop on the hot side because the hot-side value will always be larger. The cold-side relative pressure drop is lower mainly because the ambient pressure is higher but also because the cold-side fluid velocity is

lower. Furthermore, Wilson [16] states that the cold-side pressure drop might be low enough that the headers will require special techniques to ensure proper flow distribution over the core. For more information on heat-exchanger header design, see Wilson [16].

Regenerator-Performance Parameter
effectiveness, ε
$\left(\frac{\Delta P_{hot}}{P_{hot}}\right)_{core}$, hot-side-core pressure drop
$\dot{m}_{leak}/\dot{m}_{1\text{-}2}$, normalized regenerator leakage
C_{rot}

Table 5.2 Designated required regenerator-performance parameters.

5.2.2.2.2 Regenerator-Matrix Parameters

Obviously, a matrix material will have to be chosen. By specifying the material composition, then the density, specific heat, and thermal conductivity can be determined. In addition, specific matrix configuration properties will have to be furnished. Recall that rectangular passages are used. The required matrix parameters for this analysis are summarized in Table 5.3.

Porosity, hydraulic diameter, and passage aspect ratio are required since these parameters are sufficient to completely define the matrix when using rectangular passages. These parameters are defined in Section 3.3.3.

Regenerator-Matrix Parameter
material composition
ceramic solid density, ρ_{cer}
matrix porosity, Ψ_{mat}
hydraulic diameter, d_h
passage aspect ratio, AR_{pass}

Table 5.3 Designated required regenerator-matrix parameters.

5.2.2.2.3 Regenerator-Configuration Parameters

Several choices for the regenerator configuration are required and are shown in Table 5.4. The face-area ratio, *FAR*, gives the relation between the face areas (also the heat-transfer areas and number of modules) of the hot and cold sides and is

$$FAR \equiv \frac{A_{f_{hot}}}{A_{f_{cold}}} \tag{5.2},$$

where the face area, A_f, is defined as the matrix area of both voids and solid.

The channel is defined as the interface between the header and regenerator casing. In other words, it is the area at the flow entrance/exit of the ceramic matrix for one side. The designer has freedom to choose some aspects of the channel geometry. Since the modules are rectangular, the channel must conform to a similar geometry specified by the channel aspect ratio, $AR_{channel}$:

$$AR_{channel} \equiv \frac{l_{channel}}{w_{channel}} \tag{5.3},$$

where the channel lengths and widths shown in Figure 5.1.

Regenerator-Configuration Parameter
face-area ratio, FAR
number of modules exposed on cold side, $Nmod_{cold}$
cold-side channel aspect ratio, $AR_{channel_{cold}}$

Table 5.4 Designated required regenerator-configuration parameters.

5.2.2.3 Cycle Calculations and Mean Properties

With the specified gas turbine, the cycle conditions at all the stations can be determined. Then the mean properties across the regenerator are obtained.

5.2.2.3.1 Mass-Flow Rate

The leakage parameter in Table 5.2 is used only to estimate the mass-flow rates through the regenerator. Detailed leakage calculations are made later in Section 5.5. The design example in Wilson [13] assumes that the leakage occurs between the compressor outlet and heat-exchanger inlet and flows to the atmosphere. This results in equal hot and cold-side mass-flows rates. The analysis presented uses this assumption. In actuality for

the modular case, all the leakage from the cold side flows to the hot side, thus contributing to the hot-side mass-flow rate. Taking this into account complicates calculating the mass-flow rates because the actual leakage that flows into the hot side must be known; however, calculating the actual leakage requires knowing several cycle conditions which cannot be determined without knowing the mass-flow rates. Making the previous assumption eliminates this potential paradox.

Therefore, the mass-flow rate through the cold side of the regenerator (station 2-3) is

$$\dot{m}_{cold} = \dot{m}_{1-2}\left(1 - \frac{\dot{m}_{leak}}{\dot{m}_{1-2}}\right) \tag{5.4}.$$

The mass-flow rate through the turbine is

$$\dot{m}_{4-5} = \dot{m}_{cold} + \dot{m}_{fuel} \tag{5.5}.$$

The fuel mass-flow rate is generally small compared to the air mass-flow rate. Therefore, the fuel mass is assumed to be negligible. Assuming that no additional leakage occurs, mass-flow rate through the hot side of the regenerator (station 5-6) is represented as

$$\dot{m}_{hot} = \dot{m}_{cold} \tag{5.6}.$$

5.2.2.3.2 Pressures

Assuming as a reasonable approximation that the regenerator and combustor (station 3-4) provide the only pressure losses, then the cycle pressure drop can be represented as

$$\sum\left(\frac{\Delta P}{P}\right)_{cycle} = \left[\left(\frac{\Delta P}{P}\right)_{core} + \left(\frac{\Delta P}{P}\right)_{header}\right]_{cold} + \left[\left(\frac{\Delta P}{P}\right)_{core} + \left(\frac{\Delta P}{P}\right)_{header}\right]_{hot} + \left(\frac{\Delta P}{P}\right)_{3-4} \tag{5.7},$$

where the losses for the regenerator are split between the matrix core and the regenerator headers. Recall that the normalized cycle and hot-side-core pressure drops are specified as design choices, thus the remaining pressure drops need to be estimated. The actual core pressure drop on the cold side will be computed later.

Once all the pressure drops are specified, the pressures at the remaining stations can be computed as shown:

$$P_2 = r P_1 \tag{5.8}$$

$$P_3 = P_2\left(1-\left(\frac{\Delta P}{P}\right)_{cold}\right) \tag{5.9}$$

$$P_4 = P_3\left(1-\left(\frac{\Delta P}{P}\right)_{3-4}\right) \tag{5.10}$$

$$P_5 = P_6\left(1-\left(\frac{\Delta P}{P}\right)_{hot}\right) \tag{5.11}.$$

5.2.2.3.3 Temperatures

With the gas-turbine parameters specified in Table 5.1, the temperatures at all the stations can be determined. Using the definition of polytropic efficiency for an ideal gas, the temperature at the compressor exit, T_2, is found by iterating

$$T_2 = T_1\,(r)^{\frac{R}{\bar{c}_{P\ 1-2}\ \eta_{poly\ 1-2}}} \tag{5.12},$$

where the specific heat is evaluated at the mean temperature and R is the universal gas constant.

Similarly, the temperature at the turbine exit, T_5, can be determined by incorporating the normalized cycle-pressure losses in

$$T_5 = T_4 \left[r \left(1 - \Sigma \left(\frac{\Delta P}{P} \right)_{cycle} \right) \right]^{\left(-\frac{R \, \eta_{poly\ 4-5}}{\bar{c}_{P\ 4-5}} \right)} \tag{5.13}.$$

The temperature at the cold-side regenerator exit, T_3, can be calculated using the definition of effectiveness rewritten as:

$$\varepsilon = \frac{(\dot{m}\bar{c}_P)_{hot}(T_5 - T_6)}{(\dot{m}\bar{c}_P)_{min}(T_5 - T_2)} = \frac{(\dot{m}\bar{c}_P)_{cold}(T_3 - T_2)}{(\dot{m}\bar{c}_P)_{min}(T_5 - T_2)} \tag{5.14}.$$

The cold side has the smaller heat-capacity rate since the mass-flow rates are the equal and the specific heat increases with temperature. This can be written as follows:

$$(\dot{m}\,\bar{c}_P)_{min} = (\dot{m}\,\bar{c}_P)_{cold} \tag{5.15}$$

$$(\dot{m}\,\bar{c}_P)_{max} = (\dot{m}\,\bar{c}_P)_{hot} \tag{5.16}.$$

Substituting in equation (5.15) into (5.14), T_3 can be solved for directly:

$$T_3 = \varepsilon\,(T_5 - T_2) + T_2 \tag{5.17}.$$

The temperature at the hot-side regenerator exit, T_6, can be found by assuming that the heat transfer is equal for the hot and cold sides which gives

$$(\dot{m}\bar{c}_P)_{cold}(T_3 - T_2) = (\dot{m}\bar{c}_P)_{hot}(T_5 - T_6) \tag{5.18},$$

and again the specific heats are evaluated at the mean temperatures.

5.2.2.3.4 Additional Gas-Turbine Parameters

This analysis requires some additional gas turbine parameters for regenerator design. The first is the net power output of the gas-turbine engine, $\dot{W}_{GT}$. This is the sum of the compressor and turbine power:

$$\dot{W}_{GT} \equiv (\dot{m}\bar{c}_P)_{4-5}(T_4 - T_5) - (\dot{m}\bar{c}_P)_{1-2}(T_2 - T_1) \tag{5.19}$$

The next parameter is thermal efficiency, $\eta_{thermal}$, defined as the net power divided by the heat input:

$$\eta_{thermal} \equiv \frac{\dot{W}_{GT}}{(\dot{m}\bar{c}_P)_{3-4}(T_4 - T_3)} \tag{5.20}$$

The final engine parameter is the non-dimensional specific power, $\dot{W}'_{GT}$, defined as

$$\dot{W}'_{GT} \equiv \frac{\dot{W}_{GT}}{(\dot{m}\bar{c}_P)_{1-2} T_1} \tag{5.21}$$

These three equations are the basic relations used in constructing the performance curves in Section 1.2.1.

5.2.2.3.5 Mean Properties

The temperature and pressure distributions across a regenerator will probably have near-liner profiles. Therefore, using mean properties for each regenerator side should yield satisfactory results. With the temperatures and pressures known throughout the engine, the mean properties across the hot and cold sides can now be determined. The mean properties for the hot side are as follows:

$$\bar{P}_{hot} = \frac{P_5 + P_6}{2} \tag{5.22}$$

$$\overline{T}_{hot} = \frac{T_5 + T_6}{2} \tag{5.23}$$

$$\overline{\rho}_{hot} = \frac{\overline{P}_{hot}}{R\,\overline{T}_{hot}} \tag{5.24}.$$

The hot-side mean air properties such as viscosity, specific heat, Prandtl number can be determined using the equations in Section A.2 evaluated at the hot-side mean temperature.

Similarly, the mean properties for the cold side are shown below:

$$\overline{P}_{cold} = \frac{P_2 + P_3}{2} \tag{5.25}$$

$$\overline{T}_{cold} = \frac{T_2 + T_3}{2} \tag{5.26}$$

$$\overline{\rho}_{cold} = \frac{\overline{P}_{cold}}{R\,\overline{T}_{cold}} \tag{5.27}.$$

Again, the cold-side mean air properties can be found by using the equations in Section A.2 evaluated at the cold-side mean temperature.

5.2.2.4 Basic Regenerator Calculations

This section presents design calculations that are applicable for all types of periodic-flow regenerators. A regenerator's size and performance is determined using the NTU approach of heat exchanger design developed by Kays and London [14].

5.2.2.4.1 Laminar-Flow Heat Transfer and Friction Solutions

The small passages of ceramic matrices ensure laminar flow at all practical velocities [13]. Therefore, analytical solutions for fully-developed velocity and

temperature profiles can be used to develop heat-transfer and friction relations. The solutions for rectangular passage, taken from figure 6-1 of Kays and London [14], were fitted on a curve as a function of matrix-passage aspect ratio as shown:

$$C_f \, Re = 12.3810 + 1.93214 AR_{pass} - 0.113095 \left(AR_{pass} \right)^2 \tag{5.28}$$

$$\frac{St \, Pr^{\frac{2}{3}}}{C_f} = 0.267857 + 0.0191786 AR_{pass} - 0.00103571 \left(AR_{pass} \right)^2 \tag{5.29}.$$

The coefficient of friction, C_f, is the dimensionless surface shear stress, and the Prandtl number, *Pr*, is the ratio of the fluid's momentum and thermal diffusivities. The Stanton number, *St*, is a non-dimensional heat-transfer coefficient (a modified Nusselt number) defined as

$$St \equiv \frac{h_t}{\rho \, c_p \, C} \tag{5.30}.$$

The Reynolds number, *Re*, is the ratio of a fluid's inertia and viscous forces and is defined as

$$Re \equiv \frac{\rho \, C d_h}{\mu} \tag{5.31}.$$

5.2.2.4.2 Heat-Transfer Coefficients

The heat-transfer coefficient can be determined by combining and rearranging equations (5.30) and (5.31):

$$h_t = \frac{(C_f\, Re)\left(\frac{St\, Pr^{\frac{2}{3}}}{C_f}\right)\mu c_P}{Pr^{\frac{2}{3}}\, d_h} \qquad (5.32).$$

Given the passage aspect ratio and hydraulic diameter and using equations (5.28) and (5.29) for the laminar flow solutions, the heat-transfer coefficients for the hot and cold sides can be determined. This is done by using the curve fit equations for air properties (μ_{air} ,c_{Pair}, and Pr_{air}) in Section A.2, evaluated at the mean temperature specified in Section 5.2.2.3.5.

5.2.2.4.3 Matrix Geometry

The thickness of the matrix wall, th_{wall} , can be estimated by representing the matrix as only one passage surrounded by walls with one half the wall thickness. This is shown in next figure. Then, the cross-sectional area of the solid for the one passage matrix is

$$A_{solid} = 2\left(l_{pass}\frac{th_{wall}}{2}\right) + 2\left(w_{pass}\frac{th_{wall}}{2}\right) + 2\left(\frac{th_{wall}}{2}\right)^2 \qquad (5.33).$$

The void area for the passage is

$$A_{void} = w_{pass} l_{pass} \qquad (5.34).$$

Substituting in the two equations above into the definition of porosity gives the following:

$$\Psi_{mat} = \frac{w_{pass} l_{pass}}{w_{pass} l_{pass} + 2\left(l_{pass} \frac{th_{wall}}{2}\right) + 2\left(w_{pass} \frac{th_{wall}}{2}\right) + 2\left(\frac{th_{wall}}{2}\right)^2} \quad (5.35),$$

where the wall thickness is solved for iteratively.

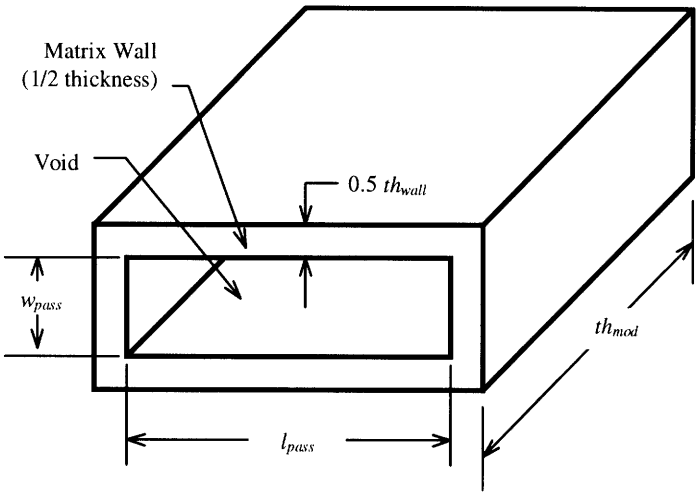

Figure 5.3 Representation of a one passage matrix.

The passage density, represented as the number of passages per square centimeter, can be found using:

$$\rho_{pass} = \frac{(0.1)^2}{\left(w_{pass} + th_{wall}\right)\left(l_{pass} + th_{wall}\right)} \quad (5.36).$$

The unit of passages per square centimeter is used to be consistent with Corning's unit convention for ceramic matrices.

5.2.2.4.4 Heat-Transfer Area Per Matrix Volume

With the matrix geometry known, the heat-transfer area per free (void) volume can be determined. Using the one passage matrix example from the previous figure, the heat-transfer area per free volume is

$$\frac{A_h}{V_{void}} = \frac{2\left(w_{pass} + l_{pass}\right)th_{mod}}{w_{pass}\, l_{pass}\, th_{mod}} = \frac{2\left(w_{pass} + l_{pass}\right)}{w_{pass}\, l_{pass}} \tag{5.37},$$

where heat-transfer area, A_h, is the "wetted" matrix surface area exposed the flow (neglecting the front and back matrix faces that are normal to the flow).
Using the previous equation and equation (3.9) for porosity, the heat-transfer area per matrix volume can be derived as:

$$\frac{A_h}{V_{mat}} = \frac{A_h}{V_{void}} \Psi_{mat} \tag{5.38}.$$

5.2.2.4.5 NTU

This study uses the NTU method for heat-exchanger design. The NTU, number of transfer units, is defined as

$$NTU \equiv \frac{U A_h}{\left(\dot{m} c_P\right)_{min}} \tag{5.39},$$

where U is the overall heat-transfer coefficient. UA_h is the net conductance for the hot and cold fluids and is related to the conductance of each fluid by the conductance equation:

$$\frac{1}{U A_h} = \left(\frac{1}{h_t A_h}\right)_{hot} + \left(\frac{1}{h_t A_h}\right)_{cold} + \left(\frac{th}{k A_h}\right)_{wall} \quad (5.40),$$

where wall resistance, $\left(\frac{th}{k A_h}\right)_{wall}$, is assumed to be negligible. Combining the previous two equations with a value of NTU, the module/matrix thickness and the heat-transfer area can be found. This will be shown in upcoming Sections 5.2.2.4.7 and 5.2.2.4.9.

Using charts in Kays and London [14] for periodic-flow heat exchangers, NTU values are obtained for a given effectiveness, C_{rot}, and C_{rat}. C_{rat} is the heat-capacity-rate ratio defined as

$$C_{rat} \equiv \frac{(\dot{m}\bar{c}_P)_{min}}{(\dot{m}\bar{c}_P)_{max}} \quad (5.41).$$

$C_{rat} = 1$ is approximated for gas-turbine cycles when using the Kays and London charts (this may produce a regenerator with a slightly higher effectiveness than specified). Most designs will have C_{rat} close to unity so the approximation should be valid.

5.2.2.4.6 Hot-Side Pressure Drop

Recall that the hot-side pressure drop is a chosen parameter. By specifying this, the module/matrix thickness and the hot-side flow velocity can be found. The following presents the necessary equations pertaining to pressure-drop performance that are required for subsequent derivations.

Making a force balance for the fluid within the matrix results in

$$\Delta P A_{ff} = \tau_{wall} A_h \quad (5.42),$$

where ΔP is the pressure drop and τ_{wall} is the wall shear stress. The wall shear stress can be eliminated using the definition for coefficient of friction:

$$C_f \equiv \frac{\tau_{wall}}{q} \tag{5.43},$$

where q is the incompressible dynamic pressure defined as (at mean properties)

$$q \equiv \frac{1}{2}\bar{\rho}\,\bar{C}^2 \tag{5.44}.$$

Substituting the above two equations into (5.42) equation results in the following:

$$\Delta P = \frac{A_h\left(\frac{C_f}{Re}\right)q}{A_{ff}\,Re} \tag{5.45}.$$

The free face area can be represented as

$$A_{ff} = \frac{\dot{m}}{\bar{C}\,\bar{\rho}} \tag{5.46}.$$

Then substituting the free face area (5.46), Reynolds number (5.31), porosity (3.9), and dynamic pressure (5.44) into equation (5.45) for the hot side simplifies to

$$\Delta P_{hot} = \frac{1}{2}\left(\frac{C_f}{Re}\right)\left(\frac{A_h}{V_{mat}}\right)\frac{\bar{C}_{hot}\,\bar{\mu}_{hot}\,th_{mod}}{\Psi_{mat}\,d_h} \tag{5.47}.$$

5.2.2.4.7 Hot-Side Fluid Velocity and Module/Matrix Thickness

The heat-transfer area can be shown as

$$A_h = A_f \, th_{mod} \left(\frac{A_h}{V_{mat}} \right) \tag{5.48}.$$

Combining the NTU equations (5.39) and (5.40) and substituting in the above equation gives

$$\frac{1}{NTU\left(\dot{m}\bar{c}_P\right)_{min}} = \left(\frac{1}{h_t A_f \, th_{mod} \left(\frac{A_h}{V_{mat}} \right)} \right)_{hot} + \left(\frac{1}{h_t A_f \, th_{mod} \left(\frac{A_h}{V_{mat}} \right)} \right)_{cold} \tag{5.49}.$$

Plugging in the face areas represented as

$$A_{f_{hot}} = \frac{\dot{m}_{hot}}{\overline{C}_{hot} \, \overline{\rho}_{hot}} \Psi_{mat} \tag{5.50}$$

and

$$A_{f_{cold}} = \frac{\dfrac{\dot{m}_{hot}}{\overline{C}_{hot} \, \overline{\rho}_{hot}} \Psi_{mat}}{FAR} \tag{5.51}$$

into equation (5.49), and solving for th_{mod}, simplifies to

$$th_{mod} = \overline{C}_{hot} \overline{\rho}_{hot} \Psi_{mat} NTU \left(\dot{m}c_P\right)_{min} \frac{h_{t_{cold}} + FAR \, h_{t_{hot}}}{h_{t_{hot}} h_{t_{cold}} \dot{m}_{hot} \left(\frac{A_h}{V_{mat}} \right)} \tag{5.52}.$$

Note that the hot-side velocity is still unknown and will be determined next.

Now th_{mod} is eliminated by inserting equation (5.52) into (5.47). After simplifying and rewriting, solving for the hot-side velocity gives

$$\overline{C}_{hot} = \sqrt{\frac{\Delta P_{hot}}{\frac{1}{2}\left(\frac{C_f}{Re}\right)\left(h_{t_{cold}} + FAR\, h_{t_{hot}}\right)\frac{\overline{\rho}_{hot}\,\overline{\mu}_{hot}\,NTU\,(\dot{m}c_P)_{min}}{h_{t_{hot}}\,h_{t_{cold}}\,\dot{m}_{hot}\,d_h}}} \tag{5.53},$$

where the hot side pressure drop is found using

$$\Delta P_{hot} = \overline{P}_{hot}\left(\frac{\Delta P}{P}\right)_{hot} \tag{5.54}.$$

So $\overline{C}_{hot}$ can now be determined since all values on the right-hand side are known (initially chosen or derived). Then, plugging the hot-side velocity into equation (5.52) will give a value for the module thickness.

5.2.2.4.8 Matrix Areas, Volume, and Mass

The hot-side free face area is found using

$$A_{ff_{hot}} = \frac{\dot{m}_{hot}}{\overline{C}_{hot}\,\overline{\rho}_{hot}} \tag{5.55},$$

and then the hot-side face area is

$$A_{f_{hot}} = \frac{A_{ff_{hot}}}{\Psi_{mat}} \tag{5.56}.$$

For the cold side, the areas are found using

$$A_{f_{cold}} = \frac{A_{f_{hot}}}{FAR} \tag{5.57}$$

and

$$A_{ff\,cold} = A_{f_{cold}} \Psi_{mat} \tag{5.58}$$

The total matrix face area, A_{fmat}, is just

$$A_{f_{mat}} = A_{f_{hot}} + A_{f_{cold}} \tag{5.59}$$

The matrix total volume, V_{mat}, is

$$V_{mat} = A_{f_{mat}} th_{mod} \tag{5.60}$$

Finally, the total matrix mass is given by

$$m_{mat} = \left(A_{f_{mat}} th_{mod}\right)\left(1 - \Psi_{mat}\right)\rho_{cer} \tag{5.61}$$

5.2.2.4.9 Heat-Transfer Areas and Matrix Conductance

The heat-transfer areas can now be calculated using equation (5.48) since the face areas and module thickness are known. For the hot and cold side, heat-transfer areas become

$$A_{h_{hot}} = A_{f_{hot}}\, th_{mod} \left(\frac{A_h}{V_{mat}}\right) \tag{5.62}$$

and

$$A_{h_{cold}} = A_{f_{cold}}\, th_{mod} \left(\frac{A_h}{V_{mat}}\right) \tag{5.63}$$

Note that by dividing the above two equations will show that the heat-transfer areas are in proportion to the face areas.

The conductance for both sides is solved using its definition:

$$\text{Conductance of hot side} \equiv \left(h_t A_h\right)_{hot} \tag{5.64}$$

$$\text{Conductance of cold side} \equiv \left(h_t A_h\right)_{cold} \tag{5.65}.$$

The conductance ratio is then defined as

$$\left(h_t A_h\right)' \equiv \frac{\left(h_t A_h\right)_{min}}{\left(h_t A_h\right)_{max}} \tag{5.66}.$$

Finally, the net conductance, UA_h, could be calculated from the conductance equation, (5.40), but can be easily determined using the NTU relations:

$$UA_h = NTU\left(\dot{m}c_P\right)_{min} \tag{5.67}.$$

5.2.2.4.10 Cold Side Pressure Drop

First, the cold-side flow velocity is needed using

$$\overline{C}_{cold} = \frac{\dot{m}_{cold}}{\overline{\rho}_{cold} A_{ff_{cold}}} \tag{5.68}.$$

The pressure drop is found using equation (5.47) evaluated at the cold-side mean values and then normalized by dividing by the cold-side mean pressure:

$$\left(\frac{\Delta P}{P}\right)_{cold} = \frac{\frac{1}{2}\left(\frac{C_f}{Re}\right)\left(\frac{A_h}{V_{mat}}\right)\frac{\overline{C}_{cold}\,\overline{\mu}_{cold}\,th_{mod}}{\Psi_{mat} d_h}}{\overline{P}_{cold}} \tag{5.69}.$$

As previously mentioned, the normalized pressure drop will be less on the cold side and may require mechanical methods to ensure proper flow distribution over the matrix [16].

5.2.2.4.11 Ceramic Matrix Temperature

Neglecting any transient effects, the heat transfer from the hot fluid (air) to the ceramic matrix equals the heat transfer from the ceramic matrix to the cold fluid (air). Evaluating at the mean temperatures gives

$$\left(h_t A_h\right)_{hot}\left(\overline{T}_{hot} - \overline{T}_{cer}\right) = \left(h_t A_h\right)_{cold}\left(\overline{T}_{cer} - \overline{T}_{cold}\right) \tag{5.70}.$$

Solving for the matrix temperature using the conductance ratio gives

$$\overline{T}_{cer} = \frac{\overline{T}_{hot} + \left(h_t A_h\right)' \overline{T}_{cold}}{1 + \left(h_t A_h\right)'} \tag{5.71}.$$

With the mean matrix temperature specified, properties such as the specific heat and thermal conductivity of the ceramic matrix can be calculated using the equations in Section A.1.

5.2.2.4.12 Matrix Mass-Flow Rate and Rotation Time

The matrix mass-flow rate, $\dot{m}_{mat}$, is needed to determine how fast the module/matrix moves (or rotates for the rotary case). The mass-flow rate can be evaluated using the definition of C_{rot} since all other values are known:

$$C_{rot} \equiv \frac{\left(\dot{m}\,\overline{c}_P\right)_{mat}}{\left(\dot{m}\,\overline{c}_P\right)_{min}} \tag{5.72}.$$

The time for a module to completely traverse the regenerator is given by

$$t_{rotation} = \frac{m_{mat}}{\dot{m}_{mat}} \tag{5.73}.$$

This is also the time for one rotation if the matrix is contiguous (rotary case).

5.2.2.5 Modular Specific Calculations

This section takes the results of the previous sections and applies them towards designing a modular regenerator. Methods for determining the module's mass, velocity, and forces are presented. In addition, the power required to move the modules is discussed. Finally, axial- conduction effects are investigated.

5.2.2.5.1 Module and Channel Size

The channel is the flow area for the fluid just leaving the inlet headers and entering the ceramic matrix. This is represented in Figure 5.1 and in Figure 5.4 below. Note from the figures that if the modules have solid-ceramic rims surrounding the core then the channel area would be a little greater than the face area to account for the rim-area exposed to the flow.

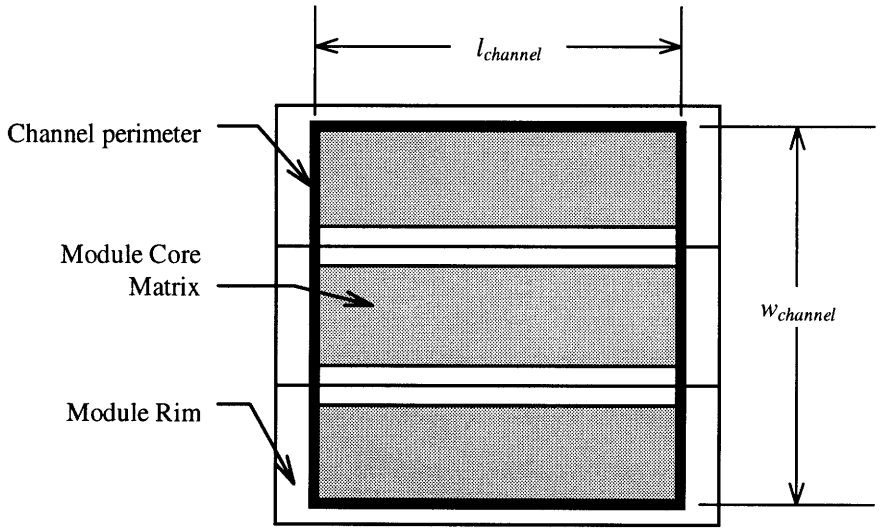

Figure 5.4 Channel configuration for one side of the regenerator showing the channel perimeter and the exposed matrix and rims.

With $AR_{channel_{cold}}$ specified, the cold-side channel dimensions can be found. Then by choosing dimensions for the module rim and using $Nmod_{cold}$, the module core

dimensions and the overall module dimensions are determined. Thereafter, the hot-side channel dimensions are obtained by using the chosen *FAR* and channel geometry.

This study chooses channel-geometry option A (see Section 4.2.2.3 for descriptions on the two options). This option stipulates that both channels (hot and cold) share identical channel lengths:

$$l_{channel_{hot}} = l_{channel_{cold}} \tag{5.74}.$$

Furthermore, this option dictates the number of modules not exposed to the flow, $Nmod_{unexposed}$, which is expressed as

$$Nmod_{unexposed} = Nmod_{cold}(FAR-1)+4 \tag{5.75}.$$

Note: If *FAR* is chosen to be unity, both channels will have the same aspect ratio and $Nmod_{unexposed}$ is fixed at 4 regardless of what channel-geometry option is used.

Module Rims

The module rim, composed of solid-ceramic material, is used for structural support and protection of the core matrix during module translation. Two dimensions for the rim are introduced. The width of the rim along the module sides is $w_{rim\text{-}side}$ and the width of the rim along the module's top and bottom faces is $w_{rim\text{-}top/bottom}$ (see Figure 5.2). The value for $w_{rim\text{-}side}$ should probably be larger than for $w_{rim\text{-}top/bottom}$ to withstand the loads on the side faces during transit (the loads on the module sides are more concentrated than on the top and bottom faces due to a smaller area) and the loads from the module-retention pins.

Cold-Side Channel Dimensions

The channel area will encompass *Nmod* number of modules. To maximize the heat-transfer performance, the total module rim-area exposed to the flow should be minimized. One method of doing this is to remove any rims along the periphery from the flow path within the channel. Thus, only the top and bottom rims of each module are exposed except

the modules at the very top and bottom of the channel (only one rim exposed each for those modules). This is shown in Figure 5.4.

The area of the cold-side channel may be written as

$$A_{channel\,cold} = A_{rim-exposed_{cold}} + A_{f_{cold}} \tag{5.76},$$

where the total rim area exposed to the flow on the cold side is

$$A_{rim-exposed_{cold}} = \left[2\, w_{rim-top/bottom}\left(\left(N\, mod_{cold} - 2\right)+1\right)\right] l_{channel_{cold}} \tag{5.77}.$$

Then, substituting in the definition of channel aspect ratio gives

$$\frac{\left(l_{channel\,cold}\right)^2}{AR_{channel_{cold}}} = \left[2\, w_{rim-top/bottom}\left(\left(N\, mod_{cold} - 2\right)+1\right)\right] l_{channel_{cold}} + A_{f_{cold}} \tag{5.78},$$

where $l_{channel}$ is solved for iteratively. Then $w_{channel}$ is calculated using the definition of $AR_{channel}$.

Multiplying the two channel dimensions yields the channel area. ζ_{mat} is defined as the proportion of channel area occupied by the core. For the cold-side, this is expressed as

$$\zeta_{mat_{cold}} = \frac{A_{f_{cold}}}{A_{channel_{cold}}} \tag{5.79}.$$

Module Dimensions and Sealing Distance

As shown in Figure 5.4, the length of the module core section equals the channel length, $l_{channel}$:

$$l_{mod-mat} = l_{channel_{cold}} \tag{5.80}.$$

The width of the module core section depends on the number of modules and the rim width for the top/bottom faces. This can be written as

$$w_{mod-mat} = \frac{w_{channel_{cold}} - 2w_{rim-top/bottom}\left[\left(Nmod_{cold} - 2\right)+1\right]}{Nmod_{cold}} \tag{5.81}.$$

After the dimensions for module core section are known, as a check, the core module area multiplied by *Nmod* should equal the face area.

The overall module dimensions are given by

$$l_{mod} = l_{mod-mat} + 2\,w_{rim-side} \tag{5.82}$$

and

$$w_{mod} = w_{mod-mat} + 2\,w_{rim-top/bottom} \tag{5.83}.$$

The sealing distance for the module-seal concept is the length of the perimeter of a module cross section multiplied by two (for each seal) which is:

$$dist_{seal} = 4\left(th_{mod} + w_{mod}\right) \tag{5.84}.$$

The seal distance is commonly referred as seal length. However, this analysis uses the term seal length, in the leakage calculations, as the length of the labyrinth seal in the direction of the leakage flow.

Number of Modules and Channel Dimensions for the Hot-Side

The number of modules on the hot side, $Nmod_{hot}$, is derived using

$$Nmod_{hot} = Nmod_{cold} FAR \tag{5.85}.$$

The hot-side channel width is then

$$w_{channel_{hot}} = w_{mod} Nmod_{hot} - 2w_{rim-top/bottom} \quad (5.86).$$

Then, the channel area and core-matrix area proportion are as follows:

$$A_{channel\,hot} = l_{channel\,hot} w_{channel_{hot}} \quad (5.87)$$

$$\zeta_{mat_{hot}} = \frac{A_{f_{hot}}}{A_{channel_{hot}}} \quad (5.88).$$

Overall Regenerator Dimensions

Assuming a seal length of module length for the module-seal concept, then the overall regenerator dimensions not including the headers, casing, or cylinders can be estimated with the following equations:

$$l_{regenerator} = 3l_{mod} \quad (5.89)$$

$$w_{regenerator} = \left(N\,mod_{hot} + 2\right) w_{mod} \quad (5.90).$$

5.2.2.5.2 Module and Regenerator Mass

The mass of the module-core section is computed using

$$m_{mod-mat} = \left(w_{mod-mat}\, l_{mod-mat}\, th_{mod}\right)\left(1 - \Psi_{mat}\right)\rho_{cer} \quad (5.91).$$

The mass of the module rims can be expressed as

$$m_{rim} = \left[\left(2\left(l_{mod} w_{rim-top/botttom} + w_{rim-side}\left(w_{mod-mat} + 2\, w_{rim-top/bottom}\right)\right)\right) th_{mod}\right]\rho_{rim} \quad (5.92).$$

If slots or fillets are used (slots are needed for the module retention mechanism and fillets are used to provide easier module entrance into the seal section), then the volume of all slots and fillets must be subtracted from the rim volume before computing the mass. The total mass of one module is simply

$$m_{mod} = m_{mod-mat} + m_{rim} \tag{5.93}.$$

The total mass of the regenerator (not including headers, casing, and actuators) is the mass of all modules:

$$m_{regenerator} = \left(Nmod_{cold} + Nmod_{hot} + Nmod_{unexposed}\right) m_{mod} \tag{5.94}.$$

5.2.2.5.3 Module-Movement Time and Velocities

This section outlines a method so that the designer can determine the duration of time when a module actually moves from one module location to the next (recall this is a one-module-movement cycle). With this information, movement profiles for acceleration, velocities, and displacement can be derived. The reader might want to review Section 4.2 to fully understand the various steps that occur during module movement.

This method begins by determining the time for a one-module-movement cycle, t_{mod}. This will also be called the time for module movement. This is an average time for a module to move to the next module location to give the specified heat-transfer performance. This is not necessarily the time when the module is actually moving. For example, if t_{mod} was equal 5 seconds, a module could move to the next module location in 2 seconds and then remain stationary for the remaining three (this is somewhat analogous the discontinuous-rotating regenerator). This type of movement actually has to occur for module motion. Movement in the present model is affected by a pneumatic cylinder that extends a piston rod to push on a module. The cylinder then has to retract to its original position for the next cycle, and the module remains stationary during this retraction step.

Therefore, the movement during cylinder-rod extension where the module is in motion will be termed "actual module movement.". If the time for cylinder-rod retraction is known, it is subtracted from t_{mod} , thus giving the time for actual module movement.

The time for module movement (one-module-movement cycle) is

$$t_{mod} = \frac{m_{mod}}{\dot{m}_{mat}} \tag{5.95}.$$

Therefore, the time for a module to completely traverse the regenerator and return to its initial location is t_{mod} multiplied by the total number of modules in the regenerator. This was actually derived earlier using equation (5.73).

Since the two-step module-movement process is used, the total time can be expressed as

$$t_{mod} = t_{mod-step1} + t_{mod-step2} \tag{5.96}.$$

The times for each step can be specified by introducing a chosen parameter, ξ_{step1}, which is the proportion of the time for module movement dedicated to step1. This is defined as

$$\xi_{step1} \equiv \frac{t_{mod-step1}}{t_{mod}} \tag{5.97}.$$

The time for step1 is calculated based on the chosen ξ_{step1}, and the time for step2 is found using equation (5.96).

The average module velocities for each step are as follows:

$$\bar{v}_{mod-step1} = \frac{l_{mod}}{t_{mod-step1}} \tag{5.98}$$

$$\bar{v}_{mod-step2} = \frac{w_{mod}}{t_{mod-step2}} \tag{5.99}.$$

The time for each module-movement step will then be divided into times for each cylinder-rod stroke. Choosing the proportion of time spent on the extension stroke, $\xi_{extension}$, defined as

$$\xi_{extension} \equiv \frac{t_{extension_{step\ 1\ or\ 2}}}{t_{mod\text{-}step\ 1\ or\ 2}} \qquad (5.100),$$

which allows $t_{extension}$, the time for the extension stroke (actual module movement), to be calculated. The time for the retraction stroke for either movement step is just

$$t_{retraction_{step1\ or\ 2}} = t_{step1\ or\ 2} - t_{extension_{step1\ or\ 2}} \qquad (5.101).$$

Earlier, two types of cylinder configurations were introduced. Cylinder configuration #1 was the general arrangement that requires two cylinder strokes (extension and retraction) for each of the module movement steps. Cylinder configuration #2 has hydraulically linked cylinders which requires an additional step1 cylinder stroke to return the cylinders at the original position. The stoke is an extension stroke but does not move a module. Therefore, the time specified in the above equation will be split to accommodate the added stroke.

The overall structure of how the times are broken down is shown in the next figure.

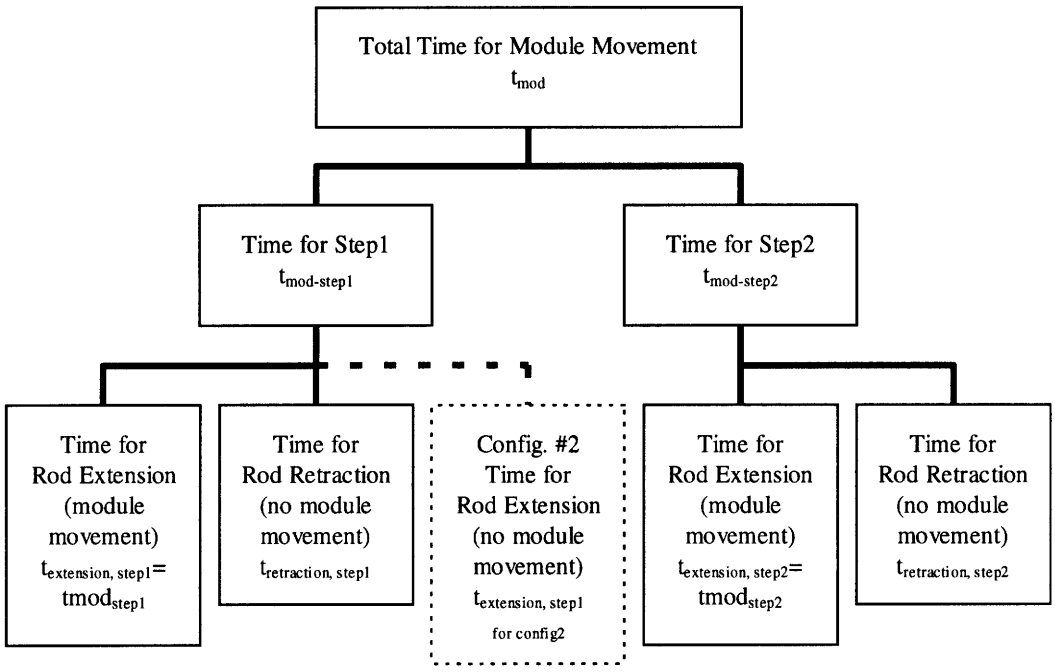

Figure 5.5 Module-movement time tree.

The following are some guidelines for specifying the time parameters:

- $\xi_{extension}$ should be selected to give the fastest allowable return stroke for the cylinder. This will maximize the time available for module movement and lower the acceleration and power required. The value selected probably will be large (relatively close to unity) since the retraction stroke does not experience any external resistance.
- The value for ξ_{step1} probably will be above 50 percent since the distance traveled for step1 is greater than step2. Moreover, ξ_{step1} affects the total power to move the modules since this parameter affects the accelerations of each step. ξ_{step1} should be chosen that minimizes the power (shown later).

In summary, the designer has a large degree of freedom in setting the times for module movement. The designer can set the time for each step and each stroke to provide the desired performance.

5.2.2.5.4 Movement Profiles for Actual Module Movement

This section presents a method to derive the module's acceleration, velocity, and displacement profiles. Choosing an acceleration profile will yield velocity and displacement profiles by integration (using two known parameters, the time for actual module movement and the distance traveled). This method will have to be performed twice to generate the profiles for each module-movement step.

As previously mentioned, actual-module-movement time is the time during cylinder-rod extension. This will be called *tmod*, and for each step this is

$$tmod_{step1} \equiv t_{extension_{step1}} \tag{5.102}$$

and

$$tmod_{step2} \equiv t_{extension_{step2}} \tag{5.103}.$$

The distance traveled during module movement is termed *dmod*. For step1, *dmod* is the length of a module and for step2, *dmod* is the width of a module. This is written as

$$dmod_{step1} = l_{mod} \tag{5.104}$$

and

$$dmod_{step2} = w_{mod} \tag{5.105}.$$

The acceleration profile is chosen to be sine wave of a half period. This was made because the sine function conveniently satisfies the boundary conditions of zero acceleration at the beginning and ending of actual module movement. Thus, the acceleration profile is

$$a_{mod}(t) = a_{max}\, sin\left(\frac{2\pi}{tmod}t\right) \tag{5.106},$$

where a_{max} is the maximum acceleration specified by the sine wave during actual module movement. The maximum acceleration is currently not known but can be solved (shown later in this section). Integrating with respect to time and applying the boundary condition (v_{mod}=0 at t = 0) gives the velocity profile:

$$v_{mod}(t) = \frac{-a_{max}\, tmod \cos\left(\frac{2\pi}{tmod} t\right) + a_{max}\, tmod}{2\pi} \tag{5.107}.$$

Integrating again with respect to time and applying the boundary conditions (s_{mod}=0 at t=0) gives the displacement profile:

$$s_{mod}(t) = \frac{-a_{max}\, tmod^2 \sin\left(\frac{2\pi}{tmod} t\right) + (2 a_{max}\, \pi\ tmod)\, t}{4\pi^2} \tag{5.108}.$$

The maximum acceleration can be determined using definitions of average velocity. The average velocity for actual module movement is just

$$\bar{v}_{mod} \equiv \frac{dmod}{tmod} \tag{5.109}.$$

In addition, the average velocity can be expressed using the integral definition for a function's average value. Thus, the average velocity is the integral of equation (5.106) divided by the time interval, *tmod*, which gives

$$\bar{v}_{mod} \equiv \frac{a_{max}\, tmod}{2\pi} \tag{5.110}.$$

Equating the above two equations and solving for a_{max} results in

$$a_{max} = \frac{2\pi\, dmod}{tmod^2} \tag{5.111}.$$

Substituting a_{max} into equations (5.106), (5.107), and (5.108) reduces to the following movement profile functions:

$$a_{mod}(t) = \frac{2\pi\, dmod}{tmod^2} sin\left(\frac{2\pi}{tmod} t\right) \tag{5.112}$$

$$v_{mod}(t) = \frac{dmod}{tmod}\left[1 - cos\left(\frac{2\pi}{tmod} t\right)\right] \tag{5.113}$$

$$s_{mod}(t) = \frac{dmod}{tmod} t - \frac{dmod}{2\pi} sin\left(\frac{2\pi}{tmod} t\right) \tag{5.114}.$$

Therefore, to get the profile functions for a particular movement step, all that is required is the appropriate *tmod* and *dmod* from equations (5.102) to (5.105).

5.2.2.5.5 Module Forces

For a cylinder to accelerate a module with the profiles in the previous section, it must overcome any resistive forces. For module-movement step1, the resistive forces are pressure and friction. For step2, the resistive force is friction and/or gravity depending on the regenerator orientation. This section presents methods to determine the force required for module movement by conducting a force balance on the modules. A force balance is made for both module movement steps. The analysis is further broken down for the two cylinder configurations and the two regenerator orientations presented earlier. These options were conceived mainly to obtain optimal results for the force and power requirements.

The following are some conventions, assumptions, and general notes pertaining to the force calculations:

- During movement within the seals, the modules are assumed to be in contact with only one seal face. This assumption is made to estimate the frictional forces for step1.

- The cross-sectional area of the cylinder rod is required when calculating the pressure forces. The rod should be sized to withstand the compressive loading placed on it. Data for sizing the cylinder rods for a specific application can be found in the *Design Engineers Handbook* by Parker Fluidpower [17].
- For step1 movement, 2 modules move together through each seal.
- For step2 movement, $Nmod_{hot}$+1 modules move together within hot side and $Nmod_{cold}$+1 modules move together within cold side.
- Some force terms in this section will contain subscripts with "high" and "low" which denote the pressure force from the high and low-pressure side respectively.
- The pressures acting on the modules are assumed to be mean pressures for the hot and cold sides calculated in 5.2.2.3.2
- The cylinder's piston-rod diameter is a chosen parameter required for step1 force computations. All cylinders used in step1 are assumed to share the same rod diameter. The cylinder-rod cross-sectional area of the, A_{rod}, is determined using:

$$A_{rod} = \pi \left(\frac{d_{rod}}{2} \right)^2 \tag{5.115}.$$

Free-body diagrams are used to determine the force required during movement. These diagrams for the various movement steps and configurations are shown next.

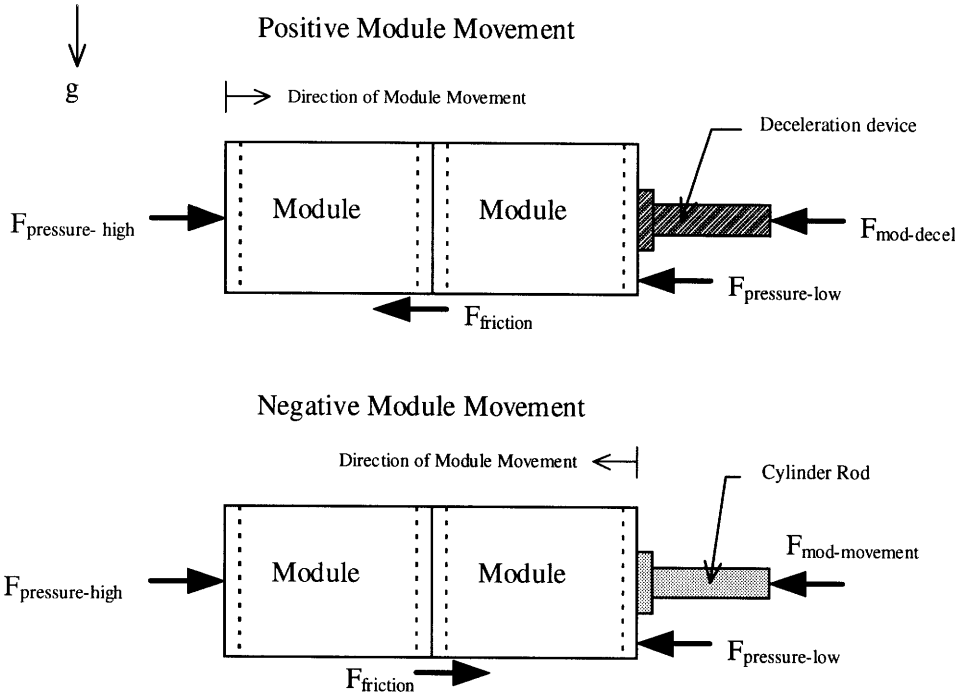

Figure 5.6 Free-body diagrams for module-movement step1, configuration #1.

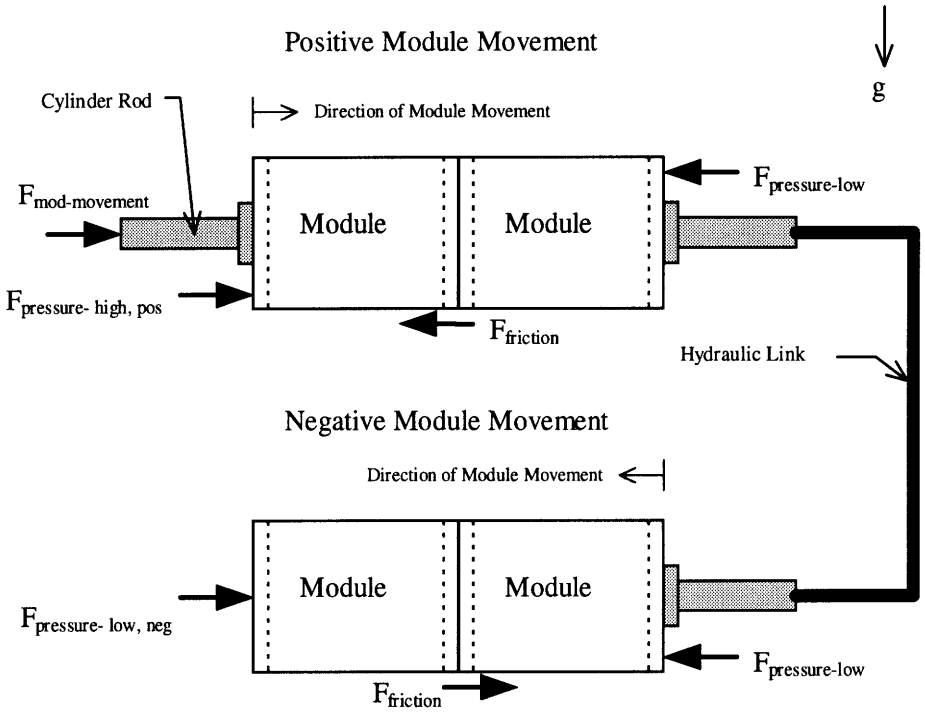

Figure 5.7 Free-body diagrams for module-movement step1, configuration #2.

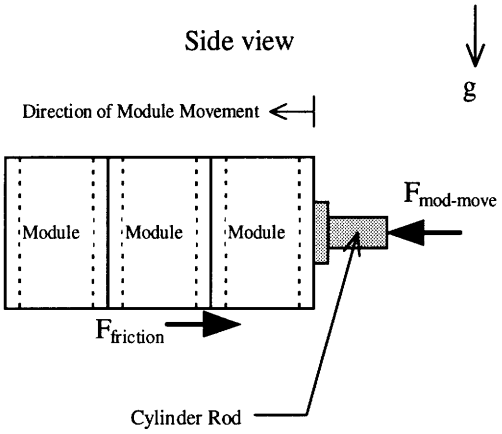

Figure 5.8 Free-body diagram for module-movement step2, orientation #1.

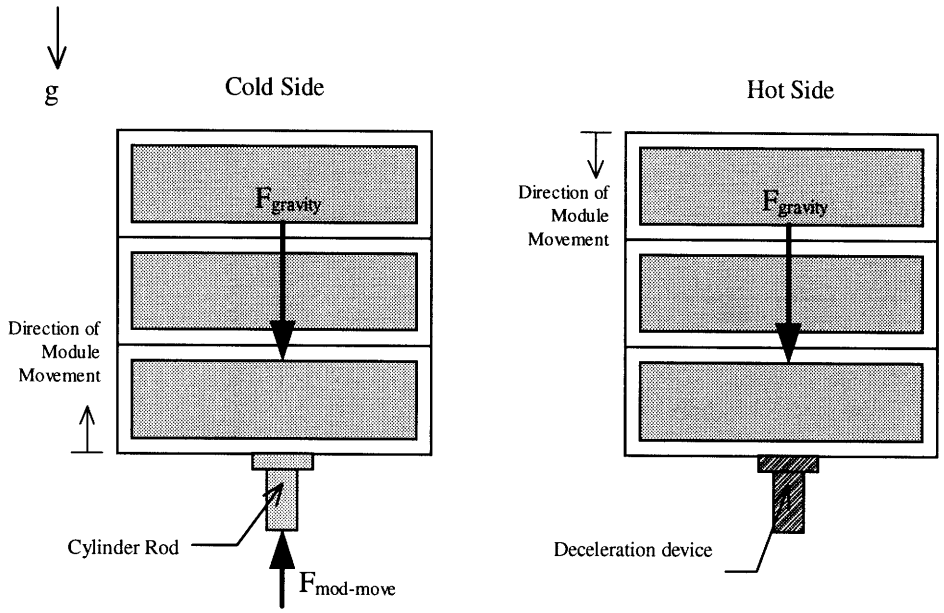

Figure 5.9 Free-body diagram for module-movement step2, orientation #2.

Forces For Step1, Cylinder Configuration #1

The forces on a module moving within the seals are dependent on the regenerator's cylinder configuration. With configuration #1, the cylinder must impart a large enough force on its piston to primarily overcome the pressure force during negative module movement. For positive module movement, the pressure force acts in the direction of travel thus no mechanical devices are required for movement. Nevertheless, a device that provides controlled linear deceleration such as a gas spring or an industrial shock absorber is required.

Using Newton's Second Law and summing forces for negative module movement in Figure 5.6 gives

$$\left(F_{mod-movement} + F_{pressure-low} - F_{pressure-high} - F_{friction}\right)_{step1,config1} = \left(2\,m_{mod}\right)a_{mod}(t) \qquad (5.116).$$

The pressure and frictional forces are as follows:

$$F_{pressure-low_{step1,config1}} = \overline{P}_{hot}\left(th_{mod}\, w_{mod} - A_{rod}\right) \tag{5.117}$$

$$F_{pressure-high_{step1,config1}} = \overline{P}_{cold}\, th_{mod}\, w_{mod} \tag{5.118}$$

$$F_{friction_{step1,config1}} = \mu_{s_{mod}}\left(2\, m_{mod}\right)g \tag{5.119}.$$

Solving for the required cylinder force for movement gives

$$\begin{aligned} F_{mod-movement_{step1,config1}} &= \overline{P}_{cold}\, th_{mod}\, w_{mod} - \overline{P}_{hot}\left(th_{mod}\, w_{mod} - A_{rod}\right) \\ &\quad +\mu_{s_{mod}}\left(2\, m_{mod}\right)g + \left(2\, m_{mod}\right)a_{mod}(t) \end{aligned} \tag{5.120},$$

where the acceleration term is given by equation (5.112).

Therefore, the net resistive pressure force is

$$\left(F_{pressure_{step1,config1}}\right)_{net} = \overline{P}_{cold}\, th_{mod}\, w_{mod} - \overline{P}_{hot}\left(th_{mod}\, w_{mod} - A_{rod}\right) \tag{5.121}.$$

For positive module movement, using Newton's Law gives (specifying that the rod for the deceleration device has the same cross-sectional area as the cylinder rod)

$$F_{pressure-high} - F_{pressure-low} - F_{friction} - F_{mod-decel} = \left(2\, m_{mod}\right)a_{mod}(t) \tag{5.122},$$

where $F_{mod\text{-}decel}$ is the force on the deceleration device.

Finally, substituting in the pressure and frictional forces, equations (5.117)-(5.119), into the above equation and solving for the deceleration-device force results in

$$\begin{aligned} F_{mod-decel} &= \overline{P}_{cold}\, th_{mod}\, w_{mod} - \overline{P}_{hot}\left(th_{mod}\, w_{mod} - A_{rod}\right) \\ &\quad -\mu_{s_{mod}}\left(2\, m_{mod}\right)g - \left(2\, m_{mod}\right)a_{mod}(t) \end{aligned} \tag{5.123}.$$

Therefore, the deceleration device must be sized to handle the loading specified above.

Forces For Step1, Cylinder Configuration #2

Configuration #2 was specifically conceived to reduce the large pressure force during negative module movement (see Section 4.2.4.2 for detailed description). Two hydraulically-linked cylinders transfer the module forces for negative module movement to the modules for positive module movement thus balancing the whole system. The result is a lower force required for movement. A small pressure force still occurs with this system since the module entering the high-pressure side during negative movement has a larger wetted area for the pressure force (see Figure 5.7).

Only one cylinder is needed to initiate the two movements (positive and negative) since the linked cylinders provide identical translation but in the opposite directions. This cylinder is positioned on the cold side for positive module movement.

Using Newton's Second Law and summing forces for the whole system in Figure 5.7 gives

$$\left(F_{mod-movement} + F_{pressure-high,pos} - F_{pressure-low} + F_{pressure-low} - F_{pressure-high,neg} - F_{friction}\right)_{step1,config2} = \left(4m_{mod}\right)a_{mod}(t) \quad (5.124).$$

Note that 4 modules are moved simultaneously for this step. As shown in the above equation, the two low-pressure forces cancel. The cold-side pressure forces on the modules during positive and negative movement are

$$F_{pressure-high,pos\,step1,config2} = \overline{P}_{cold}\left(th_{mod}\, w_{mod} - A_{rod}\right) \quad (5.125)$$

and

$$F_{pressure-high,neg\,step1,config2} = \overline{P}_{cold}\, th_{mod}\, w_{mod} \quad (5.126).$$

The frictional force is

$$F_{friction_{step1,config2}} = \mu_{s_{mod}} (4m_{mod}) g \tag{5.127}.$$

Solving for the required cylinder force for movement simplifies to

$$F_{mod-movement_{step1,config2}} = \overline{P}_{cold} A_{rod} + \mu_{s_{mod}} (4\, m_{mod}) g + (2\, m_{mod}) a_{mod}(t) \tag{5.128},$$

where the acceleration term is taken from equation (5.112).

Thus, the net resistive pressure force is

$$\left(F_{pressure_{step1,config2}}\right)_{net} = \overline{P}_{cold} A_{rod} \tag{5.129}.$$

The two pressure forces for each configuration can be compared. Taking the net pressure force for configuration #1, equation (5.121), and subtracting the pressure force for configuration #2 shown above gives

$$\begin{aligned}\left(\Delta F_{pressure}\right)_{config1-config2} &= \left(\overline{P}_{cold} - \overline{P}_{hot}\right)\left(th_{mod}\, w_{mod} - A_{rod}\right) \\ &+\mu_{s_{mod}} (2\, m_{mod}) g + (2\, m_{mod}) a_{mod}(t)\end{aligned} \tag{5.130}.$$

This is the increase in pressure force switching from cylinder configuration #2 to #1. This will ultimately lead to a larger power requirement as shown in later sections. Numerical results shown later indicate that is force is quite larger thus reinforcing the recommendation that configuration #2 should be used.

Forces For Step2, Regenerator Orientation #1

Orientation #1 places the regenerator in a horizontal plane. Therefore, the regenerator would be placed directly above the gas-turbine engine. The cylinder for

module movement only needs to overcome frictional resistance as shown in Figure 5.8. Two cylinders are required to move the modules, one for each side.

Using Figure 5.8 to make a force balance considering only movement on the cold side gives

$$\left(F_{mod-movement} - F_{friction}\right)_{step2,orient1,cold} = m_{mod}\left(Nmod_{cold}+1\right)a_{mod}(t) \qquad (5.131),$$

where the frictional force is

$$F_{friction_{step2,orient1,cold}} = \mu_{s_{mod}}\left(Nmod_{cold}+1\right)g \qquad (5.132).$$

Solving for the required module-movement force reduces to

$$F_{mod-movement_{step2,orient1,cold}} = \left(Nmod_{cold}+1\right)\left[\mu_{s_{mod}}g + m_{mod}a_{mod}(t)\right] \qquad (5.133),$$

where the acceleration term is found from equation (5.112).

If FAR=1, then the cylinder on the hot side would have identical result as shown above. If $FAR \neq 1$, the forces can be determined by using the above equations and replacing $Nmod_{cold}$ with $Nmod_{hot}$.

Forces For Step2, Regenerator Orientation #2

With Orientation #2, the regenerator is mounted horizontally. Only one cylinder, on the cold-side, is required to provide the movement. A deceleration device is required to slow the module down on the hot side. All resistive forces are gravitational forces as shown in Figure 5.8. Some frictional forces probably exist but they are assumed to be negligible.

Making a force balance on the cold side by using Figure 5.9 gives

$$\left(F_{mod-movement} - F_{gravity}\right)_{step2,orient2,cold} = \left(Nmod_{cold}+1\right)a_{mod}(t) \qquad (5.134),$$

where the gravitational force is

$$F_{gravity_{step2,orient2,cold}} = \left(Nmod_{cold} + 1\right) m_{mod}\, g \tag{5.135}.$$

Solving for the required module-movement force simplifies to

$$F_{mod-movement_{step2,orient2,cold}} = \left(Nmod_{cold} + 1\right)\left[m_{mod}\, g + a_{mod}(t)\right] \tag{5.136},$$

where the acceleration term is found from equation (5.112).

If FAR=1, then the deceleration device used on the hot side would be sized to handle the same force specified in equation (5.136). If $FAR \neq 1$, replacing $Nmod_{cold}$ with $Nmod_{hot}$ will give the force on the deceleration device.

5.2.2.5.6 Cylinder Sizing

This section presents a method for determining the minimum bore size of the cylinders. The cylinders must be sized to provide at least the maximum force required for module movement. As shown in the above section, the force varies sinusoidally. Therefore, the maximum force is determined by taking the force equations for module movement, (5.120), (5.128), (5.133), and (5.136), and then setting the time varying acceleration term to just the maximum value specified in equation (5.111). Cylinder size is dependent on the pressure fed into the cylinder. The gas-turbine engine could be outfitted with an auxiliary compressor to provide the feed air or the gas-generator compressor could be used. The auxiliary-compressor option provides more flexibility over using the gas-generator compressor. Having the freedom to specify the type of compressor allows flexibility in deciding the cylinder size. With the gas-generator-compressor option, the cylinder is fixed to a particular bore size that may not provide satisfactory results.

The minimum cylinder-bore area is calculated by the following

$$(A_{bore})_{min} = \frac{(F_{mod-movement})_{max}}{P_{feed}} \qquad (5.137),$$

where $(F_{mod\text{-}movment})_{max}$ is the maximum force for module movement and P_{feed} is the feed pressure in the cylinder.

Most pneumatic and hydraulic cylinder manufacturers specify the sizes by using the bore diameter. The minimum bore diameter is can be determined by

$$(d_{bore})_{min} = \sqrt{\frac{4(F_{mod-movement})_{max}}{\pi P_{feed}}} \qquad (5.138).$$

5.2.2.5.7 Power Requirement for Module Movement

This section presents a method to calculate the power requirement for module movement. Average power values for the two module movement steps are calculated and then added to obtain the power requirement for the regenerator. Each step has two options to choose from which gives four power results. The results should be used as a criterion when selecting the desired regenerator option. The following lists some assumptions and notes about the power requirement derivations:

- The method presented assumes that the power to move the rods back to the initial position (rod retraction) is negligible.
- The power is derived by calculating the work done by the module movement forces, as computed in Section 5.2.2.5.5. Then the average power is obtained taking the work and dividing by the time interval during module movement.
- The acceleration profile is a sine function where positive acceleration occurs during the first half of the time interval and negative acceleration during the second half. The power just to accelerate the modules to this profile is accounted only during positive

acceleration (first half of time interval). This is justified by several reasons. First, power is not needed to slow a module down when resistive forces exist that can do this job. Next, if the power accounted for the acceleration during the entire time interval, the net work would equal zero and thus zero power. Modeling the power this way is taking all of the kinetic energy back so the net acceleration energy is zero, which should not be the case. In summary, the power should account only for providing positive acceleration and overcoming resistive forces over the first half of the time interval, and accounts for overcoming only the resistive forces in the second half. As a result, the work calculations are made over two equal time intervals.

This analysis begins by deriving the power requirement on a generic basis. Afterwards, the guidelines are given on how to modify the power equation to apply to a particular step and option. The terms *dmod* and *tmod* (defined in Section 5.2.2.5.4) will be used in this generic analysis.

Generic Power Equations

First some basic definitions are given. Work done by the module-movement forces over a finite path from an initial location, s_i , to a final location, s_f, is defined as

$$W_{mod} \equiv \int_{s_i}^{s_f} F_{mod-movement}\, ds \qquad (5.139).$$

The power is defined as the time rate of doing work thus for module movement:

$$\dot{W}_{mod} \equiv \frac{dW_{mod}}{dt} \qquad (5.140).$$

The average power for this case is defined as

$$\overline{\dot{W}}_{mod} \equiv \frac{W_{mod}}{tmod} \qquad (5.141).$$

The force for module movement is basically the sum of the mass-acceleration term and any resistive forces. This can be represented as

$$F_{mod-movement_{general}} = m_{general} a_{mod}(t) + F_{resistive_{general}} \tag{5.142},$$

where the general subscript denotes a generic term. Notice that the work equation has a differential with respect to displacement but the force is function of time. Therefore, the work equation is changed to a time integral using the chain rule:

$$W_{mod} = \int_0^{t\,mod} F_{mod-movement}(t)\frac{ds}{dt}dt \tag{5.143}.$$

The differential, $\frac{ds}{dt}$, is the velocity shown in equation (5.113):

$$\frac{ds}{dt} = \frac{dmod}{tmod}\left[1 - cos\left(\frac{2\pi}{tmod}t\right)\right] \tag{5.144}.$$

Substituting equations(5.142) and (5.144) into (5.143) yields

$$W_{mod} = \int_0^{tmod}\left(m_{general}a_{mod}(t) + F_{resistive_{general}}\right)\frac{dmod}{tmod}\left[1 - cos\left(\frac{2\pi}{tmod}t\right)\right]dt \tag{5.145}.$$

Recall that work is split into two time intervals with the acceleration accounted for only during the first interval. This can be written as

$$\begin{aligned} W_{mod} = &\int_0^{\frac{tmod}{2}}\left(m_{general}a_{mod}(t) + F_{resistive_{general}}\right)\frac{dmod}{tmod}\left[1 - cos\left(\frac{2\pi}{tmod}t\right)\right]dt \\ &+ \int_{\frac{tmod}{2}}^{tmod} F_{resistive_{general}}\frac{dmod}{tmod}\left[1 - cos\left(\frac{2\pi}{tmod}t\right)\right]dt \end{aligned} \tag{5.146}.$$

Substituting in the acceleration from equation (5.112) and evaluating the integral yields

$$W_{mod} = \left[\frac{dmod\, F_{resistive_{general}}}{2} + \frac{2\, dmod^2\, m_{general}}{t\, mod^2} \right] + \left[\frac{dmod\, F_{resistive_{general}}}{2} \right] \qquad (5.147),$$

where the bracketed terms are the work for each time interval.

The average power is obtained by substituting in the above result into equation (5.141). This simplifies to the generic power-requirement for module movement:

$$\overline{\dot{W}}_{mod} = \frac{dmod\, F_{resistive_{general}}}{t\, mod} + \frac{2\, dmod^2\, m_{general}}{t\, mod^3} \qquad (5.148).$$

Dividing the power equation by the gas-turbine power output, equation (5.19), gives the normalized power-requirement:

$$\hat{\dot{W}}_{mod} = \frac{\overline{\dot{W}}_{mod}}{\dot{W}_{GT}} \qquad (5.149).$$

Power Requirement For Each Step and Option

To get the power requirement for a particular step and option, substitute the following into the generic power equations:

<u>For Step1, Cylinder Configuration #1</u>

- equation (5.102) for *tmod*
- equation (5.104) for *dmod*
- the sum the right hand side of equations (5.119) and (5.121) for $F_{resistive_{general}}$.
- $2\, m_{mod}$ for $m_{general}$

<u>For Step1, Cylinder Configuration #2</u>

- equations (5.102) for *tmod*
- equation (5.104) for *dmod*

- the sum the right hand side of equations (5.127) and (5.129) for $F_{resistive_{general}}$.
- 4 m_{mod} for $m_{general}$

For Step2, Regenerator Orientation #1

This option has two cylinders, one for module movement on the hot side and the other for module movement on the cold side. To get the power for the cold side, substitute in the following into the generic power equation:

- equation (5.103) for *tmod*
- equation (5.105) for *dmod*
- the right hand side of equation (5.132) for $F_{resistive_{general}}$.
- ($Nmod_{cold}$ + 1) for $m_{general}$

To get the power for the hot side, substitute in the same information except for the last bullet, where ($Nmod_{hot}$ +1) is substituted into $m_{general}$.

Then the net power for this option is

$$\dot{W}_{step2,orient1} = \dot{W}_{step2,orient1_{cold}} + \dot{W}_{step2,orient1_{hot}} \qquad (5.150).$$

For Step2, Regenerator Orientation #2

- equation (5.103) for *tmod*
- equation (5.105) for *dmod*
- the right hand side of equation (5.135) for $F_{resistive_{general}}$.
- ($Nmod_{cold}$ + 1) for $m_{general}$

Total Power

The total power requirement for the regenerator is the sum of the power for step1 and step2. With two options for each step, 4 total power results are made. This is summarized as shown in the following:

$$\left(\hat{\dot{W}}_{mod}\right)_{config1,orient1} = \frac{\dot{W}_{step1,config1} + \dot{W}_{step2,orient1}}{\dot{W}_{GT}} \tag{5.151}$$

$$\left(\hat{\dot{W}}_{mod}\right)_{config1,orient2} = \frac{\dot{W}_{step1,config1} + \dot{W}_{step2,orient2}}{\dot{W}_{GT}} \tag{5.152}$$

$$\left(\hat{\dot{W}}_{mod}\right)_{config2,orient1} = \frac{\dot{W}_{step1,config2} + \dot{W}_{step2,orient1}}{\dot{W}_{GT}} \tag{5.153}$$

$$\left(\hat{\dot{W}}_{mod}\right)_{config2,orient2} = \frac{\dot{W}_{step1,config2} + \dot{W}_{step2,orient2}}{\dot{W}_{GT}} \tag{5.154}.$$

Wilson [18] suggests that the normalized total power requirement should fall within one percent for typical designs. Numerical results using the power equations will be shown later and this power limit will be used to dictate the preferred configuration.

5.2.2.5.8 Axial Conduction

The thermal conductivity of the ceramic-matrix material is considerably greater than the conductivity of the fluid flowing through the matrix. As a result, conduction in the flow direction within the matrix walls, called axial conduction, may be significant. With axial conduction present, the heat contained in the ceramic material flows from the hot locations to the cold locations. Consequently, the temperature gradient for the matrix

decreases. The ultimate detrimental effect is a reduction in regenerator effectiveness. This section addresses the axial-conduction effects for a modular regenerator.

Beck [4 and 19] investigated axial conduction for regenerators taking into account the portion of the matrix under the seals (called "seal width" by Beck), not exposed to the flow. His results concluded that consideration of the seal width can increase axial-conduction effects by a factor of two. This is of particular concern for modular designs since a considerable portion of the matrix is not exposed to the flow. Beck gives a computer algorithm (commands for Matlab) to compute the regenerator effectiveness considering axial conduction with seal-width effects. The algorithm uses a finite difference technique first developed by Bahnke and Howard [20]. The following outlines a method using Beck's analysis in determining the axial-conduction effects (drop in effectiveness) for a modular regenerator.

Seven parameters are required by the algorithm to compute effectiveness (note that the parameter nomenclature presented is consistent with Beck's to avoid confusion when applying his analysis). Four parameters, NTU, C_{rat}, C_{rot}, and $(h_tA_h)'$ are already known. The remaining three are shown below.

The first parameter is seal coverage, SC, which is defined as the percentage of matrix area not exposed the flow. This can be written for the modular case as

$$SC = \frac{Nmod_{unexposed}}{Nmod_{unexposed} + Nmod_{cold} + Nmod_{hot}} \tag{5.155}.$$

Next is the heat-conduction available-area ratio, As', defined as

$$As' \equiv \frac{(As)_{min\ heat\ capacity\ side}}{(As)_{max\ heat\ capacity\ side}} \equiv \frac{As_N}{As_X} \tag{5.156},$$

where *As* is the matrix-material area available for heat conduction. *As* is essentially the cross-sectional area of the matrix exposed to the flow which can be shown for both sides as

$$As_N = A_{f_{cold}}\left(1-\Psi_{mat}\right) \tag{5.157}$$

$$As_X = A_{f_{hot}}\left(1-\Psi_{mat}\right) \tag{5.158}.$$

Thus As' is just the inverse of *FAR*:

$$As' = \frac{1}{FAR} \tag{5.159}.$$

The final parameter is the axial-conduction parameter, λ, which is a dimensionless variable that measures the axial-conduction effects. The axial-conduction parameter is defined as

$$\lambda \equiv \frac{k_{cer}\, As_N}{\left(\dot{m}\, c_P\right)_{min}\, th_{mod}}\left(\frac{1+As'}{As'}\right) \tag{5.160},$$

where k_{cer} is the thermal conductivity of the ceramic matrix evaluated at the ceramic mean temperature, equation (5.71), using equation (A.2) in the Appendix.

With all seven parameters specified, they are inputted into the algorithm to estimate the effectiveness accounting for axial conduction, $\hat{\varepsilon}_{acsw}$. Then the algorithm is run a second time but λ is changed to zero to get the effectiveness estimate assuming no axial conduction, $\hat{\varepsilon}_{nc}$. The axial conduction and seal-width effect is measured by defining

$$\left(\frac{\Delta\varepsilon}{\varepsilon}\right)_{acsw} \equiv \frac{\hat{\varepsilon}_{acsw}-\hat{\varepsilon}_{nc}}{\hat{\varepsilon}_{nc}} \tag{5.161}$$

which gives a normalized effectiveness drop.

5.2.3 Discussion and Summary

With the designated chosen parameters from Section 5.2.2.2, the modular regenerator can be sized and its performance measured using the design method just presented. The method could easily be modified to include other parameters as initial choices. Numerical results of this method are shown in later sections.

The following are some general observations made after deriving the design method.

- Configuration #2 provides a substantial reduction of the resistive forces as shown in equation (5.130). This large force drop should translate to a much lower power requirement. Actual numerical comparison verifying the force and power reduction will be shown in subsequent sections. Note that the friction force doubles with configuration #2 (as compared to #1) since the number of modules double, but this increase will be small compared to the reduction in pressure force.
- If using the two-step-movement process, the module movement for both sides must be in sync with each other during step2. Configuration #2 and orientation #1 should provide better results in performing synchronous movement since both use just cylinders for module movement. Configuration #1 and Orientation #2 uses two different mechanical devices, cylinders and deceleration devices. Matching theses two types of mechanisms for synchronous movement will require further analysis and could pose some timing problems.
- When setting the module velocities, the designer must take this into the mechanical constraints set by the particular cylinder system used. The fluid flow in the connecting lines may limit the velocity of the cylinder piston rod. Data on piston speeds for cylinders can be found in Parker Fluidpower [17] and should be correlated with the derived velocities in this analysis.

5.3 Design Optimization

5.3.1 Introduction

The initial chosen parameters designated in Section 5.2.2.2 dictate the outcome of the regenerator design. Choosing values resulting in an optimum design is not always an easy and direct task because varying a choice could provide beneficial and/or detrimental effects. Therefore, knowledge of how the choice affects the overall design is pertinent if the designer wants to optimize the regenerator to the desired specification. Choosing particular values for some parameters were straightforward because the parameter defined a desired result or was based on conclusions drawn from previous analyses for rotary regenerators. Selecting values for other parameters required numerous design iterations until satisfactory results were achieved. The purpose of this section is to give the designer some insight on how one parameter can influence other design factors.

The following section first assigns numerical values to the designated chosen parameters. After performing the design calculations outlined in the previous section, results are presented when varying certain parameters and keeping all others constant. Then a discussion is made on how these particular parameters were finally chosen. Not all chosen parameters are varied in this analysis, only the ones with possible significant design impacts or with unclear optimum values.

5.3.2 Numerical Values for Chosen Parameters

This section presents numerical values for the designated chosen parameters and the justification for the choice. Note that the following tables contain the final design choices. The reason for presenting the final choices in this section was that these values were the final chosen parameters for Section 5.3.3 analysis.

5.3.2.1 Engine Parameters

This analysis uses a hypothetical engine with the specified cycle properties listed in Table 5.5. The engine parameters specified are representative for a small gas turbine that could be fitted with a rotary regenerator. This size of gas-turbine engine is used so a direct comparison can be made between modular and rotary designs. Recall that the rotary design cannot be used for large gas turbines due to the limits on rotary regenerator sizes. Note: the temperatures and pressures given in the next table are stagnation (total) values.

Engine Parameter	Chosen Specification
compressor-inlet temperature, T_1	300 K
compressor-inlet pressure, P_1	$1 \cdot 10^5$ Pa
compressor pressure ratio, r	2
compressor total-to-total polytropic efficiency, $\eta_{poly,1\text{-}2}$	0.82
turbine inlet temperature, T_4	1400 K
heat exchanger outlet pressure, P_6	$1 \cdot 10^5$ Pa
turbine total-to-total polytropic efficiency, $\eta_{poly,4\text{-}5}$	0.90
compressor mass-flow rate, $\dot{m}_{1\text{-}2}$	1 kg/sec
$\sum\left(\frac{\Delta P}{P}\right)$, normalized pressure drops in cycle	0.08

Table 5.5 Gas-turbine engine specifications.

5.3.2.2 Regenerator-Performance Parameters

The values for the performance parameters are shown in Table 5.6. For effectiveness, the value chosen is based on the performance goal that the regenerator

should have a high effectiveness. Analysis of how effectiveness affects the design is discussed in Section 5.3.3.

For hot-side pressure drop, the chosen value of one percent is a conservative lower limit for typical heat exchangers for small gas turbines. If a smaller heat exchanger (or smaller face area) is required, then the designer should consider choosing pressure drops between 2 to 4 percent [21].

As shown in Figure 1.5, as the total cycle pressure drop increases, the thermal efficiency and specific power decrease. The total pressure drop is the sum of the individual component pressure drops so when the hot-side pressure drop is increased, the effect is just added to the cycle pressure drop. Furthermore, the regenerator headers for each side and the combustor will contribute to the total cycle pressure. When accounting for all components, the one percent value seems reasonable.

The leakage was arbitrarily chosen to give a value representative for the modular case. For C_{rot}, increasing the value increases effectiveness (beneficial effect) but also increases carry-over leakage and the required power for matrix/module movement (detrimental effects) [13]. Hagler [12] determined that setting $C_{rot} = 3.0$ provided optimal results. Furthermore, Beck [19] showed that $C_{rot} = 3.0$ does not incur any significant axial-conduction penalties.

Regenerator-Performance Parameter	Chosen Specification
effectiveness, ε	0.95
$\left(\frac{\Delta P_{hot}}{P_{hot}}\right)$, hot-side core pressure drop	0.01
$\dot{m}_{leak}/\dot{m}_{1\text{-}2}$, normalized regenerator leakage	0.02
C_{rot}	3.0

Table 5.6 Regenerator-performance specifications.

5.3.2.3 Regenerator-Matrix Parameters

The chosen matrix is based on the results in Chapter 3. The matrix consists of extruded MAS (Corning "Celcor" cordierite composition) material with rectangular passages. The ceramic solid density can vary depending on the type of cordierite composition so a value representative of typical cordierite compositions was chosen [22]. Other material properties for the cordierite material are presented in the Appendix.

Porosity was chosen based on typical rotary matrix cores that have high porosities around 70 percent. This value is close to the upper limit of manufacturing capabilities [5]. Values for hydraulic diameter and passage aspect ratio were chosen after making several design iterations and using the analysis in Section 5.3.3. The coefficient of static friction was chosen as a worst-case estimate based on experiments of ceramic matrices sliding on graphite surfaces conducted by Pfahnl [23].

Regenerator-Matrix Parameter	Chosen Specification
material composition	Extruded cordierite (MAS)
ceramic solid density, ρ_{cer}	2050 kg/m^3
porosity, Ψ	0.70
hydraulic diameter, d_h	0.82E-3 m
passage aspect ratio, AR_{pass}	4.0
matrix coefficient of static friction, $\mu_{s,mat}$	0.4

Table 5.7 Regenerator-matrix specifications.

5.3.2.4 Regenerator-Configuration Parameters

The chosen values pertaining to the regenerator configuration are listed in Table 5.8. Choosing $FAR = 1$ when $AR_{channel} = 1$ gives the simplest configuration for module movement. Otherwise some complex module-movement schemes will be required. The cold-side number of modules was chosen as a result of design iterations (see Section 5.3.3 for the analysis of how FAR and $Nmod_{cold}$ can affect other design values). The time proportion for step1 was chosen to minimize the power requirement. The time proportion for extension stroke is arbitrarily chosen. The module rim widths were also arbitrarily chosen. Additional studies will be required to optimize the rim dimensions. Finally, the cylinder-piston-rod diameter was chosen based on data from Parker Fluidpower [17].

Regenerator-Configuration Parameter	Chosen Specification
face-area ratio, FAR	1.0
channel aspect ratio, $AR_{channel}$	1.0
number of modules exposed on cold side, $Nmod_{cold}$	6
time proportion for step1 module movement, ξ_{step1}	0.70
time proportion for cylinder rod extension stroke, $\xi_{extension}$	0.75
side-rim width of module, $w_{rim\text{-}side}$	0.005 m
top/bottom-rim width of module, $w_{rim\text{-}top/bottom}$	0.015 m
cylinder piston rod diameter, dia_{rod}	0.025 m

Table 5.8 Regenerator-configuration specifications.

5.3.3 Varying Chosen Parameters

This section employs the sizing and performance method using the values assigned from the previous section. A chosen parameter is varied keeping all others constant to analyze what important design factors changed. With this knowledge, the designer should be able to optimize some of these choices.

Nine chosen parameters are varied. These nine, mainly parameters that can dictate the overall configuration and power requirement, were selected for two reasons. Some parameters were initially assigned a value arbitrarily and required further optimization. Others were selected to give additional information that would be applicable for other regenerator designs. Most of the results are shown with plots where the varying parameter is on the x-axis.

Other items pertaining to this section worth noting are presented as follows:

- All results are based on a fixed hot-side pressure drop (set at one percent). If this parameter was not initial fixed, the results could be quite different. For example, changing a parameter such as hydraulic diameter could result in unacceptable core pressure drops. This does not mean such values for hydraulic diameter cannot be used, but implies that some other parameters must be adjusted to give reasonable pressure drops.
- The power requirements between the two regenerator orientations for a particular module-movement step were nearly identical. Therefore, only one orientation is used throughout for the power analysis.

5.3.3.1 Varying Gas-Turbine Parameters

Since the modular regenerator has potential applications for a large variety of gas-turbine engines, understanding how the gas-turbine size affects the regenerator is essential. This section presents a simple approach of analyzing the gas turbine's size by varying a gas turbine's pressure ratio and mass-flow rate.

5.3.3.1.1 Varying Pressure Ratio

The pressure ratio was varied from 1.5 to 5.5 with all other inputs held constant to investigate the effects on gas-turbine performance and power requirement.

Results and Discussions

The plots showing the effect of pressure ratio on the design are as follows:

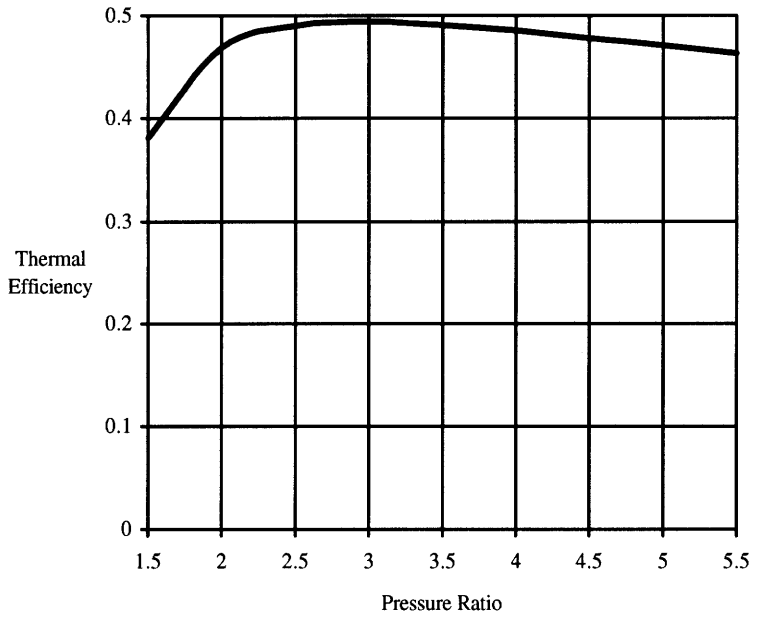

Figure 5.10 Effect of changing the pressure ratio on cycle thermal efficiency.

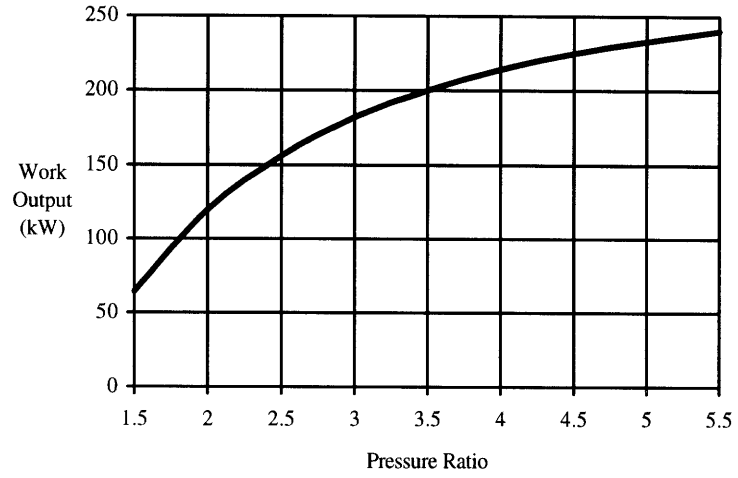

Figure 5.11 Effect of changing the pressure ratio on gas-turbine work output.

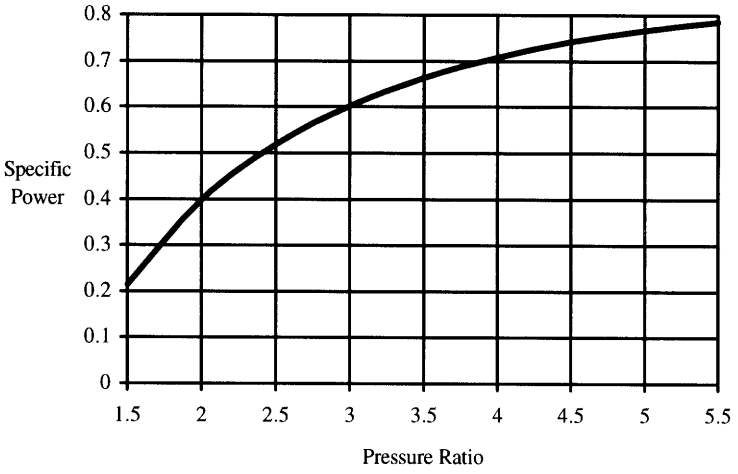

Figure 5.12 Effect of changing the pressure ratio on gas-turbine specific power.

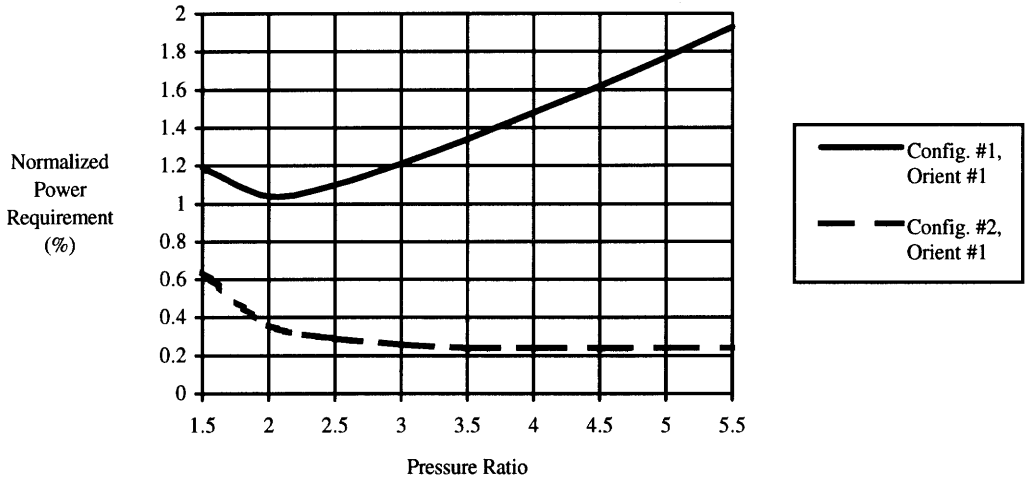

Figure 5.13 Effect of changing the pressure ratio on the power required by the regenerator to move the modules.

Discussion

The thermal efficiency peaks at r=3. This is one reason why low pressure ratio gas-turbines are used in regenerative cycles.

As expected, Figure 5.13 displays the large power discrepancy between the two cylinder configurations. The dip in configuration #1's curve is due to the increasing rate of the gas turbine's work output. As the pressure ratio increases, the work output begins to level off. The pressure forces continue to increase, thus increasing the normalized power. Since configuration #2 nearly eliminates the pressure force, the normalized power requirement decreases. Moreover, using configuration #1 further substantiates using a low-pressure ratio engine since the minimum occurs near r=2.

5.3.3.1.2 Varying Mass-Flow Rate

When the mass-flow rate increases, the power output increases in proportion without affecting the thermal efficiency and specific work. Varying this parameter gives a good measure of how a larger gas turbine affects the design. The mass-flow rate is varied

from 1 to 40 kg/s to cover gas turbines of various sizes ranging from vehicular engines to industrial power generation units.

Results

The plots showing the influence of mass-flow rate on the design are as follows:

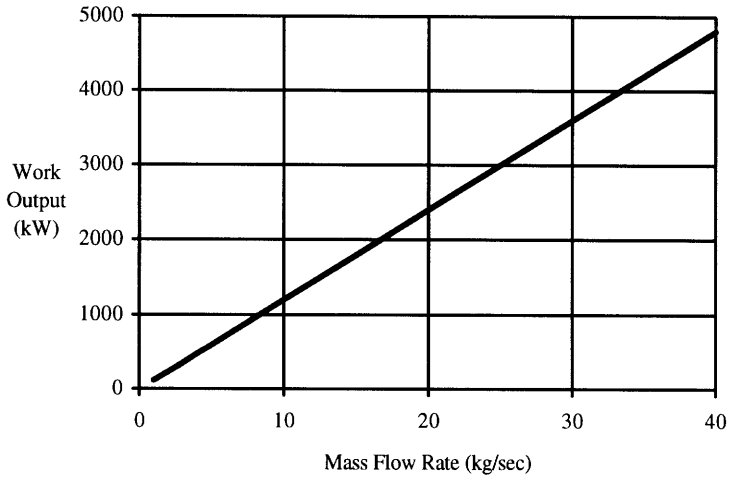

Figure 5.14 Effect of changing the gas-turbine mass-flow rate on the gas-turbine work output.

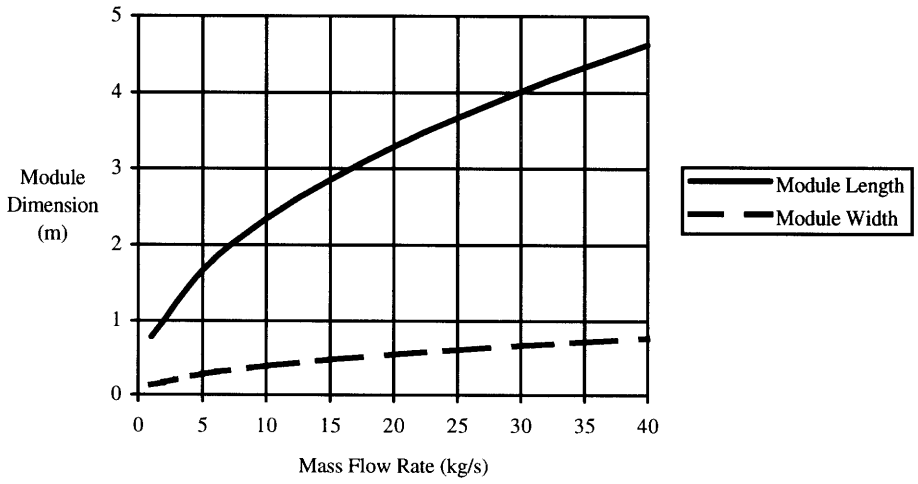

Figure 5.15 Effect of changing the gas-turbine mass-flow rate on the module width and length.

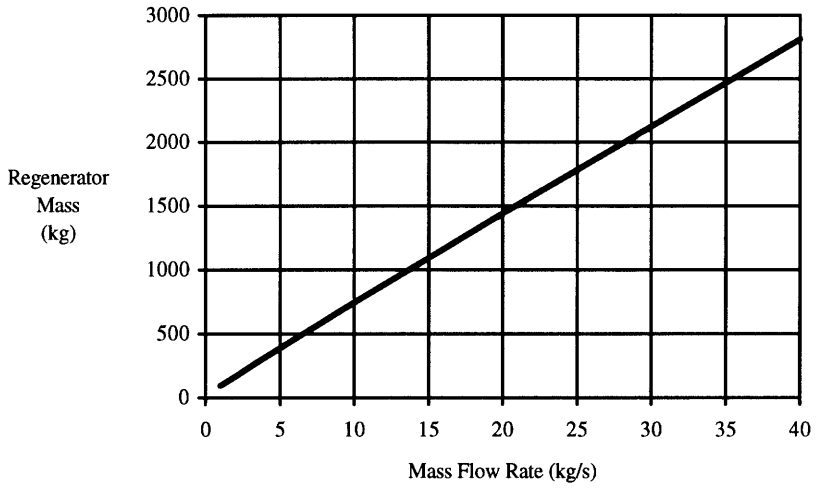

Figure 5.16 Effect of changing the gas-turbine mass-flow rate on the regenerator mass.

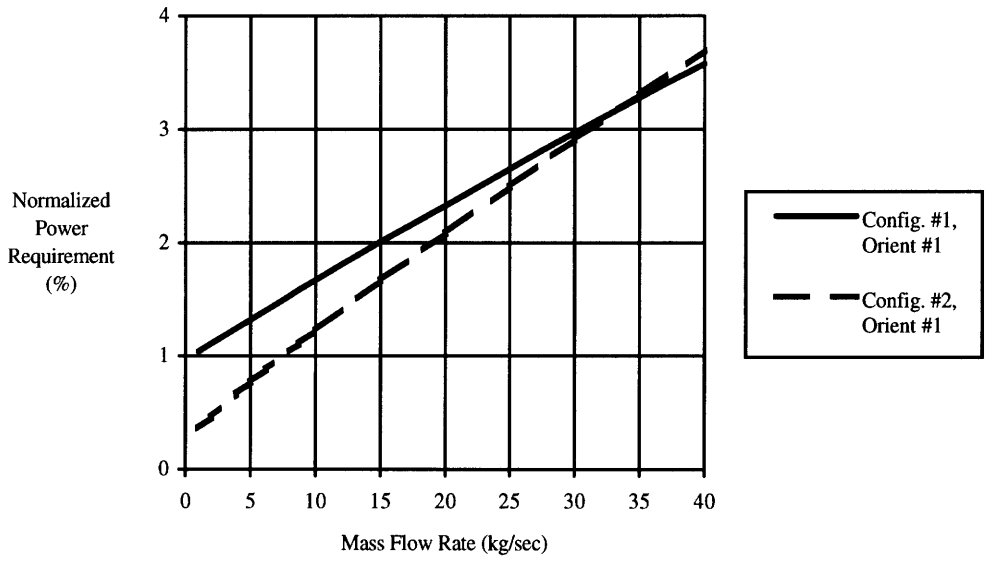

Figure 5.17 Effect of changing the gas-turbine mass-flow rate on the power required by the regenerator to move the modules.

Additional observations:

- The face area will increase in proportion to the mass-flow rate but the module/matrix thickness stays constant.

- As the face areas increase, the module dimensions increase in a way depending on the channel aspect ratio. With $AR_{channel} = 1$, the module dimensions increase non-linearly as shown in Figure 5.15.
- Since the module thickness is constant, the sealing distance will increase in proportion to the module width.
- The regenerator mass increases in proportion since the face areas increase in proportion.
- The total time for module movement is constant because both the module mass and ceramic-mass-flow rate increase by the same factor.
- Figure 5.17 shows that by increasing mass-flow rate, the power requirement increases. With very large gas turbines, attaining the one percent power goal will not be possible with either cylinder configuration.

Discussion

For large gas-turbine engines, the module size could get quite large. As shown in the plots, some results such as the module dimensions, are unrealistic. To counter this, the number of modules could be increased to reduce the dimensions but then the module velocities will increase. The effects of varying *Nmod* are presented later. Furthermore, larger dimensions correspond to heavier modules. The frictional forces resisting movement will probably become significant with larger designs. Providing rollers or dry lubricants to reduce the friction should be considered.

5.3.3.2 Varying Regenerator Choices

5.3.3.2.1 Varying Effectiveness

Since effectiveness is a measurement of the regenerator's thermal performance, a high value is desired. The effectiveness was chosen at 95 percent which should yield good results. Nevertheless, understanding how effectiveness affects the overall design could be

beneficial. The effectiveness was varied from 0.8 to 1.0. The value of unity is just a reference point since this would imply a heat exchanger of infinite size.

Results

Recall that the thermal efficiency increases as effectiveness increases. Using the design results, the increase is shown in the next figure.

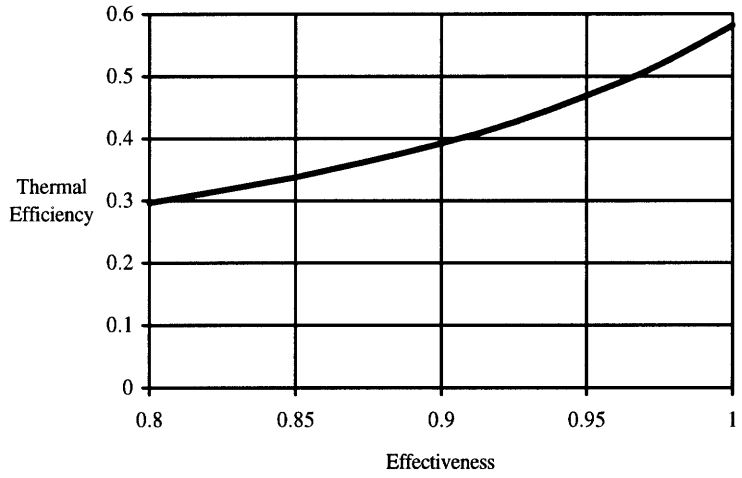

Figure 5.18 Effect of changing the regenerator effectiveness on the cycle thermal efficiency.

Additional observations as ε is increased from 0.8 to 1.0:

- Most of the other design parameters were unaffected.
- The normalized cold-side pressure drop changed from 0.14 percent to 0.2 percent.
- The module thickness increased slightly and the face areas decreased by a smaller rate. This resulted in the regenerator mass increasing by 3 kg.
- Changes in the power requirement were negligible.

Discussion

No detrimental trends were observed that would preclude using a regenerator with a high effectiveness.

5.3.3.2.2 Varying Passage Aspect Ratio

Recall that the heat-transfer performance increases as aspect ratio increases for a rectangular matrix passage (with fixed hydraulic diameter). As a result, the designer would probably choose a high aspect ratio; however, this may have detrimental effects. Therefore, this section presents the how AR_{pass} affects the design when its value is varied from 1 to 9.

Results

The following plots exhibit the influence of passage aspect ratio on the design:

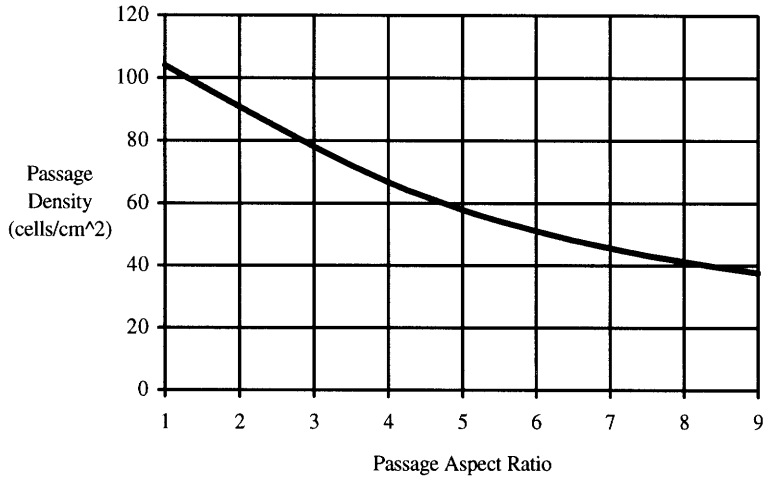

Figure 5.19 Effect of changing the ceramic-matrix passage aspect ratio on the matrix passage density.

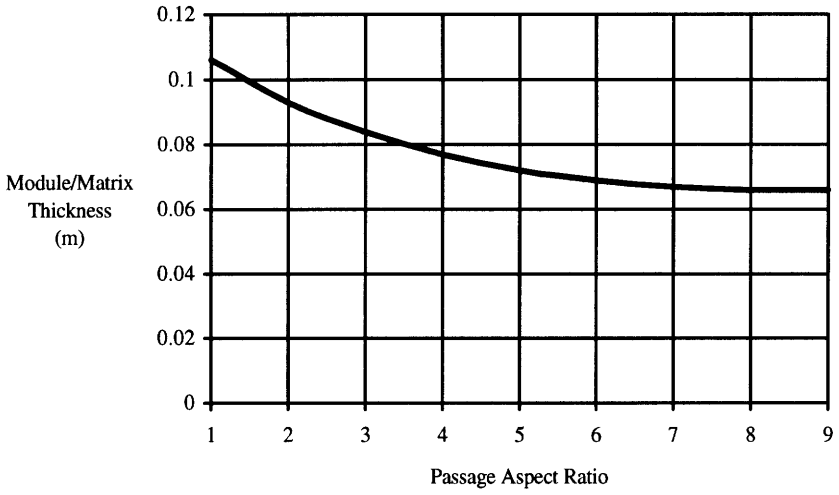

Figure 5.20 Effect of changing the ceramic-matrix passage aspect ratio on the thickness of the module/matrix.

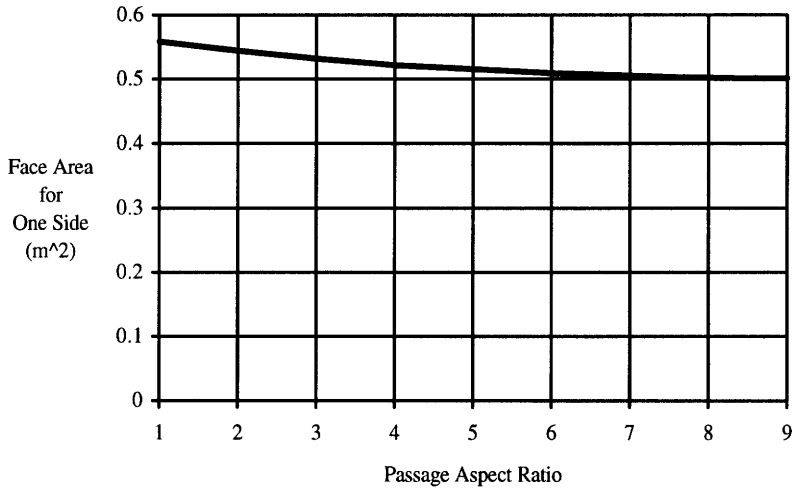

Figure 5.21 Effect of changing the ceramic-matrix passage aspect ratio on the face area for one side (hot or cold) of the regenerator.

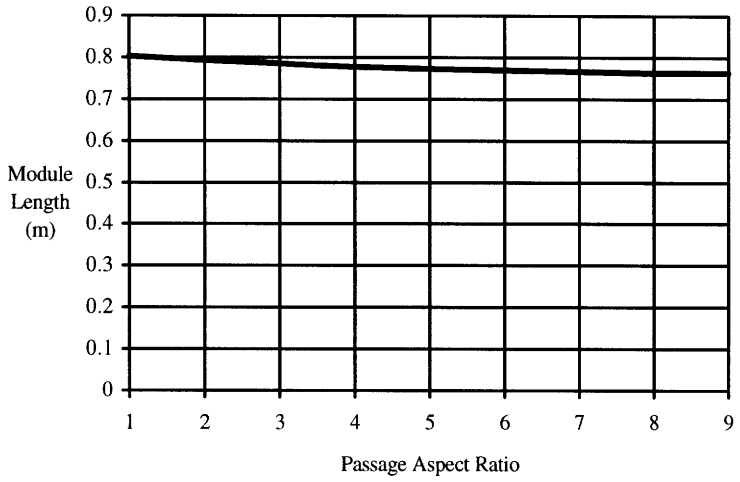

Figure 5.22 Effect of changing the ceramic-matrix passage aspect ratio on the module length.

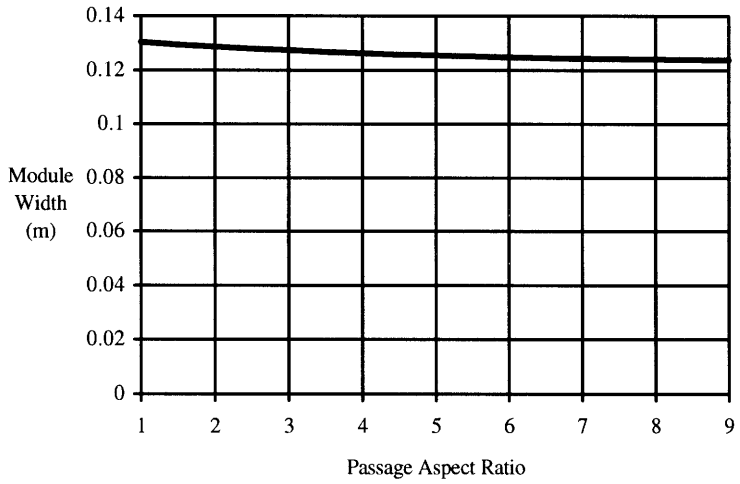

Figure 5.23 Effect of changing the ceramic-matrix passage aspect ratio on the module width.

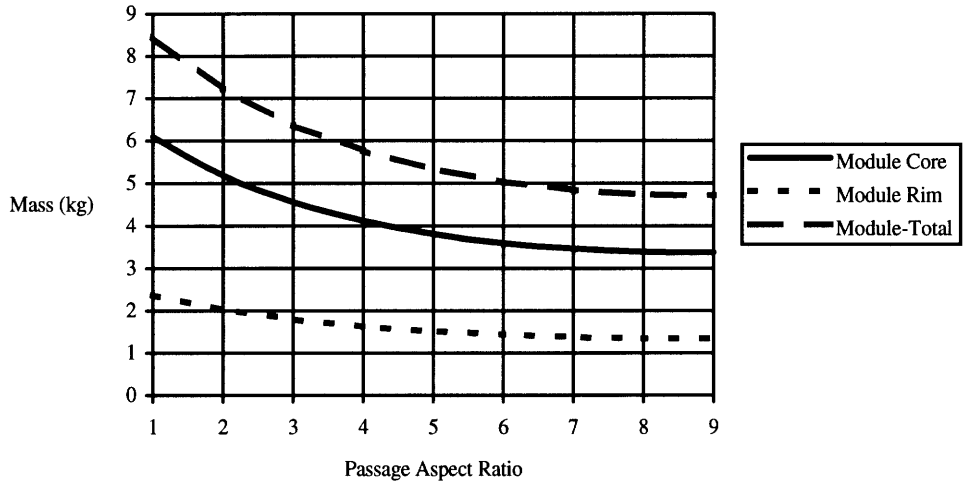

Figure 5.24 Effect of changing the ceramic-matrix passage aspect ratio on the module mass.

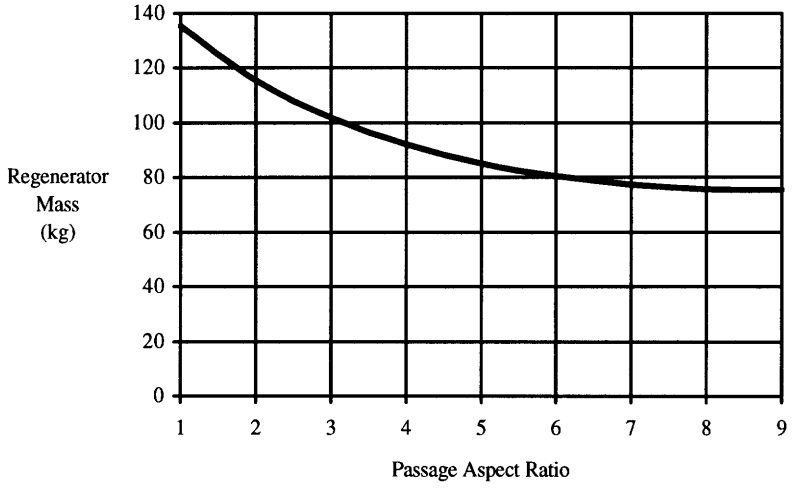

Figure 5.25 Effect of changing the ceramic-matrix passage aspect ratio on the regenerator mass.

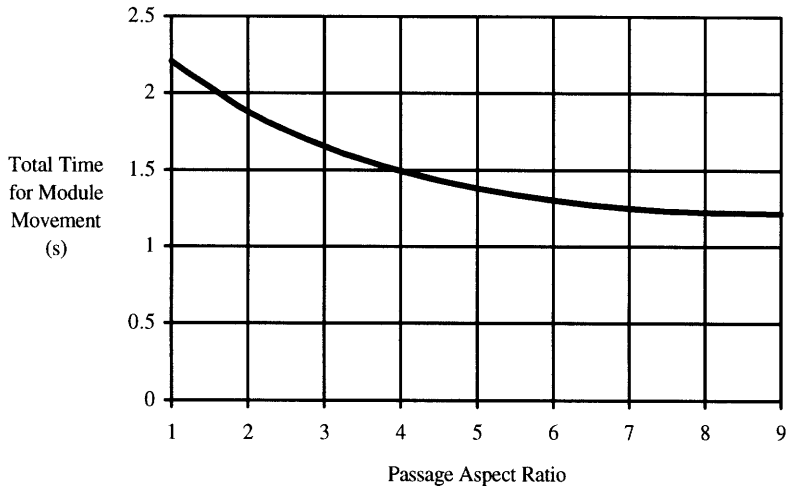

Figure 5.26 Effect of changing the ceramic-matrix passage aspect ratio on the total time for movement of one module.

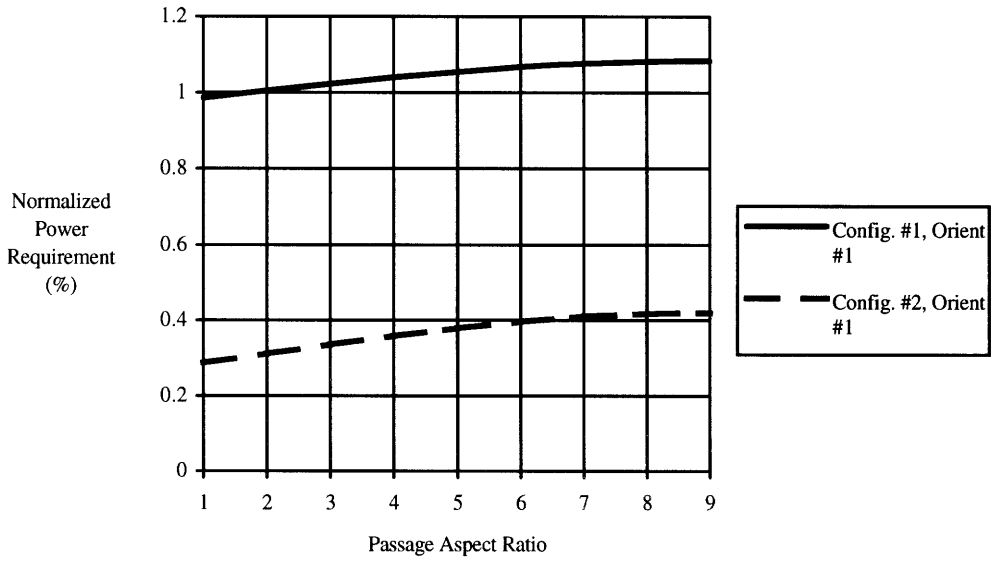

Figure 5.27 Effect of changing the ceramic-matrix passage aspect ratio on the power required by the regenerator to move the modules.

Additional observations as AR_{pass} is increased from 1 to 9:

- The face areas decreased slightly.

- Since the passage density decreased and porosity is constant, the matrix wall thickness increased.
- Cold-side pressure drop decreased slightly from 0.232 percent to 0.16 percent.
- Axial-conduction parameter increased slightly from 0.0017 to 0.0025 because the module/matrix thickness decreased and the wall thickness increased.

Discussion

Increasing the aspect ratio decreased the overall regenerator size and mass. The power requirement increased slightly but remains within acceptable limits.

5.3.3.2.3 Varying Hydraulic Diameter

Hydraulic diameter is similar to the passage aspect ratio since it specifies the passage size. Current manufacturing techniques can produce matrices with a wide range of hydraulic diameters. Thus, the designer has some freedom to select a particular value. This section presents the effects of hydraulic diameter as it ranges from 0.4 mm to 1.2 mm.

Results

The plots showing the influence of hydraulic diameter on the design are as follows:

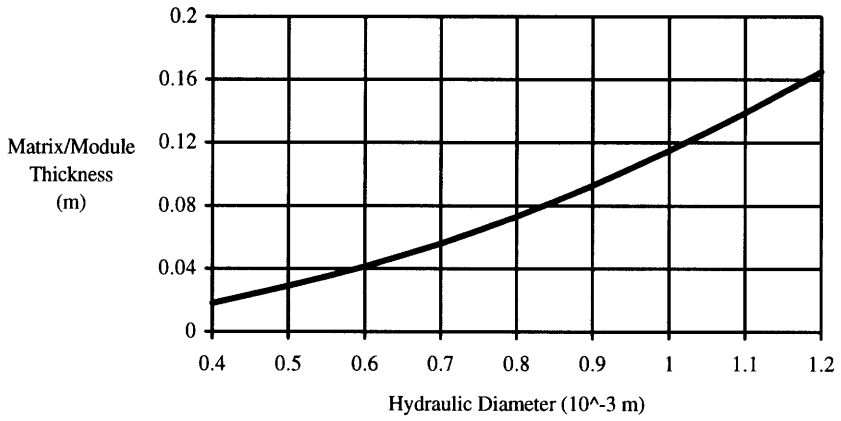

Figure 5.28 Effect of changing the ceramic-matrix hydraulic diameter on the thickness of the module/matrix.

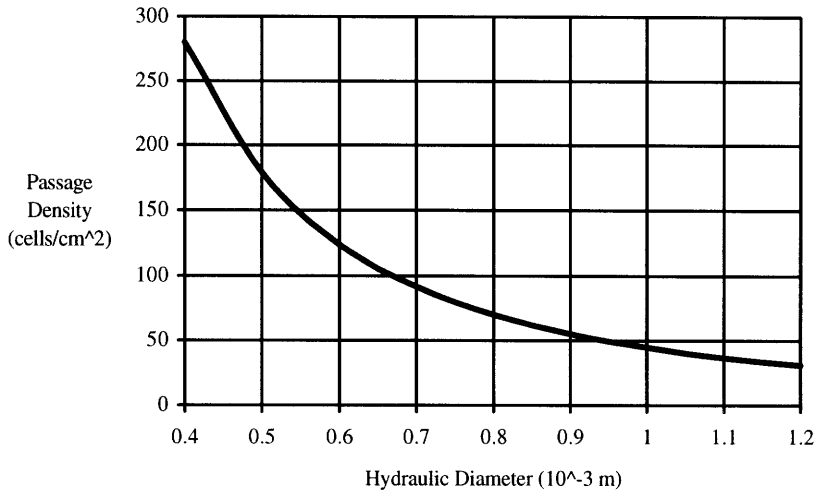

Figure 5.29 Effect of changing the ceramic-matrix hydraulic diameter on the matrix passage density.

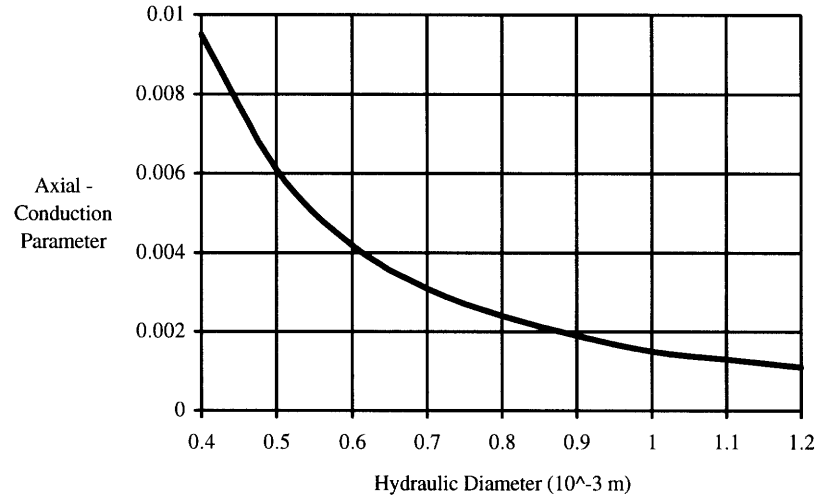

Figure 5.30 Effect of changing the ceramic-matrix hydraulic diameter on the axial-conduction parameter.

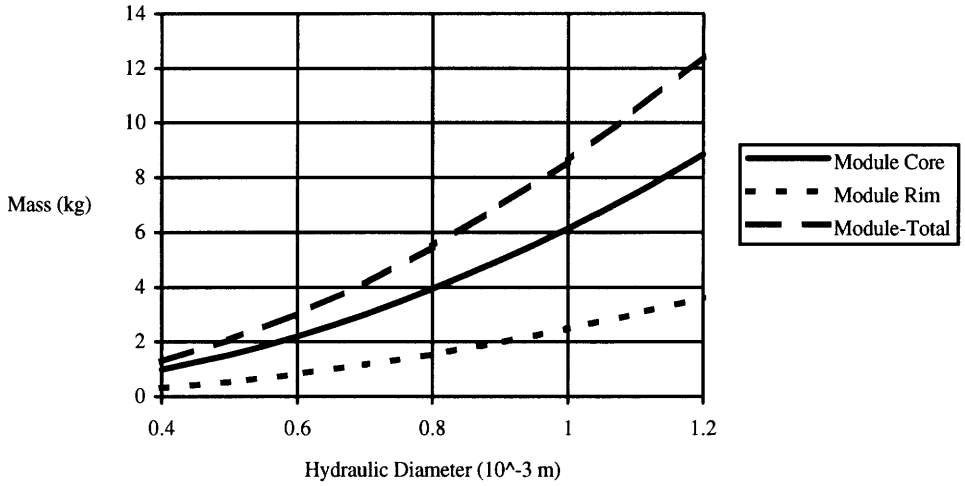

Figure 5.31 Effect of changing the ceramic-matrix hydraulic diameter on the module mass.

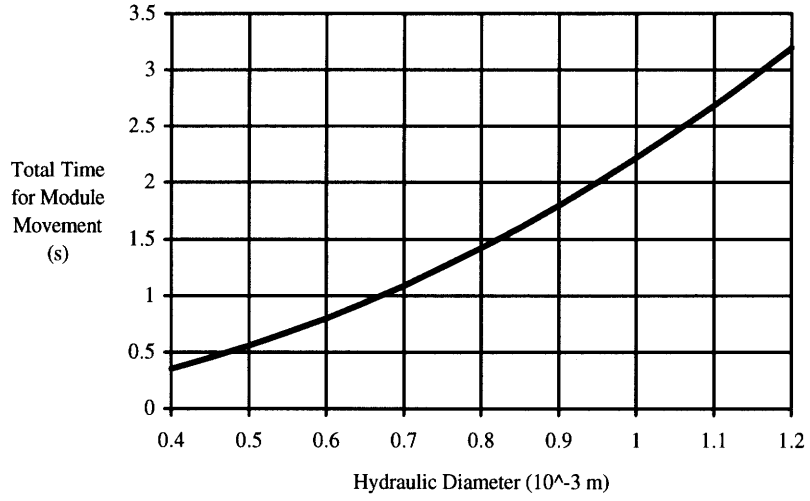

Figure 5.32 Effect of changing the ceramic-matrix hydraulic diameter on the total time for movement of one module.

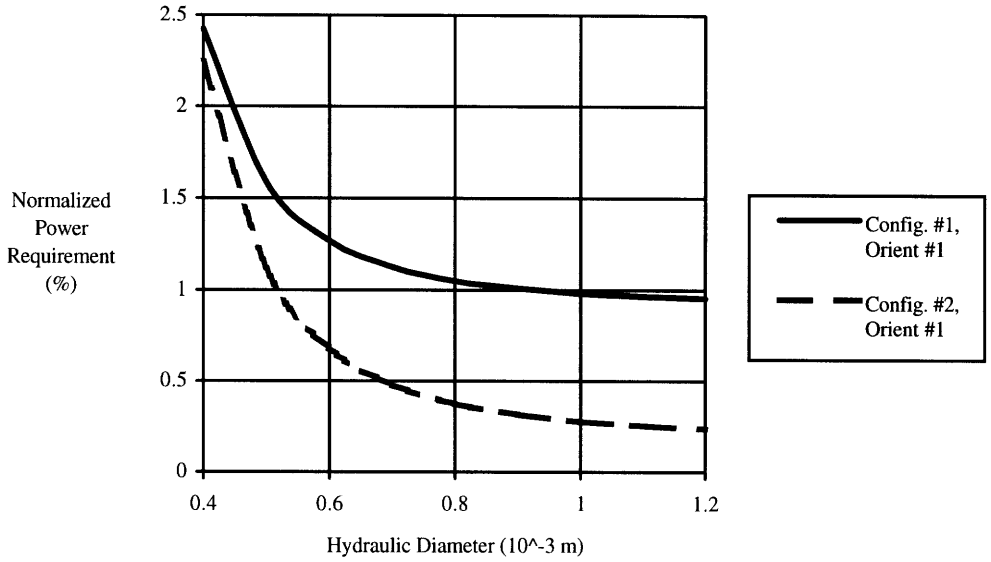

Figure 5.33 Effect of changing the ceramic-matrix hydraulic diameter on the power required by the regenerator to move the modules.

Additional observations:

- No change occurred in face areas thus the module length and width remained constant.
- No change occurred for cold-side pressure drop.

Discussion

Increasing the hydraulic diameter increased the module/matrix thickness without affecting the face areas. Thus, its value could be adjusted to obtain a specific matrix size. The axial-conduction parameter is reduced because the module/matrix thickness increases which corresponds to longer conduction lengths. The time for module movement increases which relates to lower module accelerations, velocities, and power requirement.

5.3.3.2.4 Varying Porosity

Porosity is a measure of a matrix's "openness." A low-porosity matrix has thick walls and a low passage density whereas a high-porosity matrix has thin walls and a higher passage density. The porosity was varied from 0.4 to 0.8.

Results

The plots displaying the influence of porosity on the design is shown below.

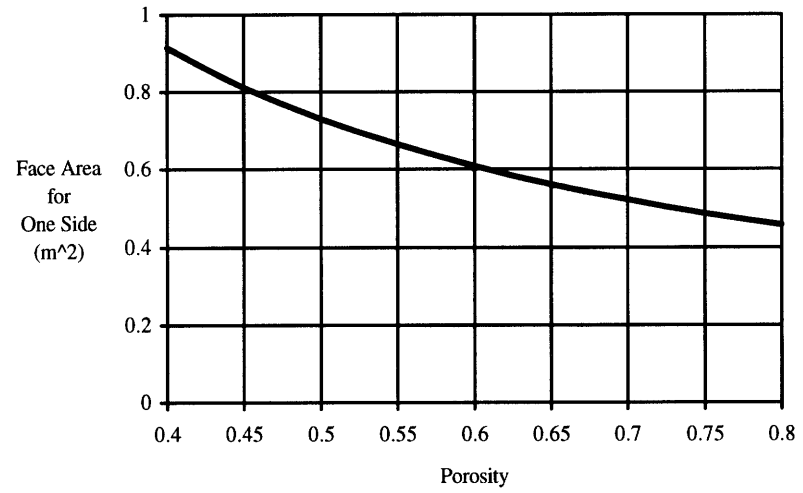

Figure 5.34 Effect of changing the matrix porosity on the face area for one side of the regenerator.

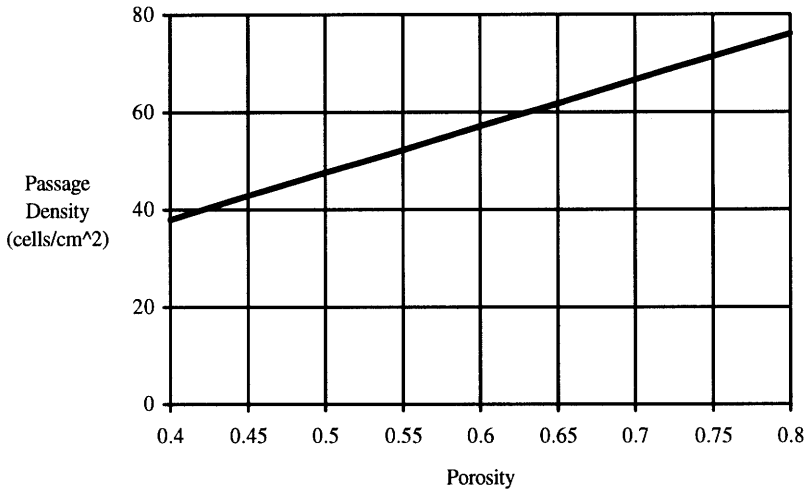

Figure 5.35 Effect of changing the matrix porosity on the matrix passage density.

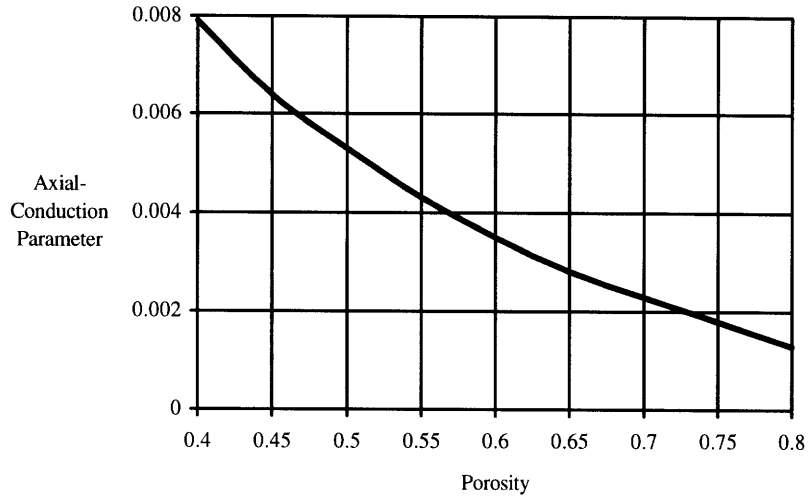

Figure 5.36 Effect of changing the matrix porosity on the axial-conduction parameter.

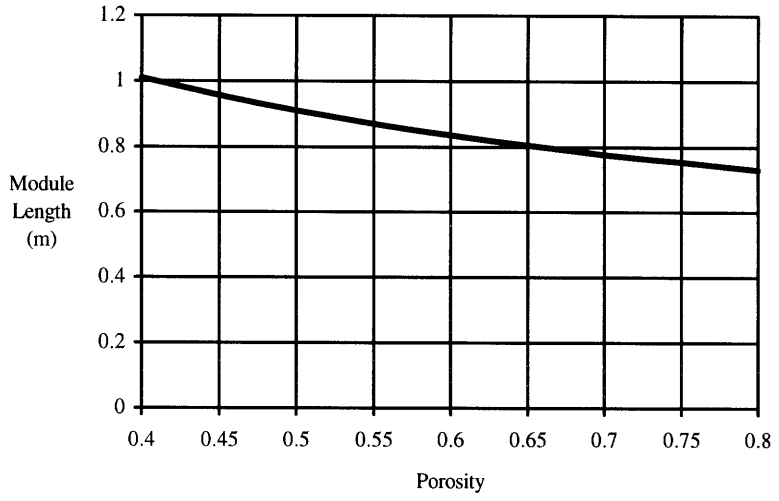

Figure 5.37 Effect of changing the matrix porosity on the module length.

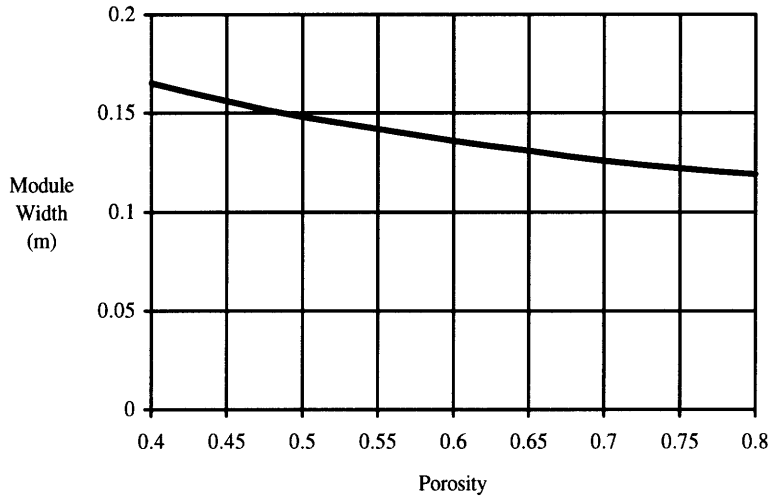

Figure 5.38 Effect of changing the matrix porosity on the module width.

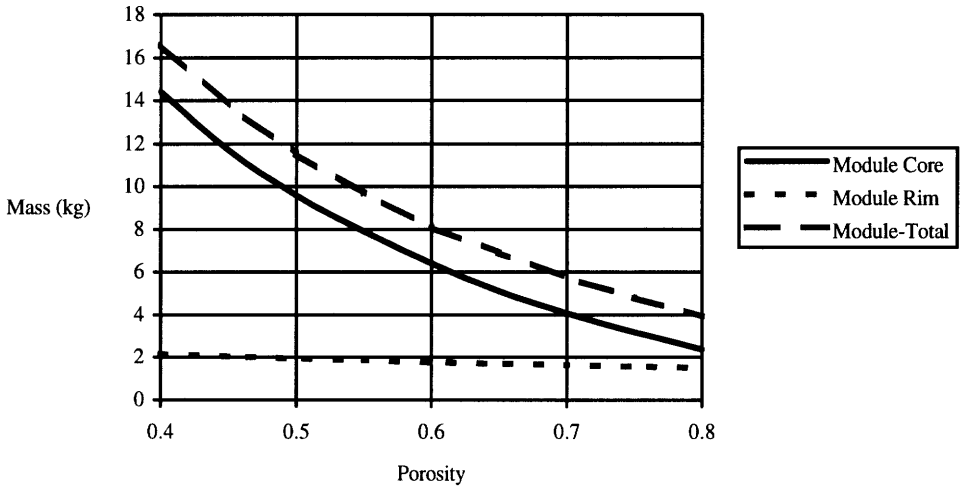

Figure 5.39 Effect of changing the matrix porosity on the module mass.

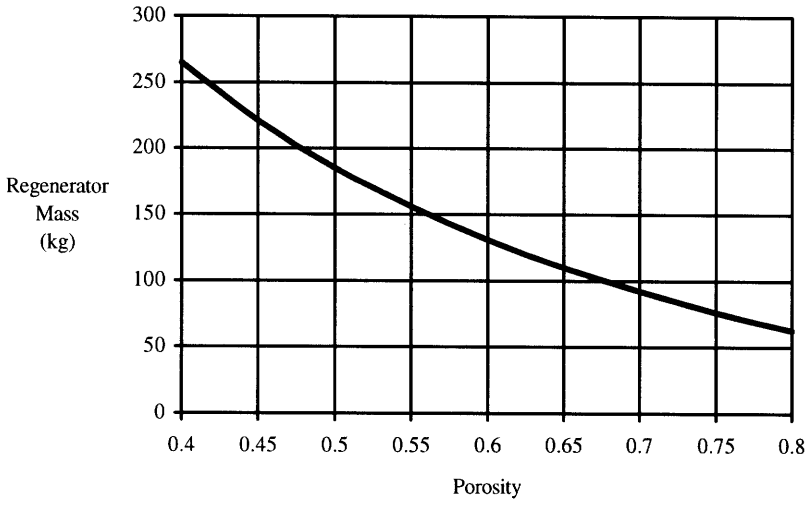

Figure 5.40 Effect of changing the matrix porosity on the regenerator mass.

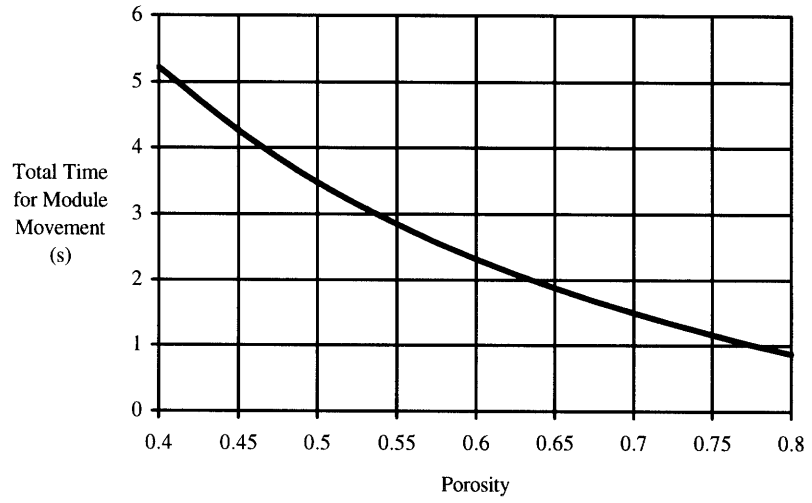

Figure 5.41 Effect of changing the matrix porosity on the total time for movement of one module.

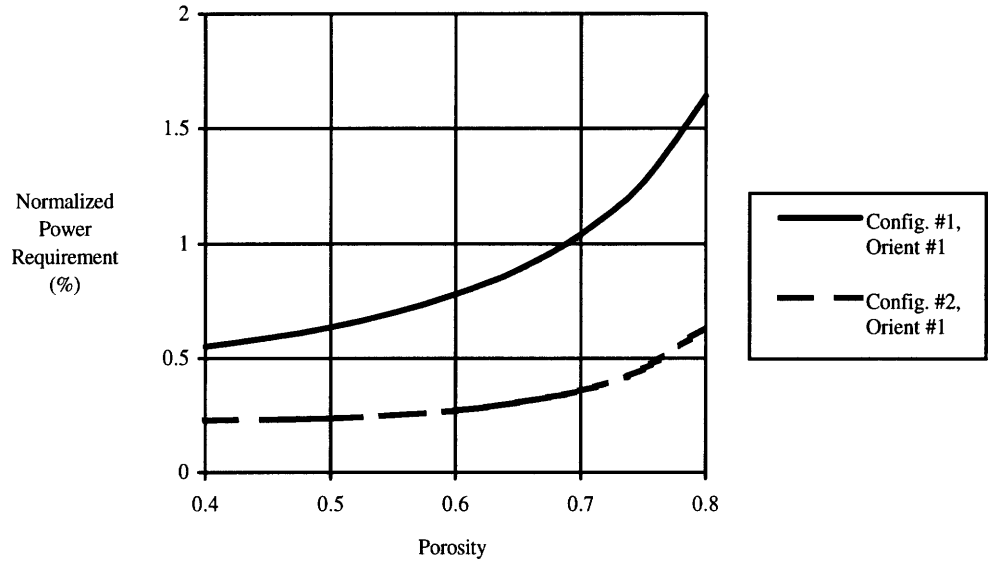

Figure 5.42 Effect of changing the matrix porosity on the power required by the regenerator to move the modules.

Additional notes:

- No change occurred for the cold-side pressure drop.
- No change occurred in module/matrix thickness.

Discussion

Increasing the porosity creates a more compact matrix thus leading to larger reductions in size and weight. This is why current rotary regenerators tend to have high porosities around 70 percent. On the other hand, this decreases the time for module movement thus contributing to the increase in power requirement. All power values are within acceptable limits except when the porosity is greater that 70 percent using configuration #2. Increasing the porosity decreased the axial-conduction parameter because the available area for heat conduction decreased and because the modules move more rapidly. In addition, increasing porosity will increase the carry-over leakage because the matrix void volume increases. The carry-over leakage is the transfer of compressed air

within the matrix from the cold side to the hot side. Carry-over leakage is addressed in later sections.

5.3.3.2.5 Varying Face-Area Ratio

Setting *FAR*=1 provides the simplest configuration for module movement. Choosing the face-area ratio greater than unity might provide the performance needed in other regenerator applications. Changing *FAR* is analogous to changing the radial-seal angle for the rotary case. This section will vary *FAR* from 0.5 to 2.5. Recall that the design method uses channel-geometry option A, stipulating that both sides have identical channel lengths.

Results

The following plots show the effect of face-area ratio on the design:

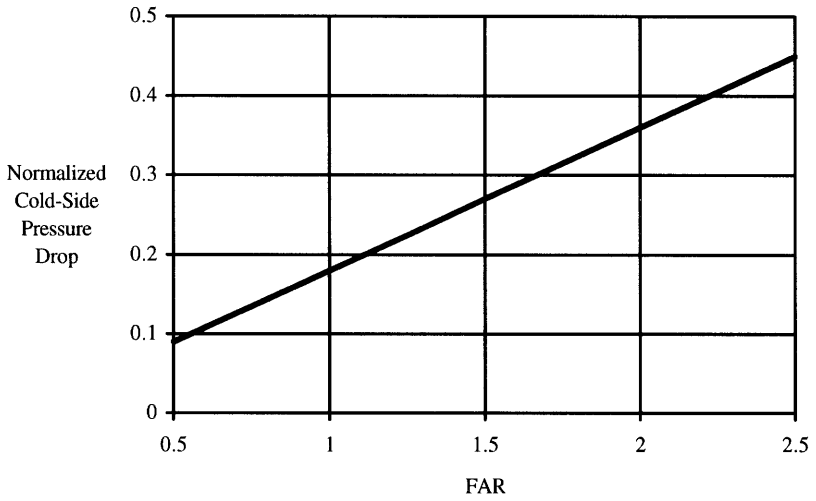

Figure 5.43 Effect of changing the regenerator face-area ratio on the pressure drop for the cold side.

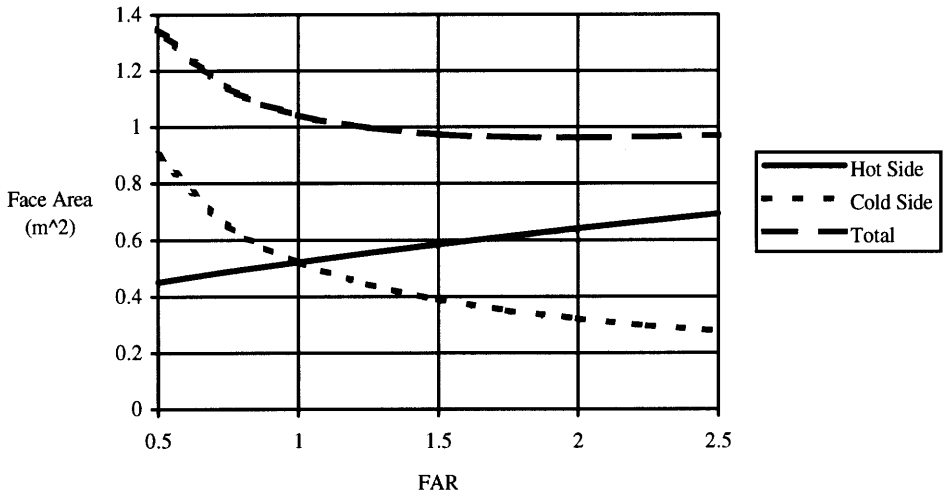

Figure 5.44 Effect of changing the regenerator face-area ratio on the regenerator face areas.

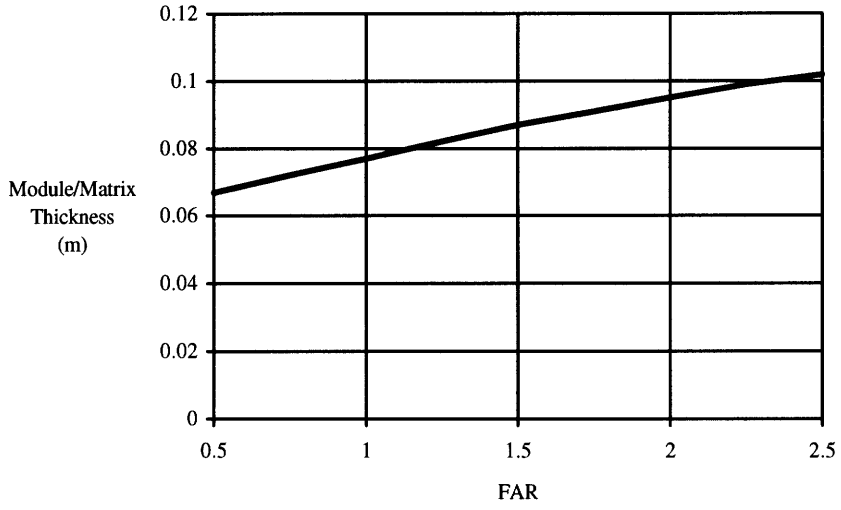

Figure 5.45 Effect of changing the regenerator face-area ratio on the thickness of the module/matrix.

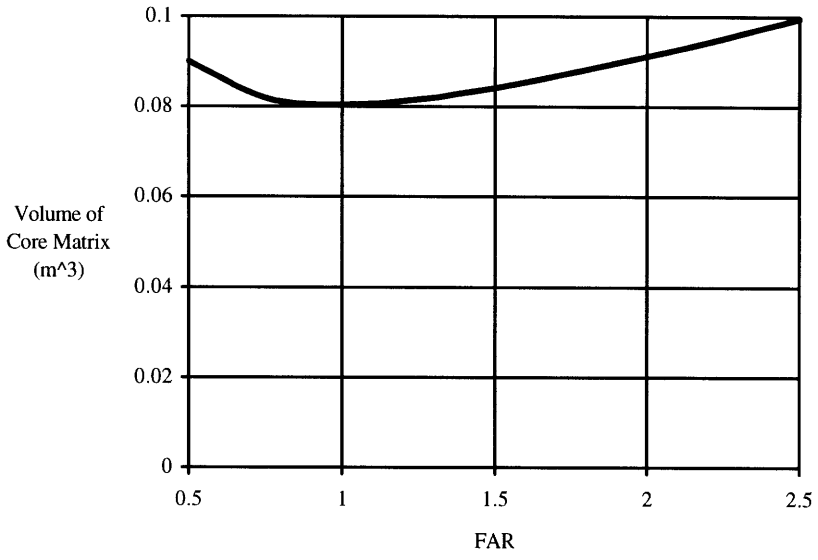

Figure 5.46 Effect of changing the regenerator face-area ratio on the volume of the core matrix.

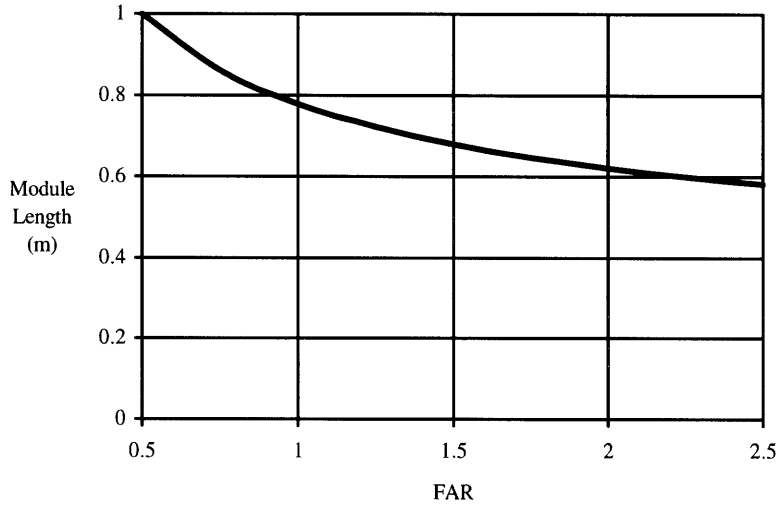

Figure 5.47 Effect of changing the regenerator face-area ratio on the module length.

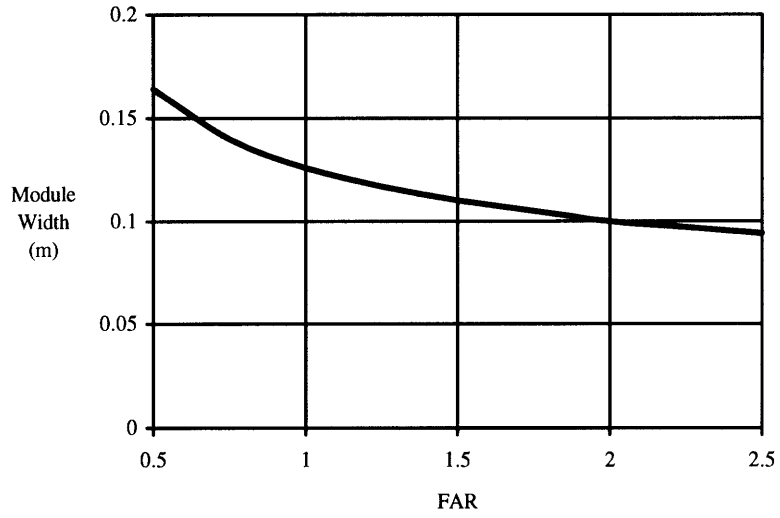

Figure 5.48 Effect of changing the regenerator face-area ratio on the module width.

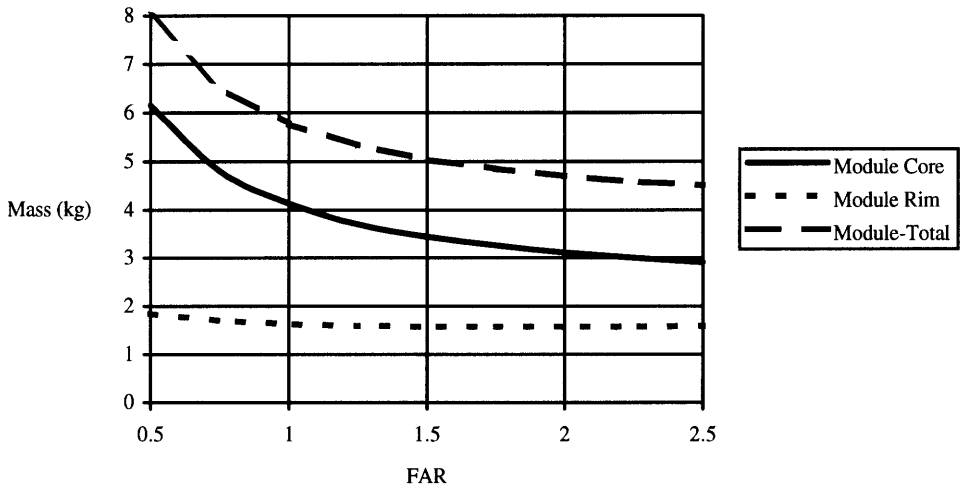

Figure 5.49 Effect of changing the regenerator face-area ratio on the module mass.

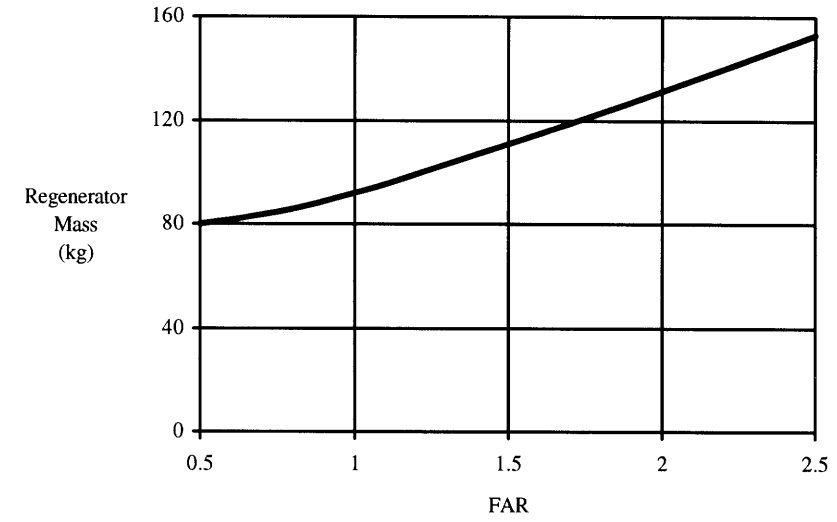

Figure 5.50 Effect of changing the regenerator face-area ratio on the regenerator mass.

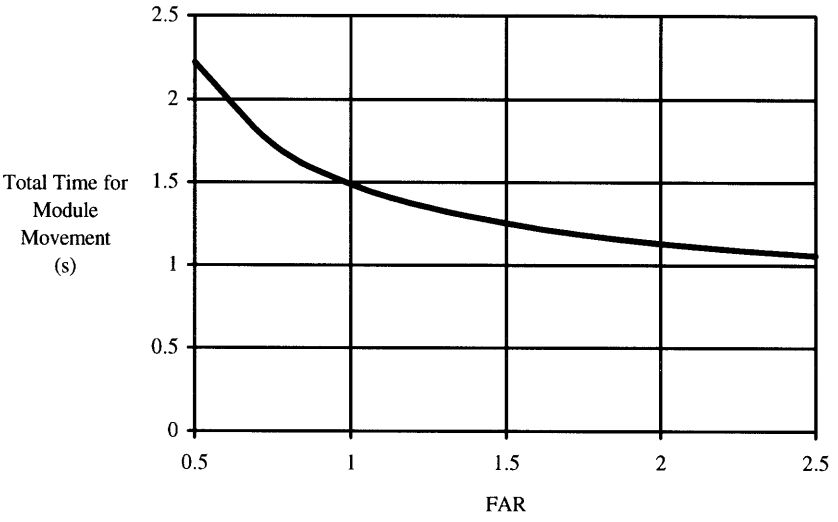

Figure 5.51 Effect of changing the regenerator face-area ratio on the total time for movement of one module.

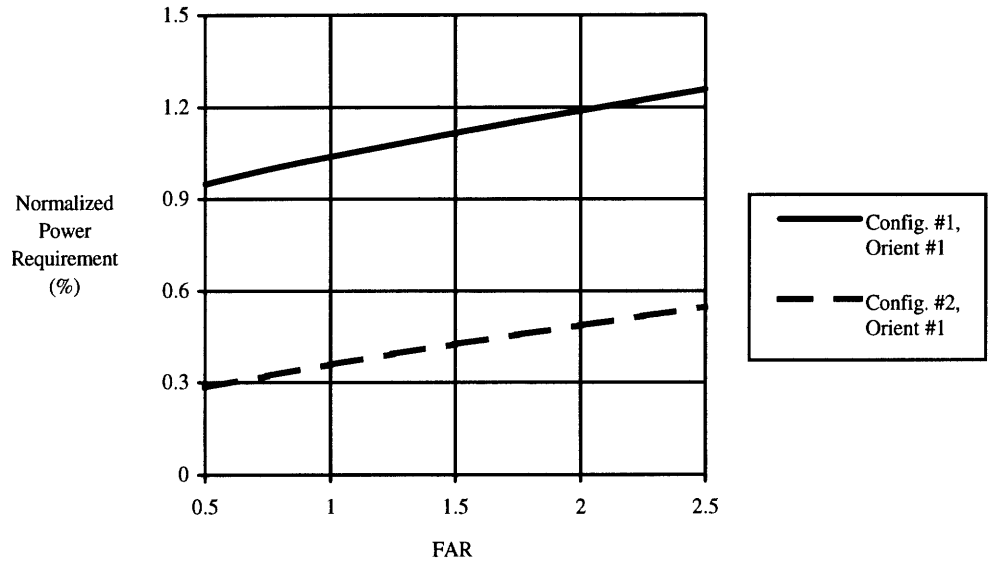

Figure 5.52 Effect of changing the regenerator face-area ratio on the power required by the regenerator to move the modules.

Discussion

The core volume reaches a minimum at *FAR*=1 due the changing effects of face area and module/matrix thickness. This decreases the module dimensions, but the number of modules increases (on the hot side) such that the total regenerator mass increases. Since the number of modules increases, the time for module movement drops thus giving a higher module acceleration and power requirement.

5.3.3.2.6 Varying Number of Cold-Side Modules

Changing the number of modules on the cold side gives the designer additional flexibility when setting the size of the modules. Increasing *Nmod* will decrease the module size. Unfortunately, this will require faster module velocities to maintain the same ceramic mass-flow rate. $Nmod_{cold}$ is varied from 2 modules to 10 module for this section.

Results

The influence of $Nmod_{cold}$ on the design is shown in the following plots:

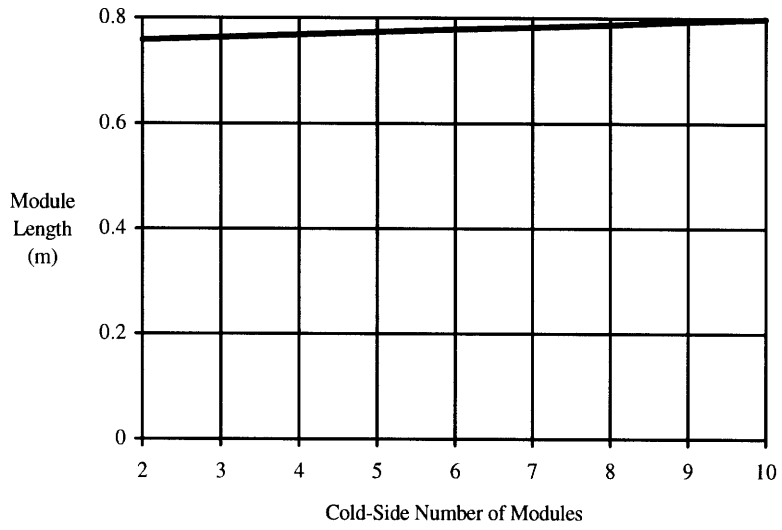

Figure 5.53 Effect of changing the cold-side number of modules on the module length.

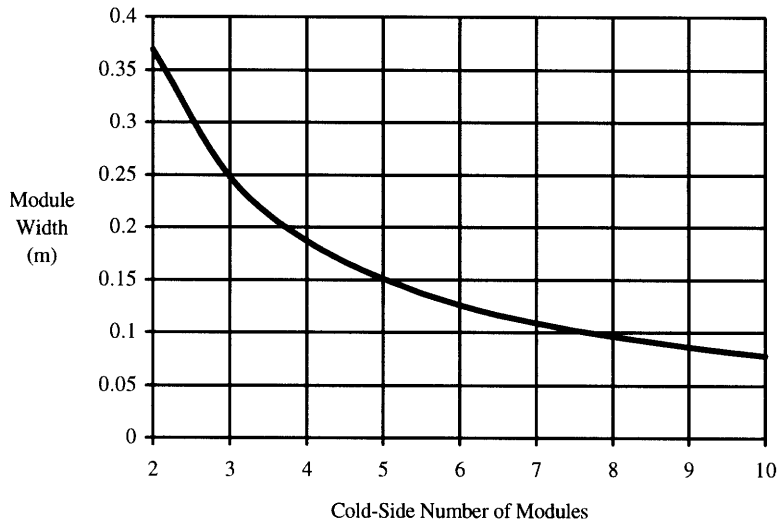

Figure 5.54 Effect of changing the cold-side number of modules on the module width.

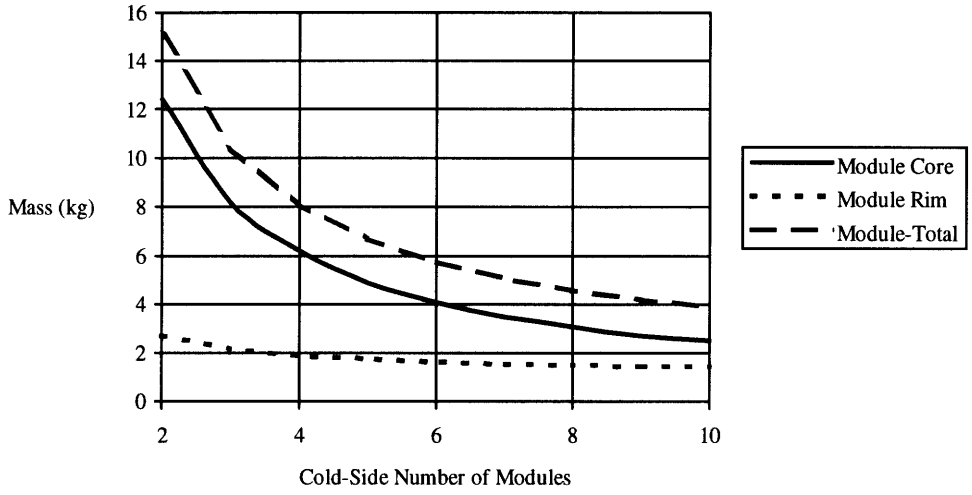

Figure 5.55 Effect of changing the cold-side number of modules on the module mass.

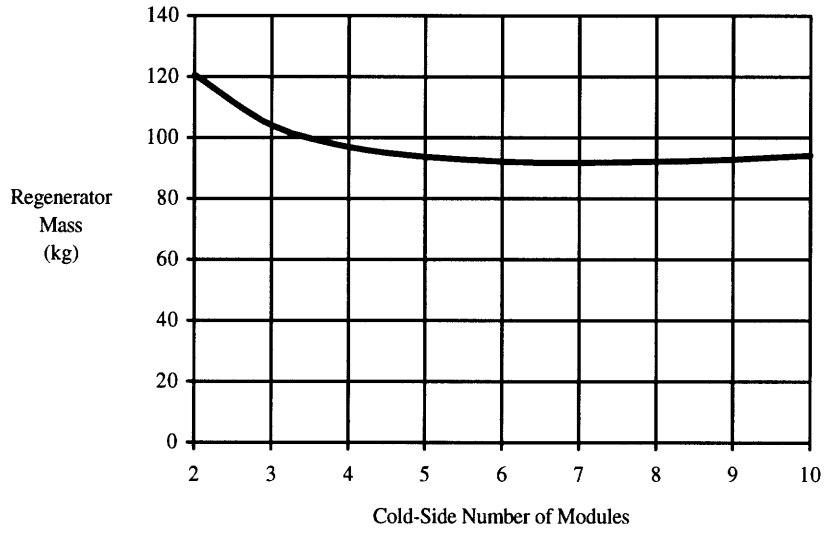

Figure 5.56 Effect of changing the cold-side number of modules on the regenerator mass.

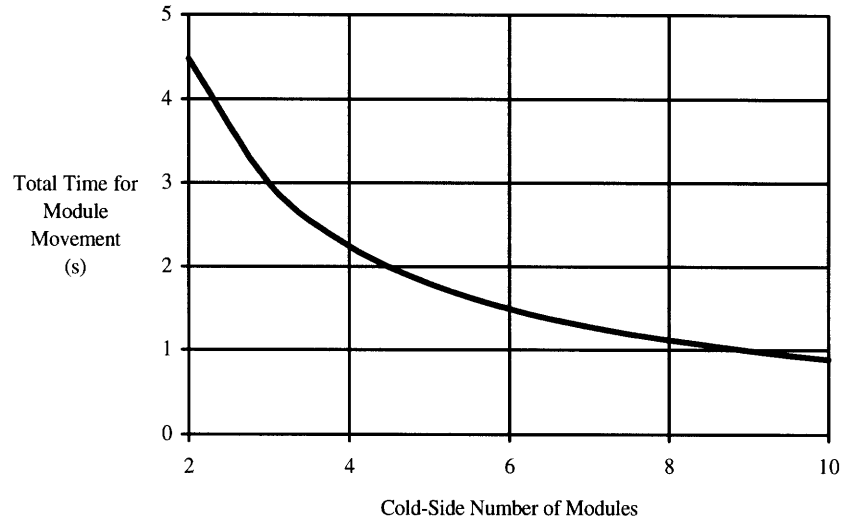

Figure 5.57 Effect of changing the cold-side number of modules on the total time for movement of one module.

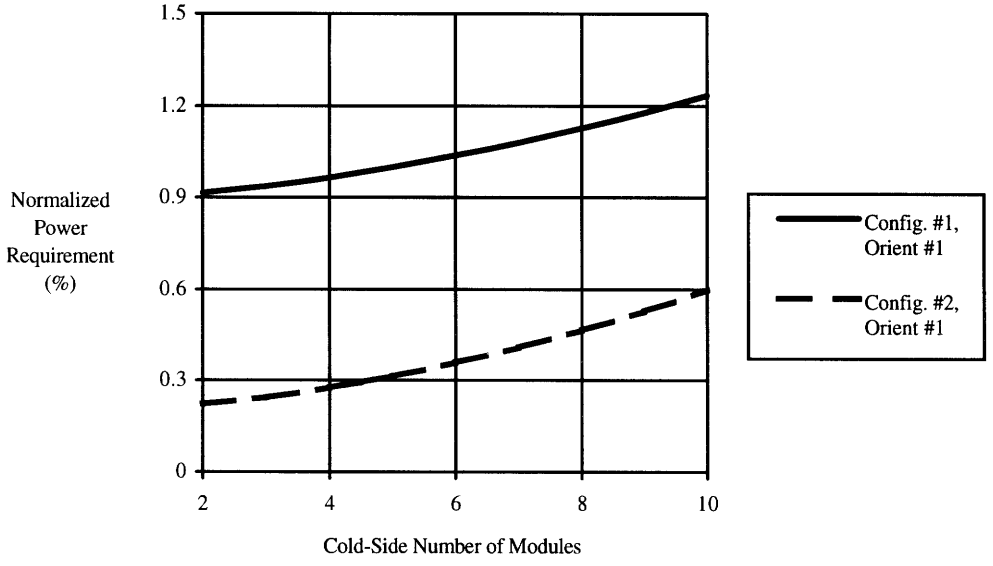

Figure 5.58 Effect of changing the cold-side number of modules on the power required by the regenerator to move the modules.

Discussion

As number of modules on the cold side increases, the reduction in module width overcomes the increase in module length to give an overall reduction in module size.

Regenerator mass reaches a minimum with 7 cold-side modules. The decrease in regenerator mass from 2 to 7 cold-side modules is attributed to the modules not exposed to the flow. As $Nmod_{cold}$ increases, the module mass decreases because the total mass for modules not exposed to the flow decreases. This effect starts to become overshadowed by the increasing rim mass when Nmod is around 7 modules. Since the rim width is constant, as the modules increase in number and get smaller, the percentage of mass composed of rim material starts to increase.

Finally, increasing $Nmod_{cold}$ decreases the sealing distance thus a reduction in leakage will occur (discussed later).

5.3.3.2.7 Varying Step1 Time Proportion

Setting the step1 time proportion, ξ_{step1}, determines the accelerations and velocities of each module movement step which affects the power requirement. ξ_{step1} was varied from 40 to 80 percent.

Results

The effect of ξ_{step1} on the power requirement is is shown in the next plot.

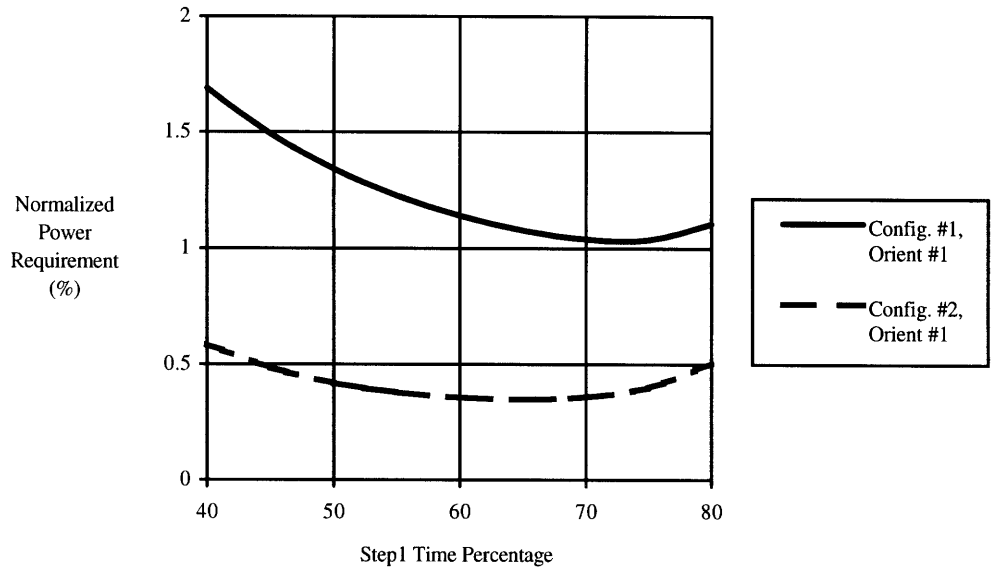

Figure 5.59 Effect of changing the percentage of time spent for step1 on the power required by the regenerator to move the modules.

Discussion

For cylinder configuration #1, a minimum of the power required occurs around 73 percent. For #2, the minimum is around 65 percent. The minimum exists because as the step1 time percentage is changed in either direction, the accelerations change for each movement step in opposite directions. The step with the positive increase in acceleration begins to dominate and thus the power required increases.

5.3.4 Conclusions

The conclusions drawn based on the optimization analysis including the rationale for the final choices are summarized below.

- The porosity was initially chosen at 95 percent to provide a high thermal efficiency. The analysis did not give any evidence that a different value should be used. Hence, the final value is 95 percent.

- Increasing the passage aspect ratio gives benefits such as the reducing the overall size, reducing the mass, and increasing the heat-transfer performance. One factor that may limit the aspect ratio is the structural integrity of the matrix material. By increasing the aspect ratio, the internal structural support of the honey-comb arrangement is decreased since the lengthwise wall distances are increased. As a compromise, AR_{pass}=4.0 was finally chosen.
- *FAR*=1 provides the simplest module configuration for movement. Furthermore, setting *FAR*=1 will probably lead to minimum axial-conduction effects since the time spent for a module going from one exposed side to the other is minimized. For the particular gas-turbine used in this analysis along with other designated parameters, *FAR*=1 yielded acceptable results.
- After the passage aspect ratio was chosen at 4.0, the hydraulic diameter was adjusted to minimize the regenerator weight. Recall that lowering the hydraulic diameter decreases the module/matrix thickness but keeps the face areas constant. Therefore, d_h was selected to minimize the weight but not to exceed the acceptable limits in the matrix thickness. Wilson [24] suggests that a matrix thickness less than 0.077 m could introduce some thermal and structural fatigue problems within the matrix. As the matrix thickness decreases, the temperature gradient within the ceramic matrix increases. Combined with the thermal cycling that the matrix sustains, the structural integrity of the core could start to deteriorate. So to remain within this matrix-thickness limit, the final value of hydraulic diameter is 0.82 mm.
- The porosity was initially set at 70 percent and this provided good results as shown previously. Thus, the final value of porosity did not change.
- The number of modules for the cold side was chosen at 6 which giving a near minimum regenerator mass as $Nmod_{cold}$ is varied.
- From the power requirement curves of Figure 5.59, a value for step1 time proportion ranging from 55 to 75 percent gives a near minimum power requirement for configuration #2. Therefore, the final value was chosen at 70 percent.

- Cylinder configuration #2 is chosen over #1 since it provided substantially lower power results throughout this analysis. The power requirement for configuration #1 sometimes provided adequate results, but the power required for #2 was always significantly lower.
- The power requirements between the two regenerator orientations were almost identical (this was not shown in the above plots). Thus, other design criteria were considered in selecting an orientation. As a result, orientation #1 is chosen because it provides a simpler module-movement system (having identical cylinder systems for each side during step2 movement). Recall that orientation #2 requires a deceleration device to slow the module down on the hot side and this will have to be synchronized with the cylinder on the cold side.

5.4 Sizing and Performance Results

5.4.1 Introduction

This section presents the results of the design and performance method using the final chosen parameters. All chosen parameters are listed in Section 5.3.2.

5.4.2 Results

The following tables present the numerical results of the cycle calculations, mean properties calculations, basic regenerator calculations, and modular specific calculations.

Parameter	Calculated Result	Parameter	Calculated Result
$\dot{m}_{cold}$	0.98 kg/s	T_3	1184.2 K
$\dot{m}_{4-5}$	0.98 kg/s	T_5	1226.5 K
$\dot{m}_{hot}$	0.98 kg/s	T_6	431.7 K
P_2	$2.0 \cdot 10^5$ Pa	$(\dot{m}\,\bar{c}_P)_{min}$	1072.8 J/K-s
P_3	$1.96 \cdot 10^5$ Pa	$(\dot{m}\,\bar{c}_P)_{max}$	1083.3 J/K-s
P_4	$1.88 \cdot 10^5$ Pa	$\dot{W}_{GT}$	120 kW
P_5	$1.02 \cdot 10^5$ Pa	$\eta_{thermal}$	0.47
T_2	381.7 K	$\dot{W}'_{GT}$	0.40

Table 5.9 Results of the gas-turbine cycle calculations.

Parameter	Calculated Result	Parameter	Calculated Result
$\bar{P}_{hot}$	$1.01 \cdot 10^5$ Pa	$\bar{P}_{cold}$	$1.98 \cdot 10^5$ Pa
$\bar{T}_{hot}$	829.1 K	$\bar{T}_{cold}$	783.0
$\bar{\rho}_{hot}$	0.425 kg/m^3	$\bar{\rho}_{cold}$	0.881 kg/m^3
$\bar{\mu}_{hot}$	$3.77 \cdot 10^{-5}$ kg/m-s	$\bar{\mu}_{cold}$	$3.63 \cdot 10^{-5}$ kg/m-s
$(\bar{P}r)_{hot}$	0.713	$(\bar{P}r)_{cold}$	0.707
$\bar{c}_{P_{hot}}$	1105.3 J/kg-K	$\bar{c}_{P_{cold}}$	1094.7 J/kg-K

Table 5.10 Results of the calculations specifying the mean properties for both sides of the regenerator.

Parameter	Calculated Result	Parameter	Calculated Result
$C_f Re$	18.3	V_{mat}	0.0851 m^3
$\frac{St\,Pr^{\frac{2}{3}}}{C_f}$	0.328	m_{mat}	49.5 kg
$h_{t_{cold}}$	367.0 W/m^2-K	$A_{h_{hot}}$	137.4 m^2
$h_{t_{hot}}$	382.6 W/m^2-K	$A_{h_{cold}}$	137.4 m^2
l_{pass}	0.00205 m	$(h_t A_h)_{hot}$	5.26 W/K
w_{pass}	0.000510 m	$(h_t A_h)_{cold}$	5.05 W/K
ρ_{pass}	66.6	$(h_t A_h)'$	0.959
$\frac{A_h}{V_{void}}$	4878.0 m^2/m^3	UA_h	2.57 W/K
$\frac{A_h}{V_{mat}}$	3414.6 m^2/m^3	$\overline{C}_{cold}$	3.04 m/s
NTU	24	$(\overline{Re})_{cold}$	60.5
$\overline{C}_{hot}$	6.32 m/s	$\overline{q}_{cold}$	4.08 Pa
th_{mod}	0.077 m	$\left(\frac{\Delta P}{P}\right)_{cold}$	0.18 %
$A_{ff_{hot}}$	0.366 m^2	$\overline{T}_{cer}$	806.5 K
$A_{f_{hot}}$	0.522 m^2	$\overline{c}_{P_{cer}}$	1164.4 J/kg-K
$A_{ff_{cold}}$	0.366 m^2	$\dot{m}_{mat}$	2.76 kg/s
$A_{f_{cold}}$	0.522 m^2	$t_{rotation}$	17.9 s
A_f	1.04 m^2		

Table 5.11 Results of the basic regenerator calculations.

Parameter	Calculated Result	Parameter	Calculated Result
$Nmod_{unexposed}$	4	t_{step2}	0.44 s
$l_{channel_{cold}}$	0.748 m	$\overline{v}_{mod-step1}$	0.75 m/s
$w_{channel_{cold}}$	0.748 m	$\overline{v}_{mod-step2}$	0.28 m/s
$A_{channel_{cold}}$	0.56 m^2	$tmod_{step1}$	0.78 s
$\zeta_{mat_{cold}}$	93.3 %	$tmod_{step2}$	0.36 s
$l_{mod\text{-}mat}$	0.748	$dmod_{step1}$	0.778 m
$w_{mod\text{-}mat}$	0.116	$dmod_{step2}$	0.126 m
l_{mod}	0.778 m	$a_{max,\ step1}$	4.48 m/s^2
w_{mod}	0.126 m	$a_{max,\ step2}$	3.96 m/s^2
$dist_{seal}$	0.407 m	A_{rod}	0.00049 m^2
$Nmod_{hot}$	6	$\left(F_{pressure_{step1,config1}}\right)_{net}$	994 N
$l_{regenerator}$	2.33 m	$\left(F_{pressure_{step1,config2}}\right)_{net}$	97.2 N
$w_{regenerator}$	1.01 m	$\left(\hat{\dot{W}}_{mod}\right)_{config2,orient1}$	0.359 %
$m_{mod\text{-}mat}$	4.13 kg	SC	25 %
m_{rim}	1.63	As'	1.0
m_{mod}	5.76	As_N	0.157 m^2
$m_{regenerator}$	92.2 kg	λ	0.0025
$t_{net_{mod}}$	1.49 s	$\left(\frac{\Delta\varepsilon}{\varepsilon}\right)_{acsw}$	0.42 %
t_{step1}	1.05 s		

Table 5.12 Results of the modular specific calculations.

The following are some notes pertaining the results in Table 5.12:

- Recall that regenerator is using cylinder configuration #2 and orientation #1.

- Since *FAR*=1, the all channel dimensions for both sides are identical.
- $\xi_{extension}$ is chosen at 0.75 to give the time for *tmod*.
- The module-side rims have 4 slots (with a radius of 0.0125 m) and are filleted (with a radius of 0.01 m).

Module Movement and Force Profiles

The movement and force profiles for step1 (configuration #2) are as follows:

$$[a_{mod}(t)]_{step1} = 4.48 \sin\left(\frac{2\pi}{0.78}t\right)$$

$$[v_{mod}(t)]_{step1} = \left[1 - \cos\left(\frac{2\pi}{0.78}t\right)\right]$$

$$[s_{mod}(t)]_{step1} = t - \frac{0.778}{2\pi}\sin\left(\frac{2\pi}{0.78}t\right)$$

$$F_{mod-movement_{step1,config2}} = 187.5 + 51.6 \sin\left(\frac{2\pi}{0.78}t\right).$$

The movement and force profiles for step2 (orientation #1) are as follows:

$$[a_{mod}(t)]_{step2} = 3.96 \sin\left(\frac{2\pi}{0.36}t\right)$$

$$[v_{mod}(t)]_{step2} = 0.35\left[1 - \cos\left(\frac{2\pi}{0.36}t\right)\right]$$

$$[s_{mod}(t)]_{step2} = 0.35t - \frac{0.126}{2\pi}\sin\left(\frac{2\pi}{0.36}t\right)$$

$$F_{mod-movement_{step2,orient1}} = 158.1 + 40.3\sin\left(\frac{2\pi}{0.36}t\right).$$

Cylinder Sizing

The cylinder-bore diameter is a function of feed pressure. The next plot shows the minimum required bore diameter for step1 (configuration #1) as the feed pressure is changed. Following that is a plot for step2 (orientation #1). Note the bore diameter is in inches since most cylinder manufactures use English units.

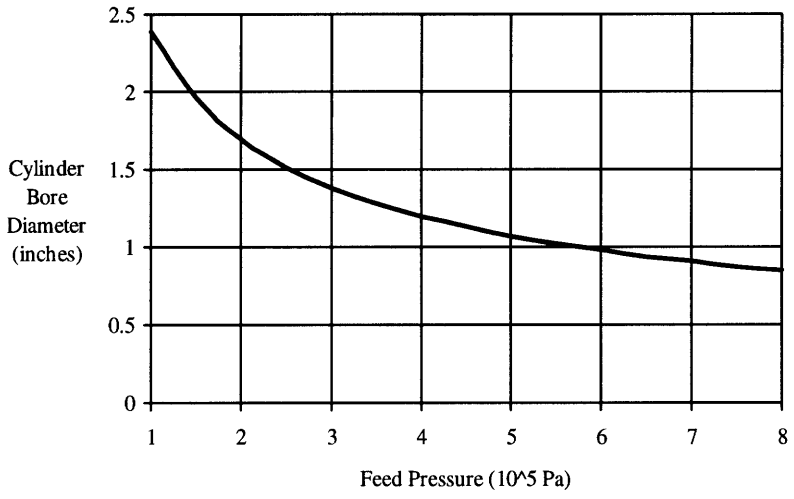

Figure 5.60 Effect of minimum required cylinder-bore diameter for step1 module movement.

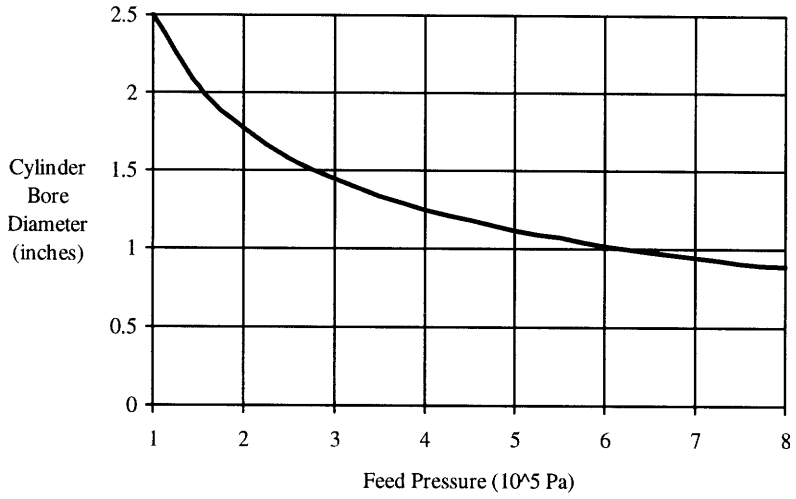

Figure 5.61 Effect of minimum required cylinder-bore diameter for step2 module movement.

5.4.3 Discussion

Cylinder configuration #2 has an 88 percent drop in the net pressure forces that resist module movement compared to configuration #1. Thus, the power required is well within the designated 1 percent limit.

As shown from the derived regenerator dimensions, a modular regenerator will always be considerably larger than a rotary regenerator. Modular regenerators have the open space (about the size of the face area for one side) between the hot and cold sides, a result of the reduced sealing distances. Several parameters could be adjusted to help reduce the size, such as increasing the hot-side pressure drop. Increasing the hot-side pressure drop to 2-4 percent might provide better results when all life-cycle costs are considered.

The drop in effectiveness due to axial conduction was only 0.42 %. Therefore, axial-conduction effects are not a factor. Most modular regenerators can be designed without substantial axial-conduction effects because most effectiveness reductions due to axial conduction are greatest for [25]:

- Metal heat exchangers with high thermal conductivities,
- High-effectiveness heat exchangers (greater than 95 percent),
- Heat exchangers with short flow lengths (module/matrix thickness) which correspond to short conduction lengths, and
- Large seal coverage (greater than 30 percent) in regenerator.

5.5 Seal-Leakage Calculations

5.5.1 Introduction

One of the significant problems plaguing rotary regenerator designs is seal leakage. The high-pressure air on the cold side escapes under the seals resulting in a reduction of thermal efficiency. As previously mentioned, reducing the area over which leakage occurs would reduce the leakage. This leakage area is the seal-clearance height, h, multiplied by the sealing distance, $dist_{seal}$. The intrinsic problem with rotary designs is a long sealing distance. The sealing distance is the periphery of the high-pressure face area across both sides of the matrix disk. For the modular case, the sealing distance is the module cross-section periphery (for the two modules located in the seal section). The result is a reduction in sealing distance as illustrated in the figure below. Furthermore, the seal length (measured in the direction of the leakage flow) can be considerably long, further contributing to leakage reduction. Therefore, one would expect to get a substantial reduction in seal leakage using a modular regenerator.

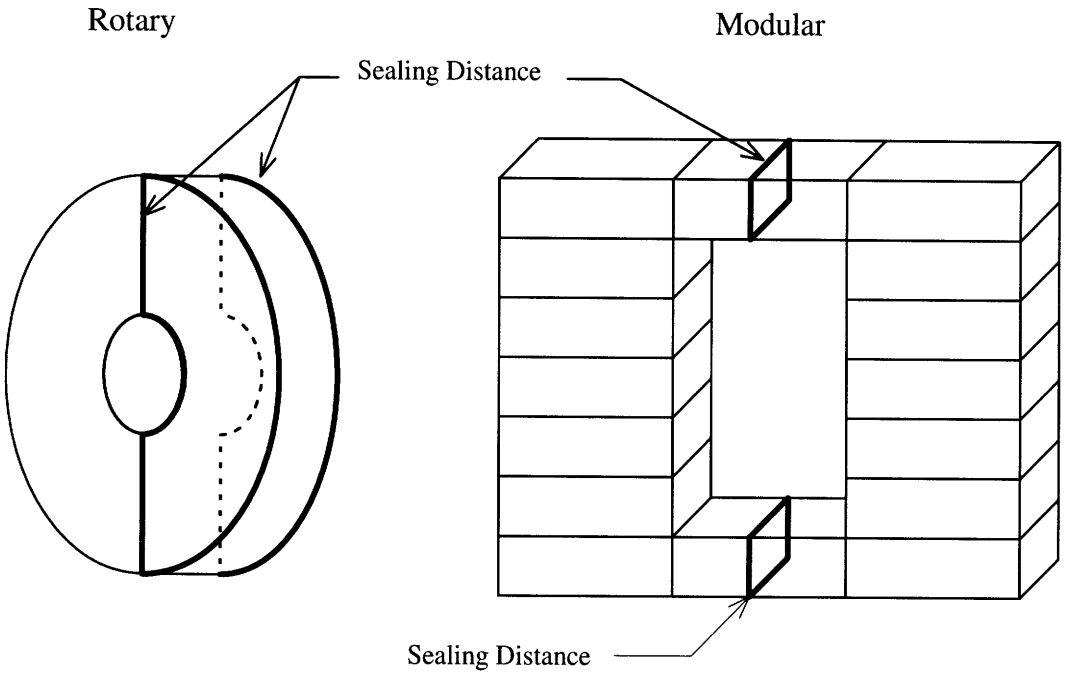

Figure 5.62 Comparison of sealing distances for rotary and modular regenerators.

The leakage can be classified into two groups, gap and carry-over. Gap leakage is the fluid flow traveling between the seals and the matrix. Carry-over leakage consists of the transfer of trapped air within the matrix passages from one side to the other. The modular concept's advantage of shorter sealing distances affects the gap leakage only.

This section presents a method of calculating the seal leakage for modular regenerators. Then, using the numerical design results, actual leakage values for the design are obtained. Then direct comparisons are made with the other concepts that are designed to the same specifications as the module-seal concept. These comparisons will validate the assertion that modular regenerators provide very low leakage rates.

5.5.2 Leakage for Module-Seal Regenerators

5.5.2.1 Introduction

This section presents the leakage analysis for the module-seal concept. The leakage occurs along 4 module faces when the module is located within each seal. Thus, four leakage calculations are required along each face. The convention for naming the sides is shown in the figure below. This analysis is based on the leakage method for rotary regenerators developed by Harper [26]. Harper's approach models the leakage flow through labyrinth seals using the analysis of Egli [27].

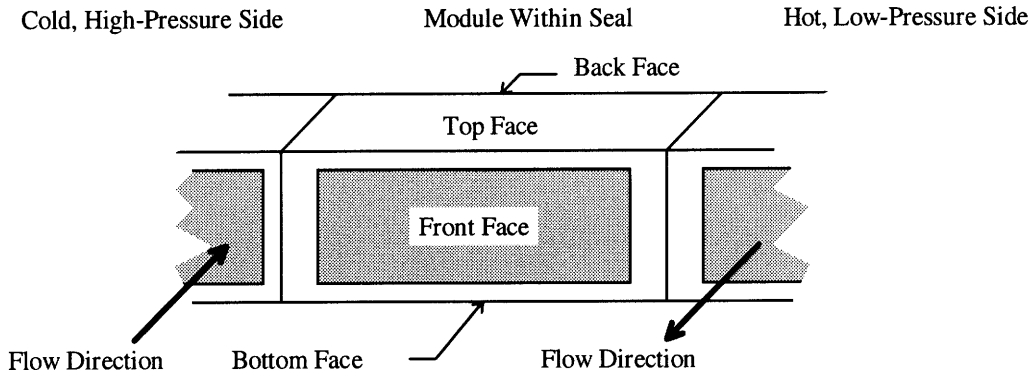

Figure 5.63 Location of module faces where the leakage occurs.

5.5.2.2 Method of Calculation

In this section the general leakage equations are derived. Afterwards, these will be modified to calculate the leakage across each module face.

Assumptions

Harper makes several assumptions as follows:

- The fluid velocity approaching the matrix is low.

- The static pressure inside the matrix passage is equal to the pressure of the corresponding seal face.
- The temperature inside the matrix channel is an appropriate mean temperature.
- The module/matrix velocity is small compared to the fluid velocity under the seals.
- The fluid flow across the end of a matrix passage is similar to the flow through an orifice.
- Enough passages exist under the seal such that the relative change in pressure ($\Delta P/P$) between adjacent passages is small.
- The air trapped in a passages undergoes isothermal compression or expansion.

In addition, the following assumptions and conventions are made for the modular case:

- The pressure along all module faces entering the seal from the cold-side is the compressor outlet pressure. Likewise, the pressure along all module faces entering the seal from the hot-side is the turbine outlet pressure. This can be expressed as:

$$P_{high} = P_2 \tag{5.162}$$

$$P_{low} = P_5 \tag{5.163}.$$

- The fluid temperature along module faces is the mean temperature for the area that the face contacts.
- The leakage calculations along the four module faces does not account for the leakage along the corners of the seal. This leakage is assumed to be negligible since the corner area is generally two orders of magnitude smaller than the total leakage area.
- Seal-clearance heights on all faces are assumed to be constant and uniform during module movement through the seals.
- Leakage due to the ceramic-material porosity is negligible.
- The top and bottom module faces consist of a smooth ceramic surface (module rim). The seals along these faces have a honeycomb structure to provide a labyrinth seal.

The honeycomb seal structure is assumed to have identical dimensions as the ceramic matrix.

- The front and back faces have the core matrix along the middle and the module rims at the edges. The leakage along the rims is modeled identically to leakage along the top and bottom faces.
- Any effects due to flow interactions at the interface of the module core and rim are assumed to be negligible.
- Seal length, l_{seal}, is the length of the seal measured in the direction of the leakage flow (x-direction). The seal width, w_{seal} is measured in the direction normal to the flow along the module face (y-direction).
- Terms with subscripts that contain "top/bottom" or "front/back" refer to a variable that has two values for each face (or share a common value). Only one value should be used at a time and must be consistent throughout the equation.
- Increasing the number of throttlings in a labyrinth seal will decrease the leakage (for a fixed seal-clearance height). Therefore, the matrix passages should be oriented such that the passage width (smaller dimension) is parallel to the direction of leakage flow. This will result in a larger number of throttlings than having the passage length aligned with the leakage flow.

Seal Configuration

The front and back module faces contain the matrix surface; therefore, the leakage along these faces consists of carry-over and gap leakage. The layout of the seal across these faces is shown in Figure 5.64. The top and bottom faces are along the smooth module rims which results in gap leakage only. The seal along these faces is illustrated in Figure 5.65.

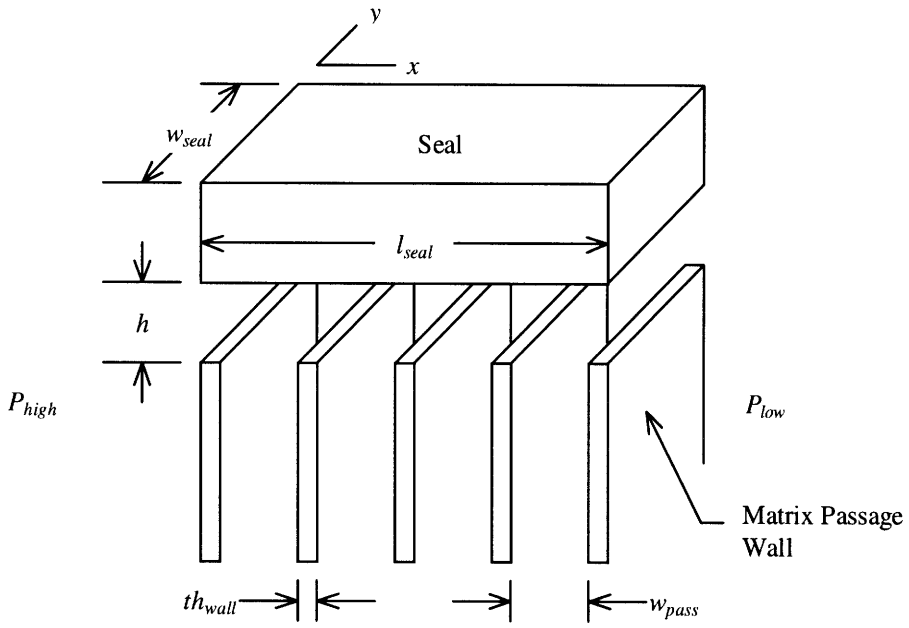

Figure 5.64 Diagram of seal along the module front and back faces showing relevant dimensions.

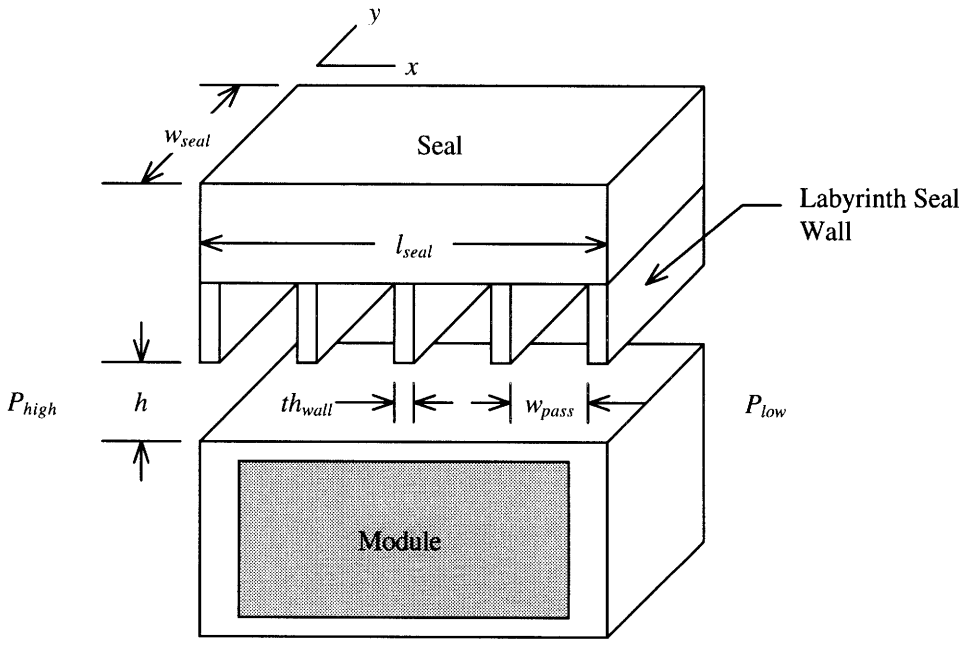

Figure 5.65 Diagram of seal along the module top and bottom faces showing relevant dimensions.

5.5.2.2.1 General Leakage Equations

Gap Leakage

First, equations for gap leakage are derived based on Harper [26]and Pfahnl [5]. The leakage is modeled as inviscid flow and then modified using a correction factor, called the flow coefficient, to account for viscosity. Using Bernoulli's equation for steady inviscid flow along a streamline gives:

$$C(x)=\sqrt{2\frac{\Delta P}{\rho(x)}} \tag{5.164}.$$

The differential mass-flow rate is

$$d\dot{m} \equiv \rho(x)\,C(x)\,dA \tag{5.165},$$

where dA is the differential leakage-flow area along a module face expressed as

$$dA = h\,dy \tag{5.166}.$$

Integrating (along the width of the seal) results in

$$\dot{m}_{gap} = \rho(x)C(x)h\,w_{seal} \tag{5.167}.$$

Substituting in equation (5.164) and the ideal gas law gives

$$\dot{m}_{gap} = h\,w_{seal}\sqrt{2\frac{P(x)\Delta P}{RT}} \tag{5.168}.$$

Now the equation is modified to account for viscosity with the flow coefficient, α. In addition, another correction factor is introduced called Egli's carry-over factor, γ. This parameter is used for account for the non-ideal effects for flow in labyrinth seals. Egli provides data for γ as function of seal height, h, and channel spacing for different values of

the number of throttlings, n. For modular seals, the number of throttlings will be large such that the data will converge to a single curve. Therefore, Egli's carry-over factor is fitted on a curve as follows:

$$\gamma = 59.2\left(\frac{h}{w_{pass} + th_{wall}}\right)^2 + 10.5\left(\frac{h}{w_{pass} + th_{wall}}\right) + 1.03 \qquad (5.169).$$

The gap leakage becomes

$$\dot{m}_{gap} = \alpha\,\gamma\, h\, w_{seal}\sqrt{2\frac{P(x)\Delta P}{RT}} \qquad (5.170).$$

Since the seal will contain a large number of passages, the pressure drop, ΔP, can be expressed as

$$\Delta P = \frac{dP}{dx}\Delta x \qquad (5.171),$$

where $\Delta x = \frac{l_{seal}}{n}$. The number of throttlings, n, can be written as

$$n = \frac{l_{seal}}{w_{pass} + th_{wall}} \qquad (5.172).$$

Substituting in equation (5.170) into (5.171) gives

$$\dot{m}_{gap} = \alpha\,\gamma\, h\, w_{seal}\sqrt{2\frac{P(x)\dfrac{dP(x)}{dx}l_{seal}}{RTn}} \qquad (5.173).$$

The seal length, l_{seal}, can be a chosen parameter with a maximum distance of module-core length, $l_{mod\text{-}mat}$. Increasing l_{seal} increases the number of throttlings leading to

reduced leakage. From the calculated results, l_{seal} can be a long as 0.748 m. Obviously, the faces seal for the rotary case could not have seal lengths this long.

Carry-Over Leakage

As the module moves from one side to the other, it transfers air trapped within the passages. This leakage, titled carry-over leakage, is dependent on the void volume of the matrix.

The carry-over mass-flow rate can be expressed as

$$d\dot{m}_{carry-over} \equiv \rho(x) C_{mod-step1}(x) dA \tag{5.174}.$$

The differential area is the matrix void area taken over one half the module/matrix thickness. This convention is used since the leakage is calculated separately over the front and back faces which includes the carry-over leakage. The differential area can be written as

$$dA = \Psi_{mat}\left(\frac{th_{mod}}{2}\right) dy \tag{5.175}.$$

Integrating and using the ideal gas law for the density term gives

$$\dot{m}_{carry-over} = \frac{P(x) C_{mod-step1} \Psi_{mat} th_{mod} w_{seal}}{2RT} \tag{5.176}.$$

5.5.2.2.2 Leakage Across Front and Back Faces

This section presents the solution for the leakage rates along the front and back module faces. A small section of these faces is occupied by the module rim; however, this section considers the portion of the face along the matrix surfaces. The rim leakage is addressed later. The calculations will have to be performed twice, for positive and negative module movement.

The leakage along a front or back face can be written as:

$$\dot{m}_{front/back} = \dot{m}_{gap} + \dot{m}_{carry-over} \tag{5.177}.$$

Substituting in equations (5.173) and (5.176)gives

$$\dot{m}_{front/back} = \alpha\gamma\, h\, w_{seal} \sqrt{2\frac{P(x)\dfrac{dP(x)}{dx} l_{seal}}{RT_{front/back}\, n}} + \frac{P(x)\, C_{mod-step1}\, \Psi_{mat} \left(th_{mod}\right)_{front/back} w_{seal}}{2RT_{front/back}} \tag{5.178}.$$

The solution for the above equation using Harper's analysis is

$$\frac{1}{1-\dfrac{\left(\dot{m}_{carry-over}\right)_{x=0}}{\dot{m}_{front/back}}} - \frac{1}{1-\dfrac{\left(\dot{m}_{carry-over}\right)_{x=0}}{\dot{m}_{front/back}}\dfrac{P_{low}}{P_{high}}} - \ln\left[\frac{\dfrac{1}{1-\dfrac{\left(\dot{m}_{carry-over}\right)_{x=0}}{\dot{m}_{front/back}}\dfrac{P_{low}}{P_{high}}}}{\dfrac{1}{1-\dfrac{\left(\dot{m}_{carry-over}\right)_{x=0}}{\dot{m}_{frontt/back}}}}\right] = \left[\frac{\dfrac{\left(th_{mod}\right)_{front/back}\Psi_{mat}\, C_{mod-step1}}{2RT_{front/back}}}{\alpha\gamma\, h\sqrt{\dfrac{2}{RT_{front/back}\, n}}}\right]^2 \tag{5.179}.$$

The carry-over leakage is evaluated at x = 0 (the seal entrance from the high-pressure side) as

$$\left(\dot{m}_{carry-over}\right)_{x=0} = \frac{P_{high}\, C_{mod-step1}\, \Psi_{mat} \left(th_{mod}\right)_{front/back} w_{seal}}{2RT_{front/back}} \tag{5.180}.$$

The seal width for the front and back faces is the width of the module core section is:

$$\left(th_{mod}\right)_{front/back} = w_{mod-mat} \tag{5.181}.$$

The leakage rates between the front and back faces will differ since the flow temperatures are different. The temperatures taken are the mean values that the flow is exposed to, thus giving

$$\overline{T}_{front} = \frac{T_2 + T_6}{2} \tag{5.182}$$

and

$$\overline{T}_{back} = \frac{T_3 + T_5}{2} \tag{5.183}.$$

All values are known so that $\dot{m}_{front}$ and $\dot{m}_{back}$ can be solved iteratively using equation (5.179) for a given a seal-clearance height.

The derivations above are applicable for positive module movement. For negative module movement, the module travels with the same velocity but in the opposite direction. The coordinate system does not change so the setting the module velocity to $-\overline{C}_{mod-step1}$ is the only required substitution.

5.5.2.2.3 Leakage Across Top and Bottom Faces

The leakage along the top and bottom faces flow along the module rim resulting in only gap leakage:

$$\dot{m}_{top/bottom} = \alpha\gamma\, h\left(w_{seal}\right)_{top/bottom}\sqrt{-2\frac{P(x)\dfrac{dP(x)}{dx}l_{seal}}{RT_{top/bottom}\,n}} \tag{5.184},$$

where the negative sign is introduced within the radical to account for the negative pressure gradient. Separating variables results in

$$\frac{R T_{top/bottom}\, n}{2\, l_{seal}} \left(\frac{\dot{m}_{top/bottom}}{\alpha \gamma\, h \left(w_{seal} \right)_{top/bottom}} \right)^2 dx = -P(x) dP(x) \tag{5.185}.$$

Integrating from $x = 0$ to $x = l_{seal}$ reduces to

$$R T_{top/bottom}\, n \left(\frac{\dot{m}_{top/bottom}}{\alpha \gamma\, h \left(w_{seal} \right)_{top/bottom}} \right)^2 = \left(P_{high} \right)^2 - \left(P_{low} \right)^2 \tag{5.186}.$$

Solving for the leakage gives

$$\dot{m}_{top/bottom} = \alpha \gamma\, h \left(w_{seal} \right)_{top/bottom} \sqrt{\frac{\left(P_{high} \right)^2 - \left(P_{low} \right)^2}{R T_{top/bottom}\, n}} \tag{5.187}.$$

The seal width for the top and bottom faces is the module/matrix thickness:

$$\left(w_{seal} \right)_{top/bottom} = th_{mod} \tag{5.188}.$$

The mean temperatures for both faces are equal since the flow on each face in contact with identical stations as shown below:

$$T_{top} = T_{bottom} = \frac{T_2 + T_6 + T_3 + T_5}{4} \tag{5.189}.$$

Since the temperatures are equal and the leakage is not a function of the module velocity, the leakage rates for all top and bottom faces are identical (for both positive and negative module movements). Therefore, the total seal leakage along the top and bottom faces is

$$\left(\dot{m}_{top-bottom}\right)_{net} = 4\left[\alpha\,\gamma\,h\left(th_{mod}\right)\sqrt{\frac{\left(P_{high}\right)^2-\left(P_{low}\right)^2}{RT_{top/bottom}\,n}}\right] \tag{5.190}.$$

5.5.2.2.4 Leakage Across the Module Rims

The leakage along the module rims on the front and back faces is modeled like the leakage on the top/bottom faces. Accounting for all 4 rims, the total rim leakage is

$$\left(\dot{m}_{rim}\right)_{net} = 2\left[\alpha\,\gamma\,h\left(w_{rim-top/bottom}\right)\sqrt{\frac{\left(P_{high}\right)^2-\left(P_{low}\right)^2}{RT_{front}\,n}}\right]+ 2\left[\alpha\,\gamma\,h\left(w_{rim-top/bottom}\right)\sqrt{\frac{\left(P_{high}\right)^2-\left(P_{low}\right)^2}{RT_{back}\,n}}\right] \tag{5.191}.$$

5.5.2.2.5 Additional Carry-Over Leakage

If the module rims contain any fillets or slots, these will contribute to the carry-over leakage. This leakage can be estimated as

$$\left(\dot{m}_{fillets-slots}\right)_{net} = \left[\frac{\left(V_{slots}+V_{fillets}\right)_{net}\overline{\rho}_{cold}}{t_{mod-steo1}}\right]-\left[\frac{\left(V_{slots}+V_{fillets}\right)_{net}\overline{\rho}_{hot}}{t_{mod-steo1}}\right] \tag{5.192}.$$

where V_{slots} and $V_{fillets}$ are the volume of the slots and fillets that are subtracted from the rim, respectively.

5.5.2.2.6 Total Leakage

The total leakage can be determined using

$$\left(\dot{m}_{seal}\right)_{net} = \left(\dot{m}_{front} + \dot{m}_{back}\right)_{pos} + \left(\dot{m}_{front} + \dot{m}_{back}\right)_{neg} + \left(\dot{m}_{top-bottom}\right)_{net} + \left(\dot{m}_{rim}\right)_{net} + \left(\dot{m}_{fillets-slots}\right)_{net} \tag{5.193}$$

Normalizing it over the cold-side mass-flow rate gives

$$\hat{\dot{m}} \equiv \frac{\left(\dot{m}_{seal}\right)_{net}}{\dot{m}_{cold}} \tag{5.194}$$

5.5.2.3 Results

The total leakage for design using the numerical results is plotted in the figure below. The seal length, l_{seal}, was chosen to be 0.7 m on all module faces.

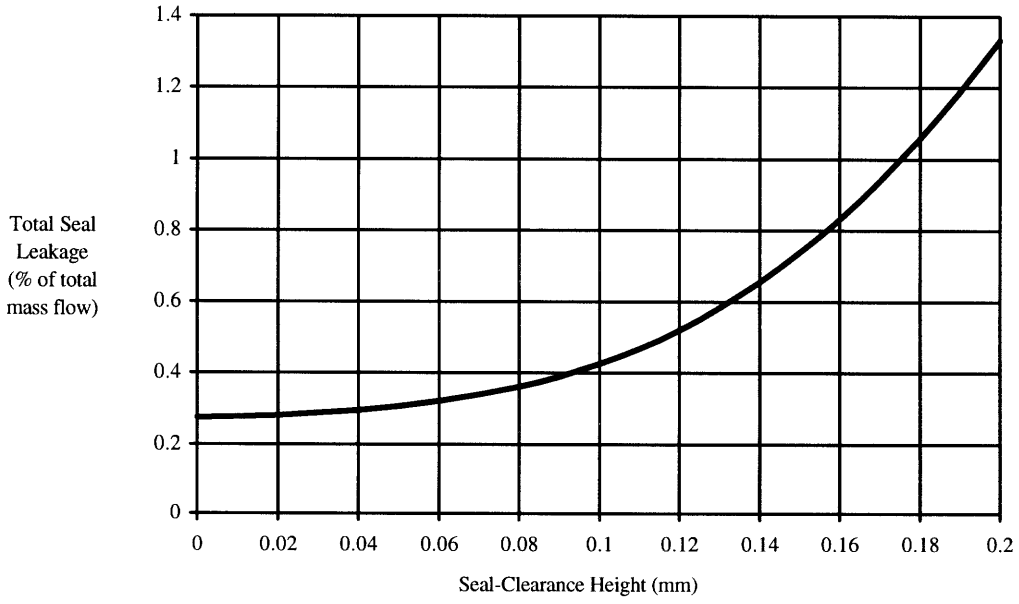

Figure 5.66 Predicted net seal leakage from the high-pressure side of the regenerator based on the design results for the module seal concept.

As the seal-clearance height approaches zero, the leakage approaches the carry-over leakage value which is less than 0.3 % of the total mass flow.

5.5.3 Leakage for Gate-Seal Regenerators

Even though the design of the gate-seal concept is not investigated, its leakage can be estimated for comparisons with other concepts. For this analysis, the gate-seal concept assumes the following:

- Only one module is used between the gates. Therefore, the leakage for each seal consists of transferring the mass of air within the chamber (the space between the two gates) over the total time for one module movement.
- The chamber-clearances height (seal height) around all module faces is constant and uniform.

The volume for the module is

$$V_{mod} = \left(l_{mod-mat}\, w_{mod-mat}\, th_{mod}\right)\left(1-\Psi_{mat}\right)+V_{rim} \tag{5.195}.$$

The volume of the chamber is based on choosing a chamber clearance height, $h_{chamber}$, such that:

$$V_{chamber} = \left(l_{mod}+2\,h_{chamber}\right)\left(w_{mod}+2\,h_{chamber}\right)\left(th_{mod}+2\,h_{chamber}\right) \tag{5.196}.$$

The volume of air within a chamber that contains a module is

$$V_{air-chamber} = V_{chamber} - V_{mod} \tag{5.197}.$$

For positive module movement, $V_{air\text{-}chamber}$ is released to the low-pressure side when the low-pressure-side chamber door opens. This occurs during every interval of one module movement. Therefore, the leakage is the rate at which this volume of air is released from the chamber. This can be expressed as

$$\left(\dot{m}_{chamber}\right)_{pos} = \frac{V_{air-chamber}\,\overline{\rho}_{cold}}{t_{mod}} \tag{5.198}$$

For negative module movement, the chamber is module-less and full of compressed air before the door opens to let a module enter from the hot side. Thus the leakage for this is

$$\left(\dot{m}_{chamber}\right)_{neg} = \frac{V_{chamber}\,\overline{\rho}_{cold}}{t_{mod}} \tag{5.199}$$

The total seal leakage is

$$\left(\dot{m}_{chamber}\right)_{net} = \left(\dot{m}_{chamber}\right)_{pos} + \left(\dot{m}_{chamber}\right)_{neg} \tag{5.200}$$

Results

The net seal leakage for the gate-seal concept is shown next.

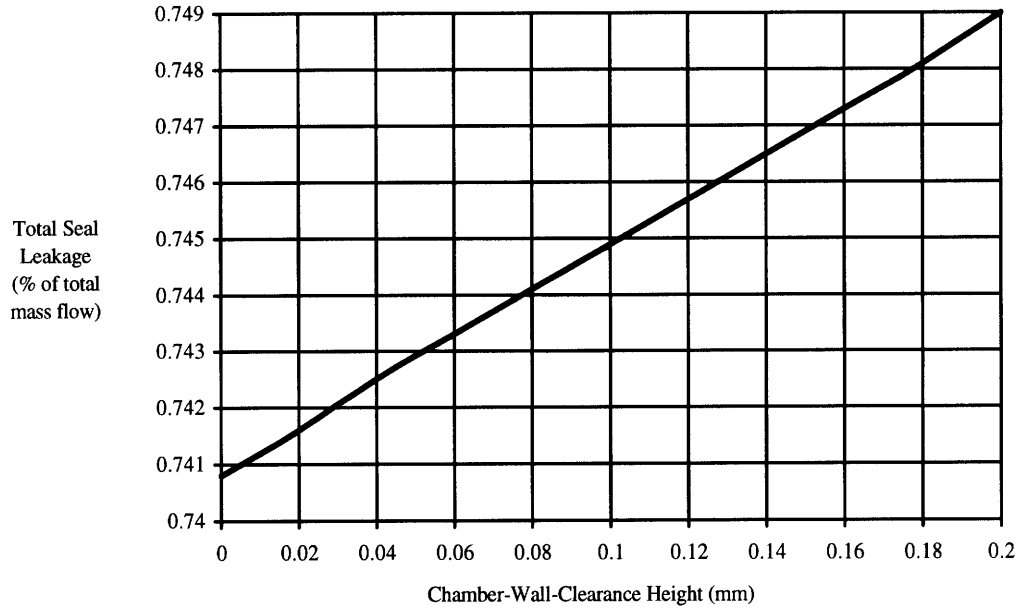

Figure 5.67 Predicted net seal leakage from the high-pressure side of the regenerator for the gate-seal concept.

At zero chamber-wall-clearance height, the leakage is the flow from the volume of one chamber (for negative module movement) plus the volume of the voids for the module in the other chamber. This is somewhat analogous to carry-over leakage and will be termed as such.

5.5.4 Leakage for Rotary Regenerators

The leakage analysis was applied to a rotary regenerator to give a direct comparison between the modular and rotary concepts.

Some additional chosen parameters were required to size a rotary regenerator. For example, the seal coverage was chosen at 5 percent, and the hub-to-tip ratio was chosen at 0.2 . This yielded a regenerator with an inside radius of 0.125 m and an outer radius of 0.625 m. Rims on the inside and outside of the core were chosen at a width of 0.03 m. For more information on sizing a rotary regenerator, see the design example in Wilson [13].

Some modifications to the leakage equations are required for rotary regenerators. The seals consist of radial and circumferential seals. The equations for the radial-seal leakage are based on the derivations from Pfahnl [5]. The circumferential seals were assumed to use labyrinth seals similar to the seals along the top and bottom module faces (Pfahnl uses flat surface circumferential seals).

Leakage calculations for a discontinuous-rotating regenerator have also been made to give a comparison of this low-leakage rotary option to the modular case. The regenerator was chosen to spend only 10 percent of the 360°-rotation time rotating. This corresponds to taking 10 percent of the gap leakage but the carry-over leakage is unchanged. See Pfahnl [5] and Beck [4] for more information on discontinuously-rotating regenerators and associated leakage.

Results

The following plot is the total seal leakage for the two rotary cases.

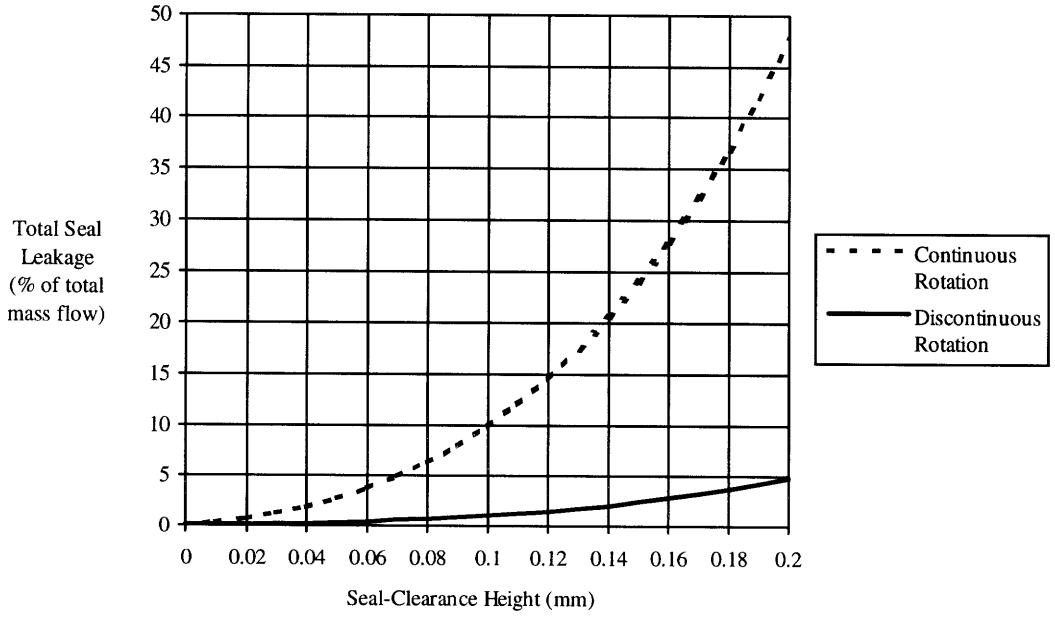

Figure 5.68 Predicted net seal leakage from the high-pressure side of a rotary regenerator with continuous and discontinuous rotation.

Obviously, the above plot show the very poor leakage performance for continuous-rotating regenerators as seal height increases. This can occur over time as the seals start to wear down thus increasing the seal clearances.

5.5.5 Discussion

By comparing the plots for the 4 concepts shown in the three previous figures, the modular concepts provide the best leakage performance. For a seal-clearance height of 0.2 mm, continuous rotation provides clearly unacceptable results. The discontinuous-rotation concept has seal leakage at 5 %, however, using a seal height of 0.1 mm resulted in leakage flow around 1 %. The module-seal concept has a net leakage rate close to 1.3 % for a seal height of 0.2 mm. If the seal height was reduced to 0.1 mm, the net leakage was close to 0.4 %. The gate-seal concept provided the lowest leakage at 0.2 mm, but at smaller seal heights, its leakage was greater than other concepts. The larger value is due to the gate-seal concept having greater "carry-over" leakage.

Despite the gate-seal's low leakage performance, this concept is more complex mechanically over the module-seal concept since mechanisms are needed to move the modules in and out of the chambers (especially for negative module movement). These mechanisms may require larger seal clearances thus increasing the leakage.

5.5.6 Conclusions

This section presented a detailed method for predicting the seal leakage for modular regenerators. The results show a dramatic reduction in leakage over comparable rotary concepts. The module-seal concept, the simplest modular regenerator, is expected to have very good leakage performance even at unacceptable seal clearances for rotary regenerators. Therefore, modular regenerators provide the better leakage performance due to the inherent reduction in sealing distances.

5.6 Pressure Gradient Within the Seals

5.6.1 Introduction

This section presents the method to determine the pressure gradient within the seal for the module-seal concept. Using the leakage results in the previous section, pressure gradient plots are presented for the design. Since different leakage rates occur along each face, different pressure gradients exist. This analysis neglects the leakage along the rims on the front and back module faces.

5.6.2 Method of Calculation

5.6.2.1 Pressure Gradient for Front and Back Faces

The pressure gradient can be determined using Harper's solution shown in equation (5.179), but rewritten to apply for a more general case:

$$\frac{1}{1-\frac{\left(\dot{m}_{carry-over}\right)_{x=0}}{\dot{m}_{front/back}}}-\frac{1}{1-\frac{\left(\dot{m}_{carry-over}\right)_{x=0}}{\dot{m}_{front/back}}\frac{P(x)}{P_{high}}}-\ln\left[\frac{\frac{1}{1-\frac{\left(\dot{m}_{carry-over}\right)_{x=0}}{\dot{m}_{front/back}}\frac{P(x)}{P_{high}}}}{\frac{1}{1-\frac{\left(\dot{m}_{carry-over}\right)_{x=0}}{\dot{m}_{front/back}}}}\right] = \left[\frac{\frac{\left(th_{mod}\right)_{front/back}\Psi_{mat}\,C_{mod-step1}}{2RT_{front/back}}}{\alpha\gamma h\sqrt{\frac{2}{RT_{front/back}\,n}}}\right]^2\left(\frac{x}{l_{seal}}\right) \quad (5.201).$$

Substituting in the results of the leakage rates for the front and back faces leaves only the pressure, x (x is the direction of the leakage flow), and seal height as the unknowns.

Therefore, the seal height will have be chosen to get the pressure gradient. These calculations are required for positive and negative module movement.

5.6.2.2 Pressure Gradient for Top and Bottom Faces

The gap leakage in equation (5.185) can be integrated from $x = 0$ to $x = x$ resulting in

$$\frac{RT_{top/bottom}\, n}{l_{seal}}\left(\frac{\dot{m}_{top/bottom}}{\alpha\gamma\, h\left(w_{seal}\right)_{top/bottom}}\right)^2 x = \left(P_{high}\right)^2 - \left[P(x)\right]^2 \qquad (5.202).$$

Solving for the pressure term gives

$$P(x) = \sqrt{\left(P_{high}\right)^2 - \frac{RT_{top/bottom}\, n}{l_{seal}}\left(\frac{\dot{m}_{top/bottom}}{\alpha\gamma\, h\left(w_{seal}\right)_{top/bottom}}\right)^2} \qquad (5.203).$$

The leakage rates for the top and bottom faces are identical, therefore the pressure gradients are the same. The pressure gradients will differ for positive and negative movement since negative module movement is going in the negative x-direction.

5.6.3 Results

Plots showing the pressure gradient along the seal based on the design results are provided below. The first four plots are the pressure gradients along the top and bottom faces for positive and negative module movement. Three seal heights (0.08, 0.14, and 0.2 mm) are used to illustrate the influence of seal height on the pressure gradient.

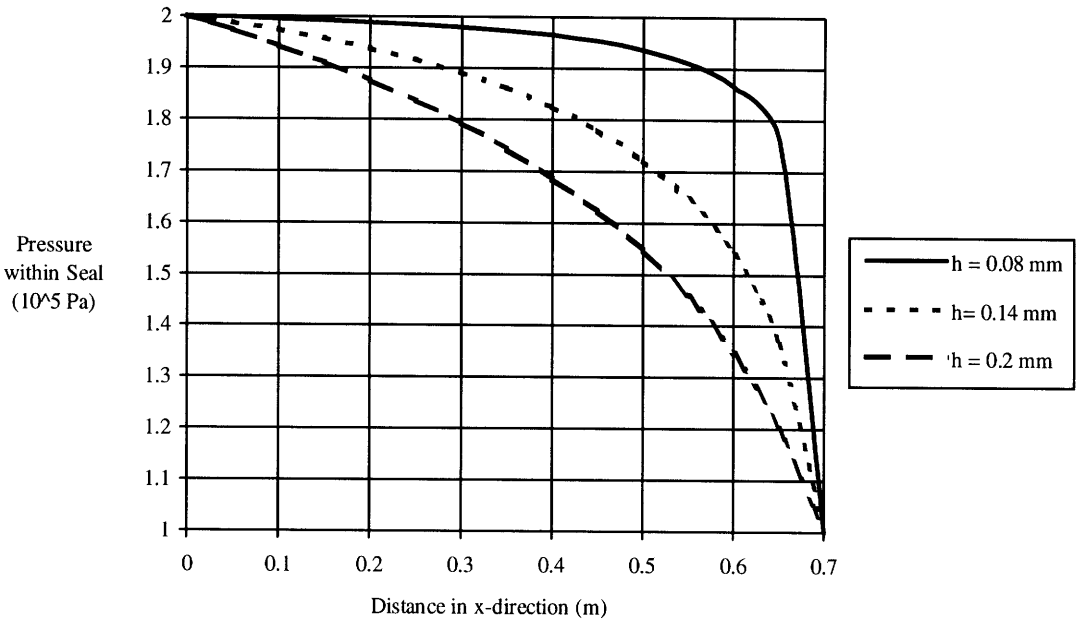

Figure 5.69 Predicted pressure gradient within the seal for positive module movement along the front face.

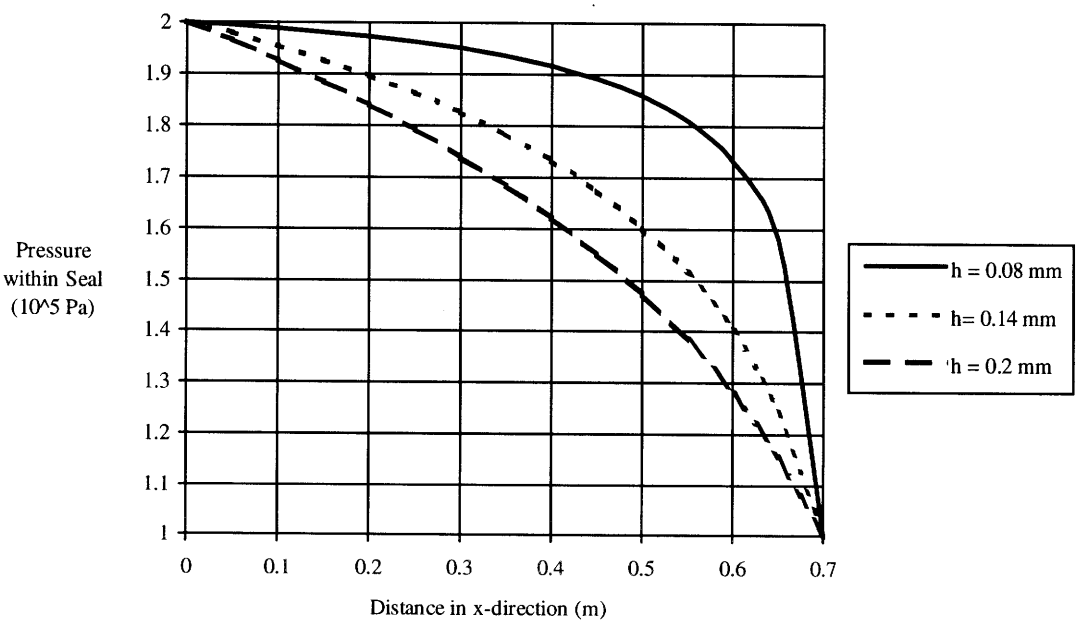

Figure 5.70 Predicted pressure gradient within the seal for positive module movement along the back face.

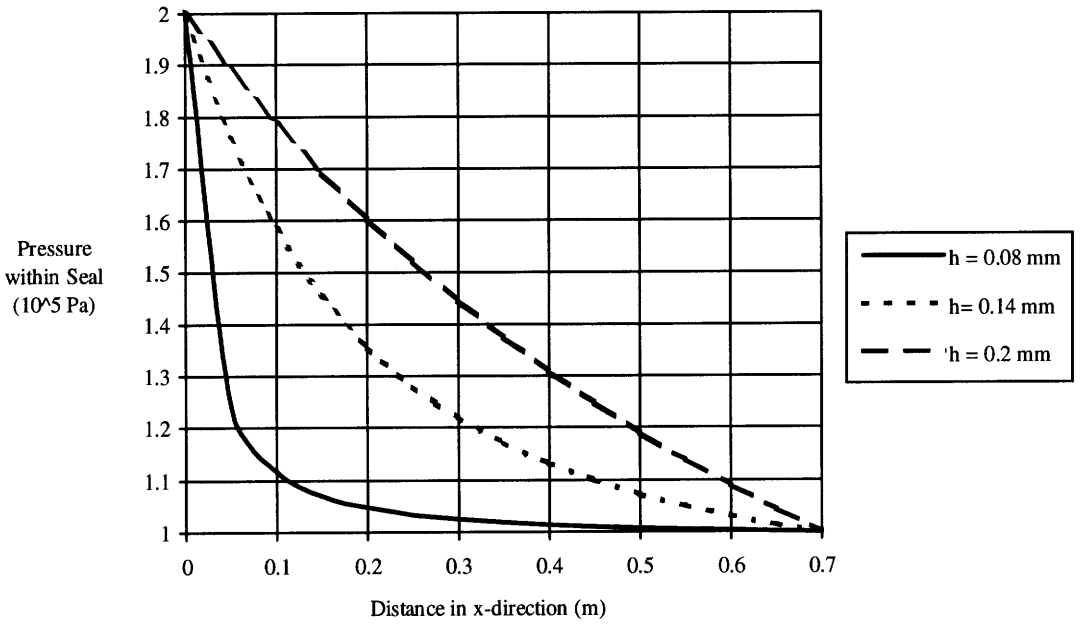

Figure 5.71 Predicted pressure gradient within the seal for negative module movement along the front face.

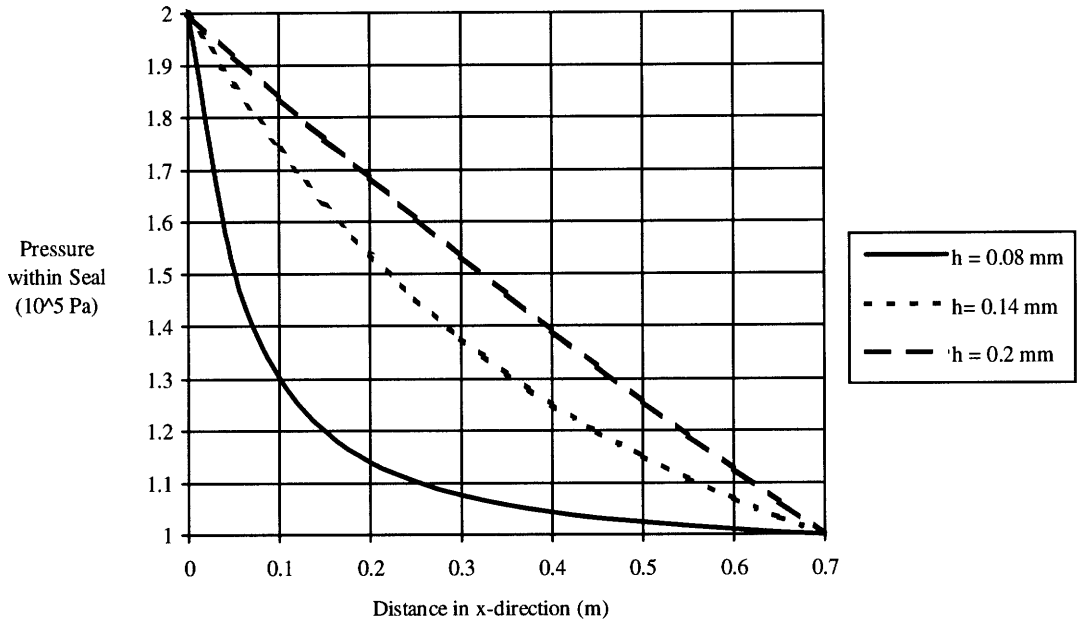

Figure 5.72 Predicted pressure gradient within the seal for negative module movement along the back face.

The next figure shows the pressure gradient along the top and bottom faces. Since the leakage is the same along all top and bottom faces, the pressure gradient is also identical.

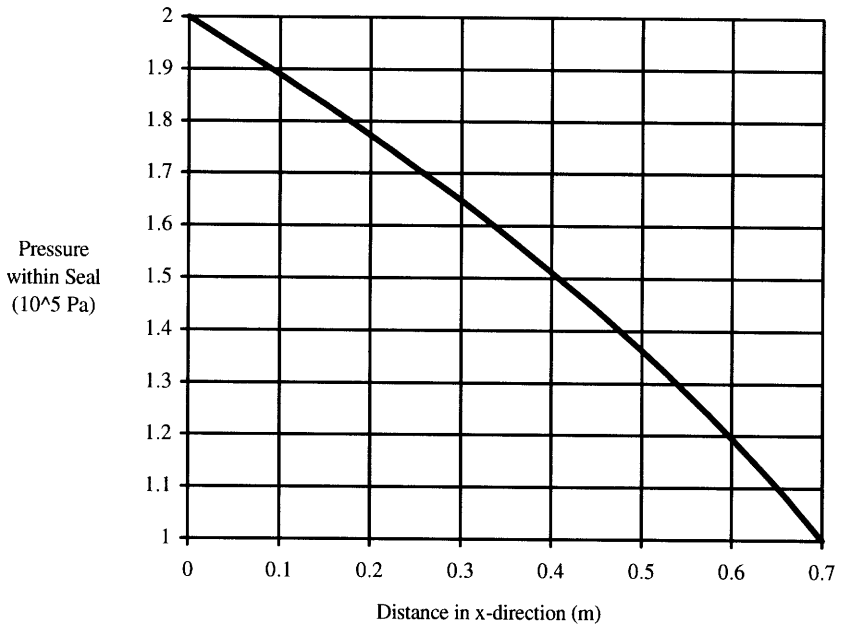

Figure 5.73 Predicted pressure gradient within the seal along all top and bottom module faces (including positive and negative module movement).

5.6.4 Discussion

The shape between the curves for positive and negative module movement differs due to the carry-over leakage. For positive module movement, the concave shape arises from transferring the high-pressure air within the passages. For negative module movement, the convex shape is from the transfer of low-pressure air within the matrix.

For the front and back faces, the pressure gradient is quite dependent on the seal height. As the seal height decreases, the gap leakage decreases but the carry-over leakage is constant. Theoretically at a zero seal height, the matrix will transfer the air within the passages without letting it travel to the seal gap (since it is at zero height). As a result, the pressure within the passages does not change until it reaches the end of the seal. The

pressure curve would experience a step change at the seal exit. The plots show that the pressure curve approaches this as the seal height decreases. On the other hand, as the seal height increases, the pressure gradient approaches a near-linear profile because the gap leakage starts to dominate over the carry-over leakage. Since no carry-over leakage occurs along the top and bottom faces, the pressure gradient is independent of seal height.

5.7 Seal-Leakage-Reduction Techniques

5.7.1 Introduction

Another advantage with the modular concept is that the design can be altered to reduce the leakage even further. Three options are presented. The first option consists of increasing the number of modules. The second consists of linking the two seals together. The last option pertains to using clampable seals around a module.

5.7.2 Increasing the Number of Modules

As shown previously, increasing the number of modules on the cold side decreases the module width (the module/matrix thickness stays constant). The net result is a reduction in sealing distance which should correspond to a reduction in seal leakage. Using the design results, the change in sealing distance as a function of cold-side modules is shown in the following plot.

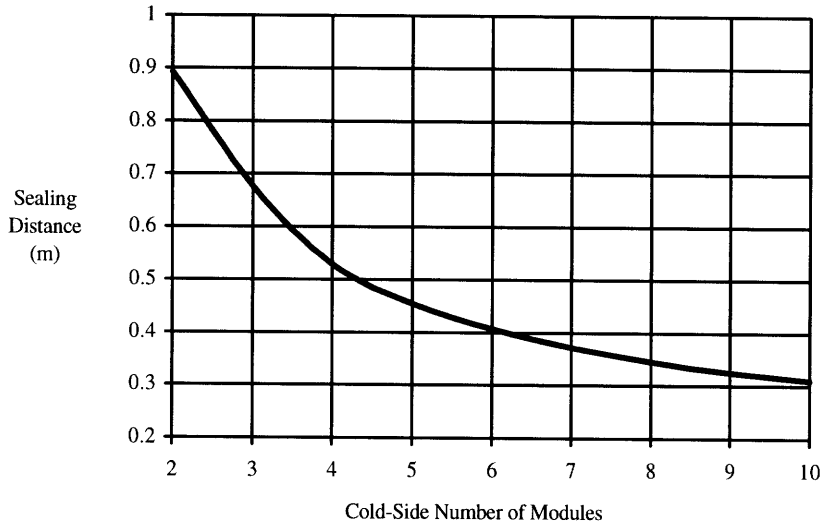

Figure 5.74 Effect of changing the cold-side number of modules on the sealing distance.

One might think the carry-over leakage increases as $Nmod_{cold}$ increases since the module velocity gets larger. This is not the case because carry-over leakage is independent of the number of modules. Carry-over leakage is dependent on the ceramic mass-flow rate, set by C_{rot} (constant). Even though the module velocity increases, the module width decreases such that ceramic mass-flow rate and thus carry-over leakage is constant. Therefore, as the sealing distance decreases according the above plot, only the gap leakage decreases. Using the design results, this corresponds to reductions in total seal leakage as $Nmod_{cold}$ is increased. This is shown in the following figure.

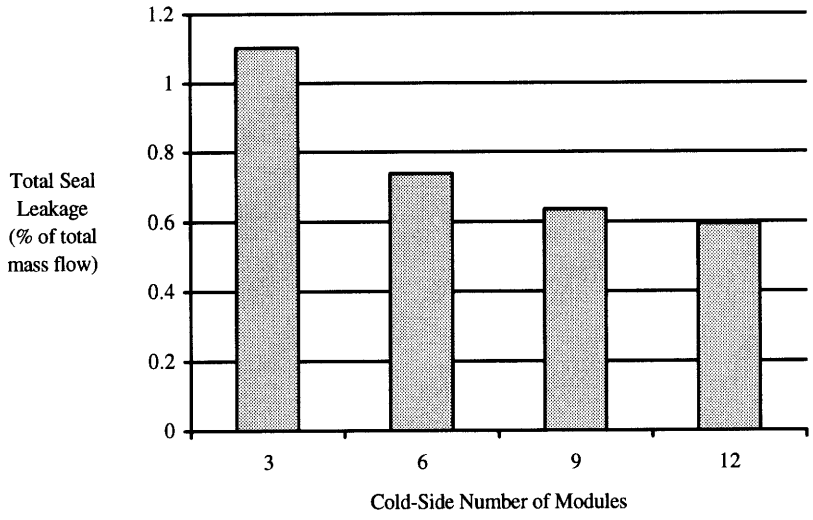

Figure 5.75 Effect of changing the cold-side number of modules on the total seal leakage.

As seen in the above figure, the leakage starts to level off around 6 cold-side modules. Therefore, choosing $Nmod_{cold}$ around 6 should give good results. If further leakage reduction is desired by increasing $Nmod_{cold}$, the designer must analyze the effects of increasing the module velocities and any constraints imposed by the cylinder system.

5.7.3 Seal-Channel Concept

5.7.3.1 Introduction

Wilson proposed that the gate-seal concept could have additional leakage reductions [28] with a slight design modification. If the chambers on one seal where connected to the chambers on the other (via the seal channel), the air pressures would equalize, thus lowering the pressure finally entering low-pressure side. If several chambers were used for one seal, the pressure in each successive chamber drops.

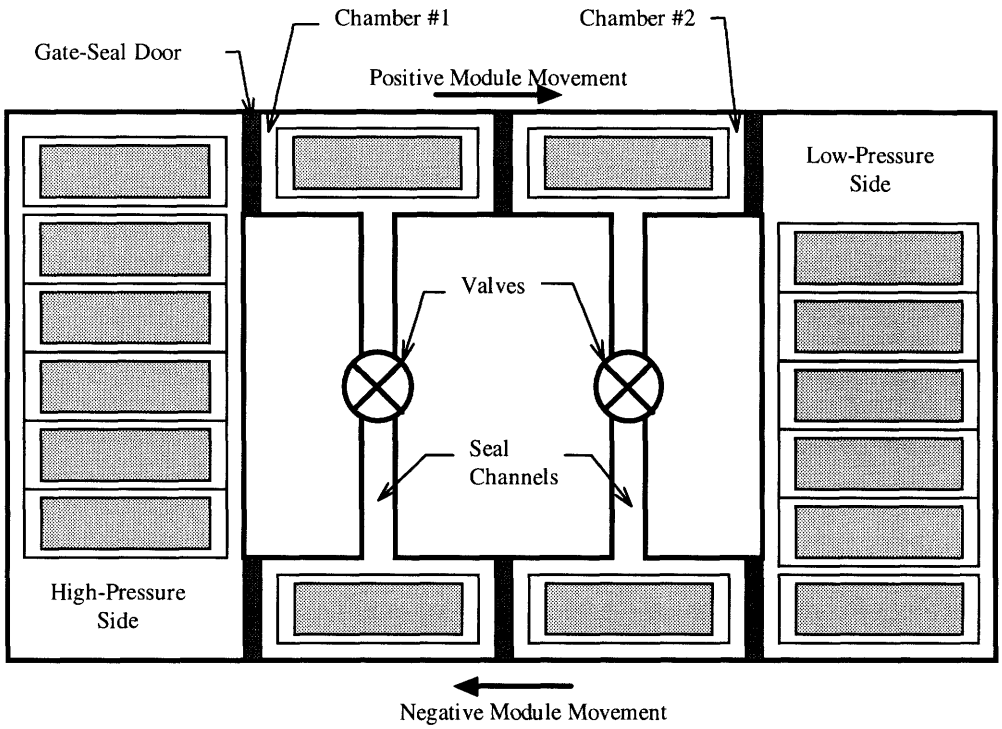

Figure 5.76 Diagram of the channel-seal concept for the gate-seal regenerator with two seal channels, proposed by Wilson [28].

For positive module movement, chamber #1 is full of high-pressure air when the module enters. Then the valve opens and it is equalized with the lower-pressure air from the chamber in the other seal. As the module enters chamber #2, the same sequence occurs, and the pressure is further reduced. By the time the module enters the low-pressure side, the leakage is reduced because the pressure is lower than not using seal channels.

This concept can be applied to the module-seal regenerator illustrated in the figures below. Each seal is essentially separated into two seals by adding a seal channel. The flow goes through one seal then enters an open space, the entrance to the seal channel, where the pressures on all module faces equalize with each other. The pressure then equalizes with the seal on the other side when the valve opens.

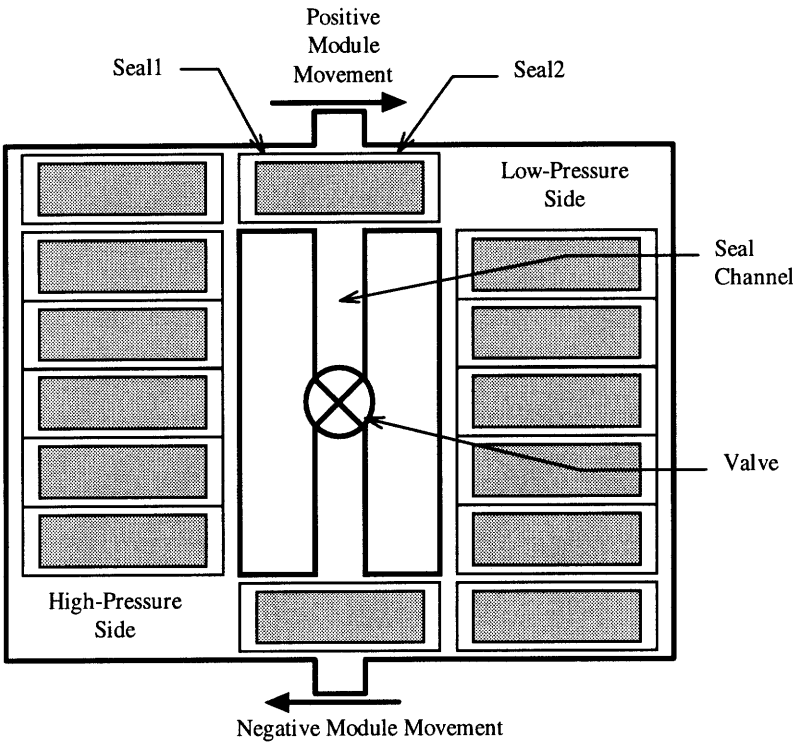

Figure 5.77 Diagram of the module-seal regenerator with a seal channel for leakage reduction.

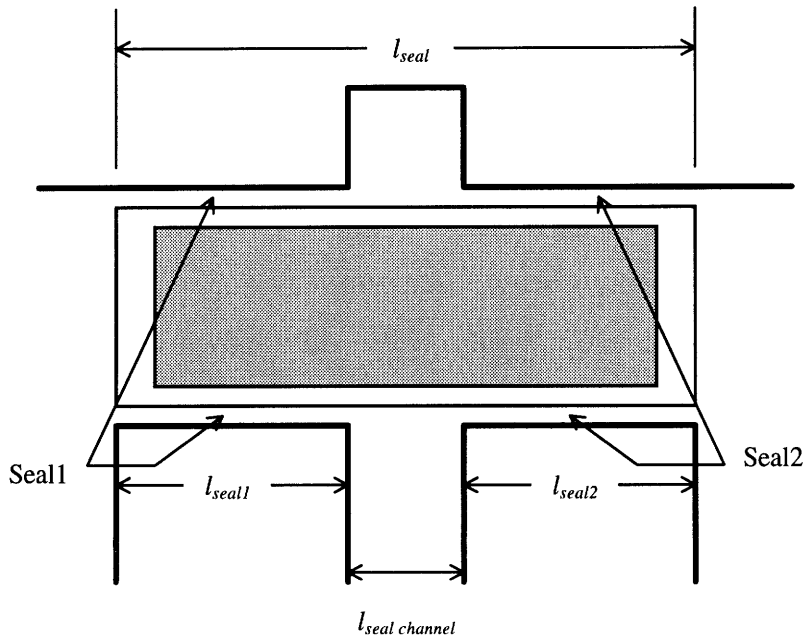

Figure 5.78 Diagram of the seals along the top and bottom module faces for the module-seal regenerator with a seal channel.

This concept of leakage reduction is essentially changing the pressure gradient for both seals towards a linear profile. Recall that a linear-profile pressure gradient occurs when the carry-over leakage is negligible or does not exist. Therefore, this technique is reducing the carry-over leakage.

Selecting a large value for the length of the open space in the direction of leakage flow, l_{space}, may increase the leakage because as l_{space} increases, then the length of the two seals, l_{seal1} and l_{seal2}, decreases (which decreases the number of throttlings). Furthermore, additional seal channels can be used. This would give another space for the pressures to equalize (and drop for positive module movement), thus possibly reducing the leakage even further. Again, if the number of seal channels increase, the length of each seal decreases which could result in additional leakage.

This following section presents a method to estimate the reduction in leakage after incorporating a seal channel.

5.7.3.2 Method of Calculation

This method uses the leakage techniques defined in earlier sections. Since adding a seal channel divides the seal into two seals, the leakage calculations will have to be done twice. First, the pressure in seal channel must be known. This can be estimated by using the pressure-gradient equations derived in the Section 5.6. Knowing the location at the end of seal1 ($x=l_{seal1}$), the pressures for each face is found using equations (5.201) and (5.203). Since all pressures are brought to equilibrium, the pressure in the seal channels for positive and negative module movement are

$$P_{seal\text{-}channel,\ pos} = \left(\frac{P_{front}\left(x = l_{seal1}\right) + P_{back}\left(x = l_{seal1}\right) + P_{top}\left(x = l_{seal1}\right) + P_{bottom}\left(x = l_{seal1}\right)}{4} \right)_{pos} \tag{5.204}$$

and

$$P_{seal\text{-}channel,\ neg} = \left(\frac{P_{front}(x = l_{seal2}) + P_{back}(x = l_{seal2}) + P_{top}(x = l_{seal2}) + P_{bottom}(x = l_{seal2})}{4} \right)_{neg} \quad (5.205),$$

where l_{seal1} is the length of the first seal entered by the module for positive movement and l_{seal2} is the length of the first seal entered by the module for each negative movement. Then the pressure of the entire seal chamber after the valve opens is

$$P_{seal\text{-}channel} = \frac{P_{seal\text{-}channel,\ pos} + P_{seal\text{-}channel,\ neg}}{2} \quad (5.206).$$

This value is substituted for P_{high} into all the leakage equations along with the new seal length set at l_{seal2}. This determines the leakage exiting seal2 which equals the total leakage.

5.7.3.3 Results

The following results are based on a seal-clearance height of 0.15 mm. The length of the seal channel was chosen at 0.05 m and situated in the middle of the seal thus l_{seal1} and l_{seal2} both equal 0.325 m. Using the pressure gradient equations resulted in $P_{seal\ channel}$ equal to $1.59 \cdot 10^5$ Pa. Then plugging this into the leakage equation gave a total seal leakage of 0.56 % of the total mass flow. The original leakage was at 0.74 %. Therefore, a 24 % drop in seal leakage occurred using the seal channel.

5.7.4 Clampable Seals

This technique basically adds a sealing mechanism to the module-seal concept. This is somewhat analogous to the discontinuous-rotation regenerator. A seal is clamped on the module faces at all times except during actual module movement for step1. Therefore, gap leakage occurs only during step1 actual module movement. This technique is probably not necessary since the module-seal concept has already shown to have low leakage. Furthermore, designing a clampable seal around rectangular objects is difficult due to the 90° corners of the module.

5.7.5 Conclusions

This section presented options to further reduce the leakage for modular regenerators. Three possible techniques were described. Increasing the number of modules and linking the two seals via a seal channel can easily be applied to the designs. Both provide significant leakage reduction to merit consideration. The third concept using clampable seals is probably too mechanically complex to warrant its use since leakage rates for module-seal concept are generally low.

5.8 Summary

This chapter first presented the necessary chosen parameters needed to design a modular regenerator. Then a method to specifically design the regenerator by sizing it and measuring various performance aspects were discussed. Afterwards, the chosen parameters were assigned numerical values, optimized, and plugged into the method to get the final design results. With these results, a procedure to determine the seal leakage and pressure gradients were described. Finally, leakage-reduction techniques were presented to provide even better performance.

The results using the module-seal design were based on a small gas-turbine engine and yielded quite acceptable results. Cylinder configuration #2 balanced the strong pressure forces resulting in a lower power requirement. Leakage calculations showed that modular regenerators have less seal leakage than rotary designs. The leakage rates could be reduced further by implementing the leakage-reduction methods.

With the information in this chapter, the designer can model a modular regenerator for many applications. The next logical step is to conduct experiments to validate the theoretical results and conclusions presented.

6. Guidelines for Future Work

The research presented is an initial design study for the modular regenerator concept. Continued investigations will be required before making a transition to designing a working prototype. The following lists some key issues that should be addressed later as the design matures:

- Further studies will be required to optimize the rim dimensions. Future work might consider analyzing how the percentage of core matrix within a channel affects effectiveness (i.e. when does increasing rim width for top and bottom faces reduce effectiveness?).
- Frictional testing should be done at all sliding module interfaces to determine coefficients of friction.
- Design work to development mechanisms (such as ceramic rollers or bearings) that reduce the frictional forces should be performed.
- Further design work is needed on the module replacement mechanism. This work addressed only the possibility of using such a mechanism.
- By using the module replacement mechanism, the new modules may not be heated prior to entering the regenerator. This will lower the regenerator effectiveness. Analysis should be made to measure the influence of effectiveness reductions as new modules are introduced.

- Actual leakage experiments should be conducted to confirm the results from the analysis and substantiate the assumptions made.
- Further analysis is required on module design. If a cement is used to join the matrices and the rims together (and separate matrix sections), then testing should be conducted to ensure the cement maintains its bonding integrity under the thermal environment.
- Additional work is needed on selecting what type of deceleration devices should be used to slow the modules down (depending on the configuration chosen).
- In terms of module movement via pneumatic/hydraulic cylinders, this research presented only the general configuration and the minimum bore sizes. Additional work is required on developing the cylinder systems including the integration of the external compressor (if used), connecting lines, valves, and control system.
- Since the module rim is solid ceramic, its mass will be significant. Therefore, the rim mass should be minimized such that it provides the necessary structural support. Further analysis is needed for this optimization.
- Comprehensive failure analysis for the regenerator should be made to identify possible failures, the magnitude of the failures (i.e., will a failure propagate), and the mean time between such failures.
- Further analysis should be made for the casing design such as performing stress analysis to ensure that the casing can withstand the pressure loads from the cold side.
- Seals must be designed at the interfaces of the cylinder rods with the casing (on the cold side). Some compressed air will escape at these interfaces and should be accounted for during the leakage calculations.

References

[1] Wilson, D. G., United States Patent, Patent Number 5,259,444, November 9, 1993.

[2] Wilson, D. G., "Turbine Cars, Major Contender, Bumpy Road," *Technology Review*, pp50-57, February/March 1995.

[3] Bathie, W. W., *Fundamentals of Gas Turbines*, John Wiley & Sons, New York, NY, 1984.

[4] Beck, D. S., *Regenerators for Gas-Turbine Applications*, Ph.D. Thesis, Massachusetts Institute of Technology, Cambridge, MA, September, 1993.

[5] Pfahnl, A. C., *Investigations in Novel Regenerator Concepts for Use in a Small Motor-Vehicle Gas-Turbine Engine*, MSME Thesis, Massachusetts Institute of Technology, Cambridge, MA, June, 1995.

[6] Wilson, D. G., "Low-leakage and high-flow regenerators for gas turbine engines," Proc. Instn. Mech. Engrs., vol. 207, pp195-202, 1993.

[7] Wilson, D. G., "The supplementary-fired exhaust-heated cycle for coal, wood and refuse-derived fuel," Proc. Instn. Mech. Engrs., vol. 207, pp203-208, 1993.

[8] Day, J. Paul, "ATTAP Extruded Ceramic Regenerator Material/Process Development," Proceedings of the Annual Automotive Technology Development Contractor's Coordination Meeting, 1994.

[9] Day, J. Paul, "A Rotary Heat Exchanger for Automobile and Other Ground Based Gas Turbines" ASME Conference Paper 94-GT-124, New York, NY, June 13-16, 1994.

[10] Frazer, J., private communication, Corning Incorporated, January 18, 1995.

[11] Carborundum Company, "Carborundum Expanding Paper, Product Specifications," Carborundum Brochure, Niagara Falls, NY, 1991.

[12] Hagler, C. D., *The Design of a Ceramic Rotary Regenerator for a Regenerated Low-Pressure Ratio Gas-Turbine Engine*, MSME Thesis, Massachusetts Institute of Technology, Cambridge, MA, April, 1987.

[13] Wilson, D. G., *The Design of High-Efficiency Turbomachinery and Gas Turbines*, The MIT Press, Cambridge, MA, 1984.

[14] Kays, W. M. and A. L. London, *Compact Heat Exchangers*, McGraw-Hill Book Company, New York, NY, 1984.

[15] Wilson, D. G., private communication, February 6, 1995.

[16] Wilson, D. G., "A Method of Design for Heat-Exchanger Inlet Headers," ASME Paper 66-WA/HT-41.

[17] Parker Fluidpower, *Design Engineers Handbook*, Bulletin 0224-B1, Parker Hannifin Corporation, Cleveland, Ohio, 1979.

[18] Wilson, D. G., private communication, April 10, 1995.

[19] Beck, D. S., "The Effect of Seal Width on Regenerator Effectiveness", ASME Conference Paper 93-GT-341, New York, NY, May 24-27 1993.

[20] Bahnke, G. D. and C. P. Howard, "The Effect of Longitudinal Heat Conduction on Period-Flow Heat Exchanger Performance,", *Transactions of the ASME Journal of Engineering for Power*, Vol. 86, 1964.

[21] Wilson, D. G., private communication, April 19, 1995.

[22] Corning Incorporated, "Celcor Honeycomb Catalyst Supports," Corning Brochure, Corning, NY.

[23] Pfahnl, A. C., "Static-Friction Coefficients Tests of Ceramic-Honeycomb Samples", Massachusetts Institute of Technology Department of Mechanical Engineering Memorandum to D. G. Wilson, 3/13/94.

[24] Wilson, D. G., private communication, March 23, 1995.

[25] Beck, D. S., private communication, March 15, 1995.

[26] Harper, D. B., "Seal Leakage in the Rotary Regenerator and Its Effect on Rotary Regenerator Design for Gas Turbines," *Transactions of the ASME*, February, 1957, pp233-245.

[27] Egli A., The Leakage of Steam Through Labyrinth Seals," *Transactions of the ASME*, FSP-57-5, 1935, pp115-122.

[28] Wilson, D. G., private communication, January 17, 1995.

[29] Lipp, D., private communication, Corning Incorporated, 1/27/95.

[30] Chappell, M. S., and E. P. Cockshutt, "Gas Turbine Cycle Calculations: Thermodynamic Data Tables for Air and Combustion Products for Three Systems of Units," NRC, Aeronautical Report LR-579, National Research Council of Canada, August, 1974.

[31] Incropera, F. P. and D. P. DeWitt, *Fundamental of Heat and Mass Transfer*, John Wiley & Sons, New York, NY, 1990.

Appendix

Supporting Curve Fits and Equations

A.1 Corning Cordierite Material Properties

The following are curve fits based on material property data for cordierite (dated 1981) supplied by Corning Incorporated [29].

Specific Heat

$$c_{p\,cer}(T) = 4186.8[0.1890 + 2.432\times10^{-4}(T-273) + 9.770\times10^{-7}(T-273)^2 - 4.332\times10^{-9}(T-273)^3 + 4.167\times10^{-12}(T-273)^4] \quad \text{(A.1)}$$

Thermal Conductivity

$$k_{cer}(T) = 418.68[1.740\times10^{-3} + 7.139\times10^{-7}(T-273) - 8.797\times10^{-9}(T-273)^2 + 1.572\times10^{-11}(T-273)^3 - 7.226\times10^{-15}(T-273)^4] \quad \text{(A.2)}$$

A.2 Thermodynamic Property Data for Dry Air

Specific Heat

The following are equations from Chappell and Cockshutt [30] to calculate specific heat of dry air.

Temperature Range 200K-800K:

$$c_{p_{air}}(T) = 1.0189134\times10^{3} - 1.3783636\times10^{-1}T - 1.9843397\times10^{-4}T^2 + 4.2399242\times10^{-7}T^3 - 3.7632289\times10^{-10}T^4 \quad \text{(A.3)}$$

Temperature Range 800K-2200K:

$$c_{p_{air}}(T) = 7.9865509\times10^{2} + 5.3392159\times10^{-1}T - 2.2881694\times10^{-4}T^{2} + 3.7420857\times10^{-8}T^{3} \quad \text{(A.4)}$$

Viscosity

The following is a curve fit for viscosity of dry air based on data from Incropera and Dewitt [31].

$$\mu_{air}(T) = 1.42742\times10^{-7} + 7.55528\times10^{-8}T - 5.4774\times10^{-11}T^{2} + 2.2113\times10^{-14}T^{3} \quad \text{(A.5)}$$

Prandtl Number

The following is a curve fit for Prandtl number of dry air based on data from Incropera and Dewitt [31].

$$Pr_{air}(T) = 0.779837 - 1.60405\times10^{-4}T - 6.94251\times10^{-7}T^{2} + 1.72069\times10^{-9}T^{3} - 9.25545\times10^{-13}T^{4} \quad \text{(A.6)}$$